

## **Towards closed-loop dynamical wind farm control: model development and control applications**

Boersma, Sjoerd

**DOI**

[10.4233/uuid:48572080-bc51-4ffe-9ba5-676ee9ab5fcc](https://doi.org/10.4233/uuid:48572080-bc51-4ffe-9ba5-676ee9ab5fcc)

**Publication date**

2019

**Document Version**

Final published version

**Citation (APA)**

Boersma, S. (2019). *Towards closed-loop dynamical wind farm control: model development and control applications*. [Dissertation (TU Delft), Delft University of Technology].  
<https://doi.org/10.4233/uuid:48572080-bc51-4ffe-9ba5-676ee9ab5fcc>

**Important note**

To cite this publication, please use the final published version (if applicable).  
Please check the document version above.

**Copyright**

Other than for strictly personal use, it is not permitted to download, forward or distribute the text or part of it, without the consent of the author(s) and/or copyright holder(s), unless the work is under an open content license such as Creative Commons.

**Takedown policy**

Please contact us and provide details if you believe this document breaches copyrights.  
We will remove access to the work immediately and investigate your claim.

**TOWARDS CLOSED-LOOP DYNAMICAL WIND FARM  
CONTROL: MODEL DEVELOPMENT AND CONTROL  
APPLICATIONS**



# **TOWARDS CLOSED-LOOP DYNAMICAL WIND FARM CONTROL: MODEL DEVELOPMENT AND CONTROL APPLICATIONS**

## **Proefschrift**

ter verkrijging van de graad van doctor  
aan de Technische Universiteit Delft,  
op gezag van de Rector Magnificus prof. ir. T.H.J.J. van der Hagen,  
voorzitter van het College voor Promoties,  
in het openbaar te verdedigen op dinsdag 15 januari 2019 om 10:00 uur

door

**SJOERD BOERSMA**

Delft Center for Systems and Control,  
Delft University of Technology, Delft, Holland,  
geboren te Hardenberg, Nederland.

Dit proefschrift is goedgekeurd door de

promotor: prof. dr. ir. J.W. van Wingerden

promotor: prof. dr. ir. M. Verhaegen

Samenstelling promotiecommissie:

Rector Magnificus,

prof. dr. ir. J.W. van Wingerden

prof. dr. ir. M. Verhaegen

prof. dr. ir. J. Meyers,

voorzitter

Technische Universiteit Delft

Technische Universiteit Delft

Katholieke Universiteit Leuven

*Onafhankelijke leden:*

prof. dr. ir. M.A. Rotea,

prof. dr. ir. S.J. Watson

prof. dr. ir. M. Wisse

dr. ir. A. Korniienko

University of Texas at Dallas

Technische Universiteit Delft

Technische Universiteit Delft

Ecole Centrale, Lyon



*Keywords:* Control-oriented wind farm modelling, closed-loop secondary frequency control, model predictive wind farm control

*Printed by:* Gildeprint

Copyright © 2019 by S. BOERSMA

ISBN 000-00-0000-000-0

An electronic version of this dissertation is available at

<http://repository.tudelft.nl/>.

*This page is for Catherine Larose, mon amour*



# CONTENTS

<b>Summary</b>	<b>ix</b>
<b>Samenvatting</b>	<b>xiii</b>
<b>1 Introduction</b>	<b>1</b>
1.1 Motivation	1
1.2 Problem statement and brief literature overview	3
1.3 Thesis contributions and outline	7
<b>2 A tutorial on control-oriented wind farm modeling and control</b>	<b>13</b>
2.1 Introduction	14
2.2 Wind and wind turbines	14
2.2.1 Wind	14
2.2.2 Wind turbine	15
2.2.3 Wake	18
2.3 Wind farm: motivation and challenges	20
2.3.1 Objectives of wind farm control	21
2.4 Control-oriented wind farm modeling	23
2.4.1 Turbine model	24
2.4.2 Flow model	24
2.4.3 Examples	25
2.5 Wind farm control	28
2.5.1 Actuators and sensors	28
2.5.2 Actuation methods for wake control	30
2.6 Wind farm control strategies	34
2.6.1 Optimization-based closed-loop control	35
2.6.2 Linear dynamic closed-loop control	36
2.6.3 Observer	37
2.7 Field tests	38
2.8 Conclusions	39
<b>3 The WindFarmSimulator Model</b>	<b>41</b>
3.1 Introduction	42
3.2 Formulation of a dynamical control-oriented wind farm model	45
3.2.1 Turbulence model	47
3.2.2 Turbine model	49
3.2.3 Discretization	50
3.2.4 Boundary and initial conditions	52



3.3	Computation time . . . . .	53
3.4	Simulation results. . . . .	55
3.4.1	Quality measures . . . . .	55
3.4.2	Axial induction actuation . . . . .	55
3.5	Conclusions. . . . .	59
3.A	Discretizing the Navier-Stokes equations. . . . .	61
3.B	PALM case study . . . . .	70
3.C	SOWFA case study . . . . .	71
<b>4</b>	<b>A constrained wind farm controller providing secondary frequency regulation: an LES study</b>	<b>73</b>
4.1	Introduction . . . . .	74
4.2	Simulation model. . . . .	76
4.2.1	The PARallelized Large-eddy simulation Model. . . . .	77
4.2.2	PALM Supervisory Controller . . . . .	77
4.2.3	Supervisory Controller implementation proposed in this work . . . . .	78
4.3	Controller models. . . . .	79
4.3.1	Dynamical model . . . . .	79
4.3.2	Steady-state model. . . . .	81
4.4	Control strategy . . . . .	81
4.4.1	Axial induction control for power tracking . . . . .	82
4.4.2	Axial induction control for power tracking with optimized yaw settings . . . . .	83
4.5	Simulation results. . . . .	83
4.5.1	Performance measures. . . . .	85
4.5.2	Simulation initialization . . . . .	85
4.5.3	Power tracking while minimizing dynamical turbine loading . . . . .	85
4.5.4	Power tracking with optimized yaw settings . . . . .	87
4.5.5	Power tracking under atmospheric perturbations . . . . .	91
4.5.6	Power tracking under turbine failure. . . . .	93
4.5.7	Power tracking close to and above greedy power . . . . .	93
4.5.8	Computation time . . . . .	96
4.6	Conclusions. . . . .	97
4.A	Turbulence intensity . . . . .	98
<b>5</b>	<b>Conclusion and recommendations</b>	<b>99</b>
5.1	Conclusions. . . . .	99
5.2	Recommendations . . . . .	102
	<b>Bibliography</b>	<b>105</b>
	<b>Preface</b>	<b>121</b>
	<b>Curriculum Vitae</b>	<b>123</b>
	<b>List of Publications</b>	<b>125</b>

# SUMMARY

Electricity consumption is increasing on a global level. In 2017, non-renewable energy sources such as crude oil, natural gas and coal provided 76% of the required energy, while 24% came from renewable sources such as hydro, wind and solar. Non-renewable sources are finite because they do not replenish rapidly enough relative to the rate at which they are being used, and harvesting these resources is environmentally costly. Since renewable energy sources replenish naturally in a relatively short period of time and are cleaner, they are suitable for the sustainable production of electricity.

Wind overtook coal as the second largest form of power generation capacity in Europe in 2016 and is approaching gas, which is currently the largest contributor. However, in 2017 in The Netherlands, only 9.6% of the average annual electricity demand is covered by wind, indicating that there is still room for improvement. A goal described in the Dutch 2018 climate agreement is to increase the offshore wind turbine power to 4450 MW by 2023 (this with respect to 357 MW in 2015). Nevertheless, it is not sufficient to only increment the number of turbines to increase the overall share of wind energy. It is also necessary to reduce the cost of wind energy, which will in turn stimulate further investments in the wind energy industry.

Another cost reduction strategy is by placing turbines in each other's proximity since this reduces maintenance as well as cabling costs. A collection of turbines placed together is called a wind farm. However, a wake develops downstream of each turbine, which is a region of air flow characterized by a flow velocity deficit and an increased turbulence intensity. Since wind turbines are placed together in a farm, the wakes of upstream turbines influence the performance of downstream turbines. For example, the flow velocity deficit reduces the potential power production of downstream turbines and it can deteriorate the provision of ancillary services such as wind farm power reference tracking. An increased turbulence intensity will increment the turbine's fatigue loads, which can reduce its lifetime. The idea of wind farm control is to take wake interactions into account when necessary, and to find control signals such that the levelized cost of wind energy decreases through, *e.g.*, power optimization or load reduction. An advantage of control is that, for existing farms, wind energy cost can be reduced and ancillary services can be delivered. That is, there is no need for redesigning the wind farm though, performance is enhanced by the implementation of wind farm control.

Research on wind farm (control-oriented) models and wind farm controllers has been carried out since the eighties with different results presented in a vast variety of papers. This thesis provides an elaborate overview of the published results. From this overview it is concluded that not many closed-loop wind farm controllers that employ a dynamical control-oriented model are evaluated in a high-fidelity wind farm model

(a first serious step towards practical implementation). Closed-loop control is necessary because 1) it can partially compensate for modelling errors and 2) it can reject time-varying disturbances. Employing a dynamical model allows for utilizing model predictive control, a strategy that admits for control under constraints. This thesis presents a closed-loop control framework for such an approach. One major building block of this closed-loop framework is a control-oriented model. In this thesis, a control-oriented model is defined as a model that can be employed in a controller that works in real-time, *i.e.*, the controller evaluates new control signals within one sample. The control-oriented model's parameters are subsequently updated according to new measurements to increase its accuracy.

This thesis develops a control-oriented model that is based on the three-dimensional unsteady Navier-Stokes equations. Since the closed-loop framework should work in real-time, model assumptions are made. However, which assumptions can be made while ensuring controller performance is an open question in wind farm control. An answer to this question depends, *i.a.*, on the control objective. It is possible to adapt the spatial and temporal resolution of the developed control-oriented model to change its fidelity according to a specific control task. For two case studies, the developed model estimates flow velocities at hub-height and turbine power data. The results are evaluated and validated with a high-fidelity wind farm model. Additionally, the controller model has been employed in several wind farm closed-loop control applications, which illustrates its potential.

This thesis also develops a complete closed-loop wind farm control solution for power reference tracking by utilizing the closed-loop framework presented in this thesis. Therefore, this thesis develops a second dynamical (parameter-varying) wind farm model that is employed in a model predictive controller. Although more modelling assumptions were made during the development of this model with respect to the model presented previously, this control application illustrates that wind farm power tracking is ensured in several simulation cases. Consequently it is concluded that, in order to ensure power tracking, no full wake information needs to be included in the control-oriented model. This results in a time efficient controller implementation that is suitable for online control. The closed-loop control solution also demonstrates that by applying optimized yaw angles, the set of feasible signals for power reference tracking is enlarged. The optimized yaw angles are found by employing a steady-state wind farm model. It is concluded that, in order to find the optimized yaw settings, a full wake model (minimal steady-state) needs to be employed in the controller.

The control application in this part of the thesis also demonstrates that different controller settings result in 1) wind farm power tracking and 2) different distributions of the control signals among the turbines. Accordingly it is concluded that there are multiple solutions to the wind farm power tracking problem. A second performance indicator (besides power tracking) referred to as dynamical loading is included in the controller. It is shown that tracking can be ensured while also dynamical loading can be reduced. The developed control solution is evaluated in a high-fidelity wind farm model, which is a serious first step towards practical implementation.

---

Overall, this thesis demonstrates that the necessary control-oriented model's fidelity depends on the controller's objective, and that in one control solution, different control-oriented models can be employed for different tasks.



# SAMENVATTING

Elektriciteitsconsumptie stijgt wereldwijd. In 2017 namen niet duurzame bronnen zoals ruwe olie, natuurlijk gas en kolen 76% van de benodigde energie voor hun rekening terwijl 24% van duurzame bronnen zoals water, wind en zon kwam. Niet duurzame bronnen zijn eindig omdat ze niet snel genoeg aangevuld worden vergeleken met de snelheid waarmee ze worden verbruikt en het delven van deze bronnen is kostbaar voor het milieu. Duurzame energiebronnen aan de andere kant zijn (bijna) altijd aanwezig, worden natuurlijk aangevuld in een relatief korte periode en zijn schoner. Ze zijn daarom geschikter voor de duurzame productie van elektriciteit.

Wind nam in 2016 de tweede plaats over van kolen in de lijst van capaciteit om vermogen op te wekken en het is gas, de huidige nummer 1, aan het naderen. Desalniettemin werd in 2017 maar 9.6% van de Nederlandse jaarlijkse gemiddelde elektriciteitsvraag door wind geleverd, wat aantoont dat er nog werk aan de winkel is. De Nederlandse regering heeft echter als doel (zie klimaat akkoord 2018) om voor 2023 minimaal 4450 MW vermogen aan windturbines op zee te hebben geplaatst. Dit ten opzichte van de 357 MW in 2015. Desalniettemin is het plaatsen van meer windturbines om het aandeel windenergie te verhogen niet voldoende. De reductie van de kosten moet ook een speerpunt zijn, wat dan de industrie weer zal stimuleren om nog meer te investeren in windenergie.

Een andere kostenvermindering kan behaald worden door turbines bij elkaar te plaatsen omdat dit de onderhoudskosten en ook de netwerkbekabelingskosten vermindert. Een verzameling bij elkaar geplaatste windturbines noemt men een windpark. Echter, (stroomafwaarts) achter de turbine ontwikkelt zich dan een zog. Een zog is een regio lucht die is gekarakteriseerd door windsnelheid vermindering en een verhoging van de turbulentie intensiteit. Het zog van stroomopwaartse turbines zal de prestatie van stroomafwaartse turbines beïnvloeden omdat deze windturbines dicht bij elkaar zijn geplaatst. De windsnelheidsvermindering bijvoorbeeld vermindert de potentiële vermogensproductie van stroomafwaartse turbines en kan het leveren van aanvullende diensten, zoals het volgen van een windparkvermogenssignaal, negatief beïnvloeden. Een verhoging van de turbulentie intensiteit verhoogt de vermoeiingsintensiteit van de turbines wat de levensverwachting van de turbine vermindert. Het idee achter windparkregeltechniek is om, waar nodig, zog interactie in acht te nemen in de regeltechnische oplossing om zo de windenergie kosten verder te verminderen, door bijvoorbeeld vermogensoptimalisatie en vermoeiingsvermindering. Een voordeel van regeltechniek is dat, voor bestaande parken, de kosten voor windenergie verminderd kunnen worden en er aanvullende services geleverd kunnen worden. Met andere woorden, het is niet nodig om een windpark opnieuw te ontwerpen, maar de prestatie kan verbeterd worden door regelaars te ontwerpen.

Onderzoek naar windpark (regeltechnische) modellen en windparkregelaars wordt sinds de jaren tachtig gedaan en heeft verschillende resultaten opgeleverd die in meerdere artikelen zijn gepubliceerd. Deze dissertatie geeft de lezer een uitgebreid overzicht van deze gepubliceerde resultaten. Hieruit is geconcludeerd dat er niet veel resultaten zijn behaald met een gesloten lus windparkregelaar die online (real-time) gebruik maakt van een dynamisch regeltechnisch model en die is getest in een hoogwaardig (precies) windparkmodel (een eerste serieuze stap richting praktische implementatie). Gesloten lus regeltechniek is nodig omdat 1) het gedeeltelijk voor modelleringsfouten kan compenseren en 2) het tijd variërende perturbaties weg kan regelen. Het gebruik van een dynamisch model staat toe dat een model-voorspellende regelaar gebruikt kan worden, een strategie die signaalbeperkingen in de regelaar toelaat. Deze thesis presenteert een gesloten lus raamwerk voor een dergelijke aanpak. Een bouwsteen hiervoor is een regeltechnisch model. In deze thesis is een regeltechnisch model gedefinieerd als een model dat gebruikt kan worden in een regelaar die real-time werkt. Met andere woorden, de regelaar berekent nieuwe regelsignalen binnen één sample. De parameters van het regeltechnische model kunnen dan herzien worden op grond van nieuwe metingen, met een verhoogde modelprecisie als gevolg.

Deze dissertatie ontwikkelt een regeltechnisch model gebaseerd op de drie dimensionale onstabiele Navier-Stokes vergelijkingen. Model aannames zijn gemaakt omdat het gesloten lus raamwerk gebruikt moet worden in real-time. Desalniettemin, welke aannames precies doorgevoerd kunnen worden om nog steeds regelaarsprestatie te kunnen garanderen is een open vraagstuk in windparkregeltechniek, en hangt onder andere af van het doel van de regelaar. Het is mogelijk om de spatiële en temporale dichtheid van het ontwikkelde model te veranderen om zo een modelprecisie te verkrijgen die past bij de specifieke regeltechnische taak. In twee casussen wordt aangetoond dat het ontwikkelde windparkmodel in staat is om windsnelheden op hub-hoogte en turbinevermogenssignalen van een hoogwaardig windparkmodel te schatten. Tevens is het regeltechnische model gebruikt in meerdere windpark gesloten lus regelapplicaties wat het model potentieel aangeeft.

Deze dissertatie ontwikkelt ook een geheel gesloten lus windpark regeltechnische oplossing voor het volgen van een vermogensreferentiesignaal, gebruikmakend van het eerder gepresenteerde gesloten lus raamwerk. Hiervoor ontwikkelt deze dissertatie een tweede dynamisch (parameter-variërend) regeltechnisch windpark model dat in een model-voorspellende regeltechnische oplossing wordt gebruikt. Alhoewel meer modelaannames zijn gemaakt tijdens het ontwikkelen van dit model ten opzichte van het model gepresenteerd in deze dissertatie, laat de regelapplicatie gepresenteerd in dit gedeelte zien dat windparkvermogensvolging gegarandeerd kan worden in meerdere simulatiecasussen. Vervolgens is geconcludeerd dat geen volledige informatie over het zog aanwezig hoeft te zijn in het regeltechnische model als windparkvermogensvolging het regeldoel is. Dit resulteert in een tijdsefficiënte regelaar implementatie die in real-time (online) gebruikt kan worden. De gesloten lus regeltechnische oplossing gepresenteerd in dit gedeelte van de thesis laat ook zien dat door het toepassen van

geoptimaliseerde gierhoeken, de mogelijke set van vermogenssignalen die gevolgd kunnen worden, wordt vergroot. De geoptimaliseerde gierhoeken worden gevonden door gebruik te maken van een statisch windparkmodel. Om de geoptimaliseerde gierhoeken te vinden is er geconcludeerd dat een volledig (minimaal statisch) zogmodel aanwezig moet zijn in de regelaar.

De regelapplicatie in dit gedeelte van deze dissertatie laat ook zien dat verschillende regelaarsinstellingen resulteren in 1) windpark referentievolling en 2) verschillende verdelingen van de regesignalen over de turbines. Vervolgens is geconcludeerd dat er meerdere oplossingen zijn voor het windpark referentievollingsprobleem. Er is geconcludeerd dat de regelapplicatie een tweede prestatie indicator (genaamd dynamische belasting) kan doen verbeteren, terwijl het referentievolling garandeert. De voorgestelde regeltechnische oplossing is geëvalueerd in een hoogwaardig windparkmodel: dit is een eerste serieuze stap naar praktische implementatie.

In zijn algemeenheid laat deze thesis zien dat de noodzakelijke regeltechnische modelprecisie afhangt van het doel van de regelaar, en dat in één regeltechnische oplossing verschillende regeltechnische modellen gebruikt kunnen worden.





# 1

## INTRODUCTION

This introductory chapter provides a motivation for the research presented in this thesis, followed by the problem statement and a brief literature overview. This chapter concludes with the presentation of the thesis contributions and outline.

### 1.1. MOTIVATION

Electricity consumption is increasing on a global level (Enerdata, 2017). In 2017, non-renewable energy sources such as crude oil, natural gas and coal provided 76% of the required energy, while 24% came from renewable energy sources such as hydro, wind and solar (Enerdata, 2017). Non-renewable sources are finite because they do not replenish rapidly enough relative to the rate at which they are being used, although this argument has lost some significance due to the shale gas revolution (Boersma and Losz, 2018). However, the environmental costs related to the harvesting of non renewable resources is high. Since renewable energy sources replenish naturally in a relatively short period of time and have a smaller environmental impact, they are suitable for the sustainable production of electricity. In fact, in 2017, 97.9% of Norway's electricity stemmed from renewable sources, and this mode of production represents 84.0%, 82.0% and 37.3% of New Zealand's, Colombia's and Italy's electricity, respectively (Enerdata, 2017). Although on a global level, the majority of the electricity production is still generated using non-renewable sources, a clear trend towards renewable sources is observed. In fact, their share in global energy generation is expected to grow to 40% in 2040 (International Energy Agency, 2017). The fact that renewable sources accounted for 85% of all new power installations in European Union countries in 2017 (WindEurope, 2018) indicates that we are heading in the right direction.

One of these renewable energy sources is wind, which consists of a bulk movement of air. This movement is due to, *i.a.*, temperature changes that are caused by the sun. In Europe, wind overtook coal as the second largest form of power generation capacity in 2016 and it is approaching gas, which is currently the largest form of power generation capacity (see Fig. 1.1).

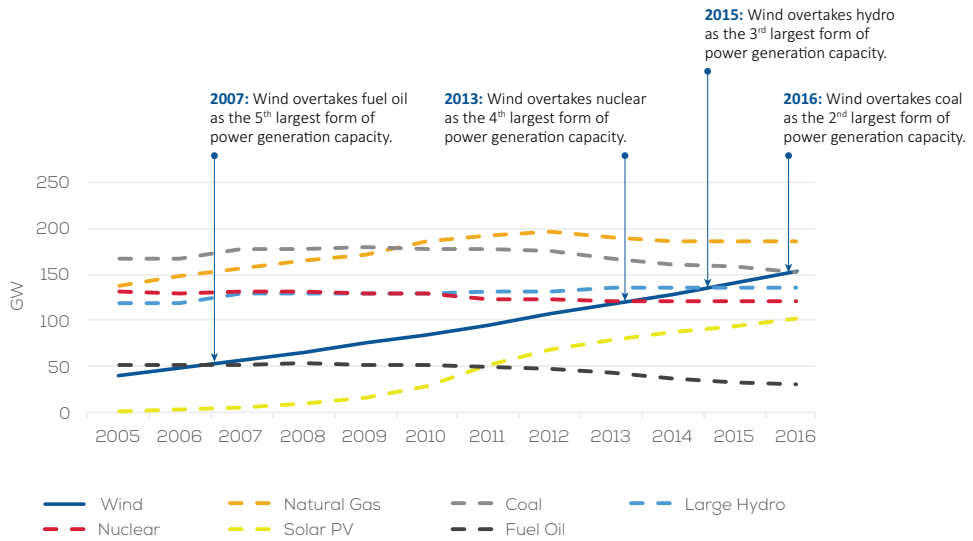


Figure 1.1: Total power generation capacity in the European Union 2005-2017 (WindEurope, 2018).

For example, 44% of Denmark's average annual electricity demand was covered by wind energy in the year 2017. On the other hand, in Holland, this is only 9.6% (WindEurope, 2018) indicating that there is still room for improvement. This should not only be realized by increasing the percentage of wind energy through the placement of additional wind turbines, but also by reducing the cost of wind energy, which will in turn stimulate further investments in the wind energy industry (hence more wind turbines). Figure 1.2 illustrates the coast of Holland with existing and future wind turbine locations, indicating that the previously mentioned 9.6% will increase significantly. A cost reduction can

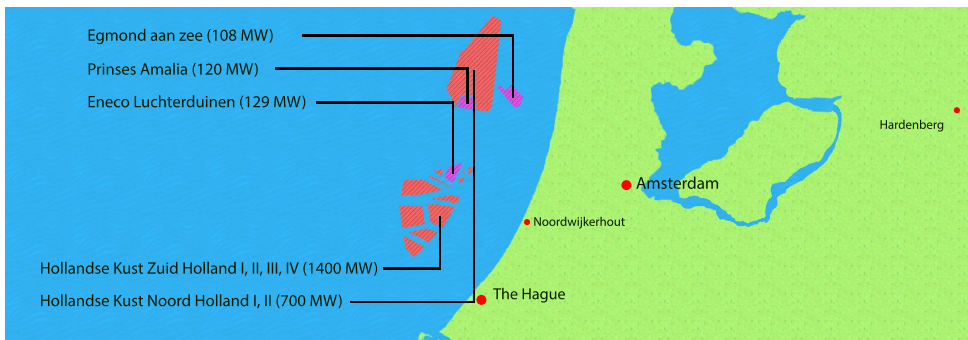


Figure 1.2: Coast of Holland with existing (purple) and future (red) locations where wind turbines are or will be placed, respectively. Figure taken from (International Renewable Energy Agency, 2016) and adapted.

be achieved by, *e.g.*, improving the turbine's structural design such that its lifetime can be extended. Additional cost reduction can be realized by increasing the turbine's energy extraction efficiency and optimizing the turbine's power curve by correctly designing the turbine's controller. Placing turbines in each other's proximity reduces maintenance as

well as cabling costs. It is also easier to provide ancillary services to the electricity grid due to the fact that large power output variations can be regulated more easily when controlling multiple turbines that operate in similar atmospheric conditions. A collection of turbines placed together is called a wind farm. On a farm level, additionally cost reductions can be achieved by, *e.g.*, optimizing the wind farm topology with respect to annual averaged atmospheric conditions and by utilizing wind farm control to optimize turbine fatigue and the wind farm power curve. This last optimization entails, *i.a.*, the maximization of power output or the wind farm's ability to track a power reference signal. The latter is a so called ancillary service that could be delivered by the wind farm (Aho et al., 2012). An advantage of control is that, for existing wind farms, wind energy cost can be reduced and ancillary services can be delivered. In other words, without redesigning the wind farm, but by having proper controllers, performance can be enhanced. Wind farm modelling and control have been research topics since the eighties (Clayton and Filby, 1982; Jensen, 1983; Ainslie, 1988; Katic et al., 1986; Steinbuch et al., 1988).

## 1.2. PROBLEM STATEMENT AND BRIEF LITERATURE OVERVIEW

It was stated before that it is beneficial to place turbines together in a so called wind farm. However, when doing so, a wake develops downstream of each turbine as illustrated in Fig. 1.3.



Figure 1.3: Horns Rev offshore wind farm with, normally invisible, wakes. Source: Christian Steiness. See also (Hasager et al., 2013) for more information on the picture.

A wake is a region of air flow that is characterized by a flow velocity deficit and an increased turbulence intensity (Barthelmie et al., 2007). Since wind turbines are placed together in a farm, the wakes of upstream turbines influence the performance of downstream turbines. For example, the flow velocity deficit reduces the power production of downstream turbines (Barthelmie et al., 2010) and it can deteriorate the provision of ancillary services such as wind farm power reference tracking. An increased turbulence intensity will increment the turbine's fatigue loads as suggested in (Rosen and Sheinman, 1995), which possibly can reduce the turbine's lifetime. The idea of wind farm control is to take wake interactions into account when necessary and find control signals such

that the levelized cost of wind energy decreases through, *e.g.*, power optimization or load reduction. Wind farm control emerged in science around the eighties and is slowly finding its way to industry. Three common wind farm performance objectives are generally considered:

- maximization of power generation,
- minimization of fatigue loading,
- provision of ancillary services.

In current practice, wind farm control typically relies on greedy control, in which structural loading and power production are optimized for a single turbine. However, this often appears to be suboptimal for the overall performance of the wind farm since wake interactions are not taken into account (Pao and Johnson, 2009). On a wind farm level, greedy control could be considered as open-loop control, since no measurements are fed back into a wind farm controller and new controller settings are evaluated locally.

Current research on wind farm control aims to provide plant-wide improvement of the wind energy cost, while (partially) taking wake interactions into account in a closed-loop controller. Closed-loop control is interesting since it can partially compensate for model mismatches and it can reject time-varying disturbances. It can be done by designing a controller offline using a wind farm model, or by incorporating a model in the controller itself, and employ this to evaluate optimized control settings online (within one sample) using measurements (referred to as “online model-based closed-loop wind farm control”). The latter approach will be detailed later, but includes a major challenge due to the complex nonlinear dynamics in a wind farm. This challenge can be circumvented by approaching the wind farm control problem with model-free methods Extremum-seeking control (Ciri et al., 2016, 2017, 2018). The challenge in using model-free methods remains the relatively long convergence time of the algorithms, especially when large wind farms need to be considered, although not enough data is available to make definite statements on its applicability. A model free open-loop approach that does not deal with the convergence time challenge is the application of pre-defined time-varying control signals as proposed in (Munters and Meyers, 2018b).

When putting more information in the controller, the problem requires a turbine and flow model that can be complex and high dimensional, as will be discussed in Chapter 2 and Chapter 3. It should already be clear that different wind farm models exist, and that one categorization of these models can be according to the model's fidelity. In general, an increase in model fidelity results in an increase in computational time and the other way around, as indicated in Fig. 1.4. Here, four model categories are defined and their corresponding computational time is depicted in a graph. The first-principle models are the discretized three-dimensional Navier-Stokes equations and could include a subgrid scale model and high-fidelity turbine model. The physics-based models typically solve a set of simplified and discretized Navier-Stokes equations. Simplification can be made by, *e.g.*, neglecting terms in the three-dimensional Navier-Stokes equations, by including a simplified subgrid scale model or by neglecting the vertical dimension. The engineering

models are heuristically found wind farm models. These models are generally based on multiple different and relatively simple expressions that, *e.g.*, approximate the turbine's power generation and wind velocities in the farm. These expressions are then coupled and tuning parameters are generally used to match wind farm data or initially, data from a high-fidelity wind farm model. The pre-calculated models can be seen as lookup tables that contain heuristically found models, each tuned for specific atmospheric conditions. Consequently, when an atmospheric condition, such as wind velocity, changes, another simplified wind farm model is used from the lookup table to evaluate optimized control settings (something that can be done offline). Chapter 2 and Chapter 3 provide the reader with examples and a more elaborate discussion on wind farm models.

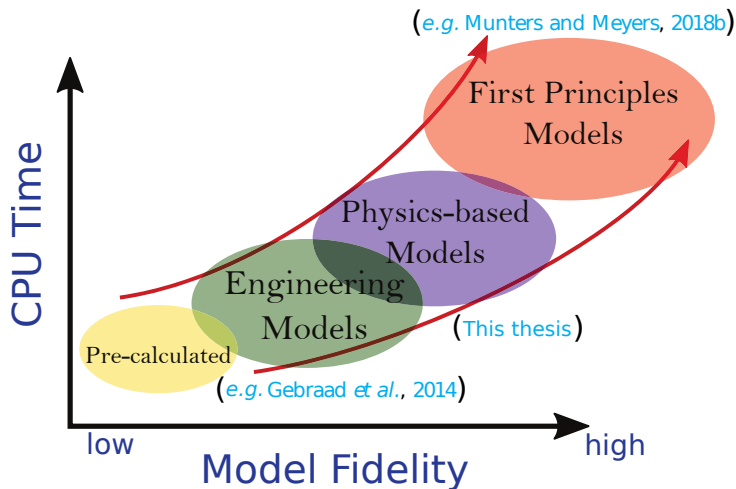


Figure 1.4: Model fidelity versus computational time (CPU time). Figure taken from (Mann et al., 2006) and adapted.

A controller model is defined as a model that is employed in a controller. Wind farm control results that are obtained with a high-fidelity controller model can be found in, *e.g.*, (Munters and Meyers, 2018a) in which the objective is to maximize the wind farm energy production by employing Economic Model Predictive Control as control strategy. Due to the large controller computation time, practical implementation is not feasible. However, the results are scientifically interesting and can serve as an upper bound on the possibilities. Wind farm control results that are obtained using a steady-state engineering model can be found in, *e.g.*, (Gebraad et al., 2014). Due to the fact that the model is found heuristically and contains many tuning parameters, it is difficult to interpret the results. Generally, the conclusions can be summarized as whether the controller provides satisfactory performance or not. However, researching why the controller does not work properly by, *e.g.*, including missing wind farm characteristics is difficult due to the heuristic nature of the employed controller model. Additionally, the inclusion of more heuristic expressions results in more tuning parameters and consequently increases the model's complexity. Despite these limitations, these types of controller models are very suitable for practical implementation and can be updated online based on past

measurements due to the relatively low computational cost (Bottasso and Schreiber, 2018). The results given in (Munters and Meyers, 2018a) and (Gebraad et al., 2014) employ controller models that can be found on the spectrum's edges of controller model fidelity currently known in literature (see Fig. 1.4). Wind farm control results that can be found in the spectrum's middle are not widely present in literature. One example of this is (Shapiro et al., 2017a). The controller model employed in (Shapiro et al., 2017a) is based on a dynamical version of the Jensen model (Jensen, 1983) and additionally utilizes the wake superposition principle of (Katic et al., 1986). There is however no controller that employs a controller model based on the governing flow equations, the unsteady Navier-Stokes equations and that can potentially find optimized control signals in an online closed-loop control framework. In Chapter 2 and Chapter 4, a more elaborate overview on the state-of-the-art in wind farm control and related topics is presented.

1

A topic under investigation in the online model-based closed-loop wind farm control approach is the necessary fidelity of the controller model. Which wind farm dynamics should be taken into account in a controller model and which can be neglected is still an open question. In any case, a trade-off has to be made between controller model fidelity and computational time. Another topic under investigation is the necessary controller sample period, *i.e.*, how often do new control signals need to be applied. For example, this can occur anywhere from every second to every fifteen minutes. An answer to this question has a major impact on the possible choice of the controller model since, if every fifteen minutes new control signals are applied, the computational cost of the controller model becomes less of a critical issue and consequently, the controller's fidelity can increase.

It was previously mentioned that another option is to synthesize a controller offline using a dynamical wind farm model (Soleimanzadeh et al., 2013). In such a case, computational time is not really an issue because once the controller is derived, it can be applied in a wind farm and no online forward nor (possibly) backward propagation is necessary, like in Model Predictive Control (MPC). However, currently known controller synthesis methods are in general limited to linear models and it is an open question whether these type of models can be employed for designing a controller for offline wind farm control. These type of controllers are especially interesting when power reference tracking is the objective.

### 1.3. THESIS CONTRIBUTIONS AND OUTLINE

Many wind farm models and wind farm control algorithms exist in current literature. The first question that this thesis investigates is:

1. What is the state-of-the art in wind farm modelling and control, what is missing and contributes to the current state of wind farm control?

One contribution of this thesis is a categorisation and overview of wind farm models and control results that have been published (see Chapter 2). The main conclusion drawn from this overview is that wind farm controllers utilizing a medium-fidelity control-oriented dynamical wind farm model are not extensively researched, while it is hypothesized that these models can be employed in wind farm control. In this thesis, a control-oriented model is defined as a model that is employed in a controller that works in real-time, *i.e.*, the controller evaluates new control signals within one sample. This thesis proposes an online model-based closed-loop wind farm control approach that employs a medium-fidelity dynamical control-oriented wind farm model. The objective in online model-based closed-loop wind farm control is to, within one sample period of the controller:

1. update the employed dynamical control-oriented model's parameters based on current measurements,
2. estimate wind farm states that can not be measured by employing an observer,
3. find optimized control settings such that a predefined performance measure is ensured.

It is necessary to update the employed control-oriented model's parameters according to measurements (*e.g.*, mean wind direction) due to the fact that modelling assumptions are made. Consequently, the controller model does not capture all temporally and spatially varying nonlinear wake dynamics and is not suitable for all atmospheric conditions. By properly updating the control-oriented model's parameters according to measurements, the control-oriented model can be adapted to match the current atmospheric conditions. The control-oriented model in the proposed framework is dynamical so that wake delays and flow transients can be captured by propagating the model forward in time in a model predictive controller. Estimating system states such as flow velocities in the wind farm is interesting because one can then predict the incoming flow for each turbine in the farm and consequently power production and a measure of fatigue can be predicted. These predictions can, in turn, be used in a control strategy such as MPC. With MPC one can evaluate optimized control settings such that a predefined performance (quadratic cost) is ensured (minimized), which is the objective of wind farm control. The above can schematically be represented in a block scheme as depicted in Fig. 1.5.



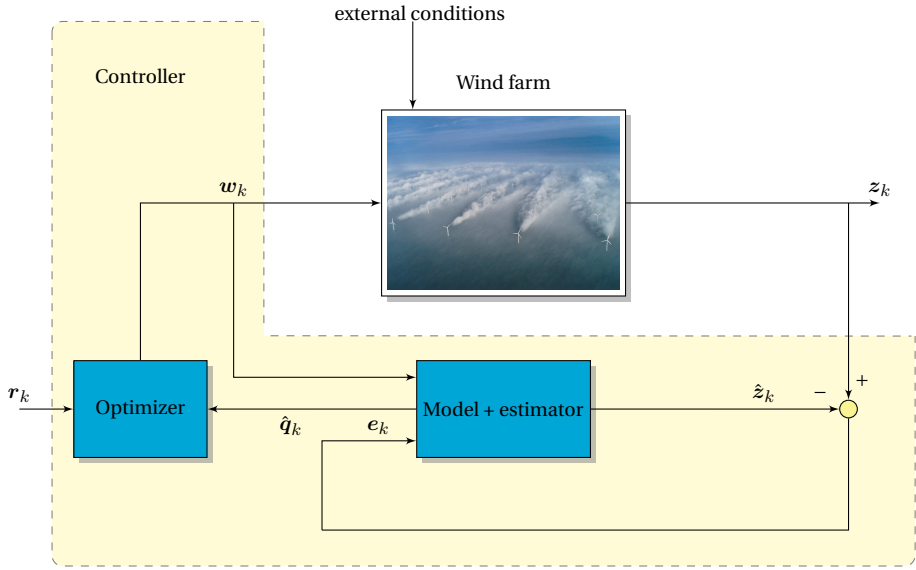


Figure 1.5: General dynamical closed-loop control framework with measurements  $z_k$  and its estimation  $\hat{z}_k$  and state estimation  $\hat{q}_k$  at time index  $k$ . The signals  $r_k$  and  $w_k$  are reference and control signals, respectively. The observer is the model and estimator combined.

An example of the signal  $z_k$  can be the power generated by the turbines, and  $\hat{q}_k$  can be wind velocity components in the wind farm. The reference  $r_k$  can be a wind farm power reference signal and  $w_k$  the generated torque, pitch and yaw angle of all turbines in the farm. The framework presented in Fig. 1.5 contains three main building blocks:

1. a control-oriented (surrogate) model,
2. an estimator (state observer),
3. an optimizer (model predictive controller).

The first objective of the closed-loop control framework proposed above is to develop a dynamical control-oriented model that is suitable for online control. As discussed above, modelling assumptions need to be made such that the control-oriented model becomes employable in the closed-loop control framework described above. The following question is formulated:

- II. Which wind farm dynamics need to be captured in a control-oriented wind farm model such that the model can be employed in the online closed-loop control framework, while the control objective is ensured?

One major factor that influences the answer to the above formulated question is the defined control objective. In other words, what is the wind farm controller's objective? For example, if reducing the turbine's fatigue is not included in this objective, no such

information needs to be present in the controller model. Following this line of reasoning, the above question can be stated more specifically as:

III. Which wind farm dynamics need to be captured in a control-oriented wind farm model such that the model can be employed in the online closed-loop control framework, while wind farm power tracking is ensured?

As will be detailed in Chapter 4, the objective in wind farm power tracking is to follow a predefined reference signal with the wind farm power by de- and up-rating the power output of the turbines. This problem has in general multiple solutions. For example, suppose that a 12 [MW] reference signal needs to be followed with six turbines. One solution is to let each turbine produce 2 [MW], but another solution is to let two turbines produce each 6 [MW], while shutting down the other four turbines. In order to have a unique solution, additional objectives should be defined. An example of such an additional objective could be the minimization of turbine fatigue. Consequently, when assuming that wind farm power tracking is the objective, a fourth question can be formulated:

IV. Can we impose additional objectives on the controller while providing wind farm power tracking and what is the consequence on the control signal distribution among the turbines?

Different aspects of the closed-loop control framework proposed above and a complete wind farm control solution are presented in this thesis and in the related publications. The presented results aim to provide leverage for answering the stated questions above. Each chapter in this thesis is self contained. Consequently, chapter abstracts and parts of their introductions are repeated in different chapters.

- Chapter 2 is based on

**S. Boersma, B.M. Doekemeijer, P.M.O. Gebraad, P.A. Fleming, J. Annoni, A.K. Scholbrock, J.A. Frederik and J.W. van Wingerden**, *A tutorial on control-oriented modelling and control of wind farms*, [American Control Conference](#), 2017.

**B.M. Doekemeijer, S. Boersma, J. Annoni, P.A. Fleming and J.W. van Wingerden**, *Wind Plant Controller design*, ModSim book, 2018.

and presents a tutorial on control-oriented wind farm modelling and wind farm control. This chapter elaborates on basic concepts and definitions that are used in the wind farm scientific and engineering community. Additionally, the chapter provides an elaborate state-of-the-art overview of wind farm control and provides ideas on possible future research directions. Two of these conclusions are 1) there is a potential need for a medium-fidelity control-oriented model that can be employed in a closed-loop control framework as depicted in Fig. 1.5 and 2) controller solutions require thorough validation in a high-fidelity environment.

- Chapter 3 is based on

**S. Boersma, B.M. Doekemeijer, M. Vali, J. Meyers and J.W. van Wingerden**, *A control-oriented dynamic wind farm model: WFSim*, [Wind Energy Science](#), 2018.

**S. Boersma, P.M.O. Gebraad, M. Vali, B.M. Doekemeijer and J.W. van Wingerden**, *A control-oriented dynamic wind farm flow model: WFSim*, [Journal of Physics: Conference Series](#), 2016.

and develops a nonlinear dynamical control-oriented medium-fidelity wind farm model. The model originates from the three-dimensional Navier-Stokes equations that are simplified such that a two-dimensional control-oriented wind farm model is obtained that includes an approximation of the third dimension. A new parametrization of the mixing length turbulence closure model is proposed that allows for spatially varying wake recovery. The model is agile in a sense that the model's spatial and temporal discretization can be adapted. It will be demonstrated that the former has a large influence on the computational time of the model, but also influences its accuracy. In other words, the model allows for a trade-off between model accuracy and computational time. The presented model is employed in an observer

**B.M. Doekemeijer, S. Boersma, L.Y. Pao, T. Knudsen and J.W. van Wingerden**, *Online model calibration for a simplified LES model in pursuit of real-time closed-loop wind farm control*, [Wind Energy Science](#), 2018 (under review).

and in an adjoint-based model predictive wind farm controller

**M. Vali, V. Petrović, S. Boersma, J.W. van Wingerden, L.Y. Pao and M. Kühn**, *Adjoint-based model predictive control of wind farms: Beyond the quasi steady-state power maximization*, [Control Engineering Practice](#), 2018 (under review).

All these elements together form the basis of the framework schematically depicted in Fig. 1.5. The control-oriented model is additionally utilized in a wake redirection application

**S. Raach, S. Boersma, B.M. Doekemeijer, J.W. van Wingerden and P.W. Cheng**, *Lidar-based closed-loop wake redirection in high-fidelity simulation*, [Journal of Physics: Conference Series](#), 2018.

- Chapter 4 is based on

**S. Boersma, B.M. Doekemeijer, S. Siniscalchi-Minna and J.W. van Wingerden**, *A constrained wind farm controller providing secondary frequency regulation: an LES study*, [Renewable Energy](#), 2018 (under review).

**S. Boersma, V. Rostampour, B.M. Doekemeijer, J.W. van Wingerden and T. Keviczky**, *A Model Predictive Wind Farm Controller with Linear Parameter-Varying Models*, [IFAC Conference on Nonlinear Model Predictive Control](#), 2018.

and proposes a complete closed-loop wind farm control solution. The time efficient controller utilizes a second proposed dynamical control-oriented wind farm model that is updated online according to measurements. Furthermore, the proposed controller provides an ancillary service called power tracking in which the objective is to track a wind farm power reference signal. It additionally reduces dynamical loading on a farm level. The controller is tested in a high-fidelity wind farm model for which software is developed that allows for evaluating wind farm controllers in a high-fidelity wind farm model.

This thesis is concluded in Chapter 5.



# 2

## A TUTORIAL ON CONTROL-ORIENTED WIND FARM MODELING AND CONTROL

*Do the things you like and find others  
who like to do the things you don't like.*

*Wind turbines are often sited together in wind farms as it is economically advantageous. However, the wake inevitably created by every turbine will lead to a time-varying interaction between the individual turbines. Common practice in industry has been to control turbines individually and ignore this interaction while optimizing the power and loads of the individual turbines. However, turbines that are in a wake experience reduced wind speed and increased turbulence, leading to a reduced energy extraction and increased dynamic mechanical loads on the turbine, respectively. Neglecting the dynamic interaction between turbines in control will therefore lead to suboptimal behaviour of the total wind farm. Therefore, wind farm control has been receiving an increasing amount of attention over the past years, with the focus on increasing the total power production and reducing the dynamic loading on the turbines. In this chapter, wind farm control-oriented modeling and control concepts are explained. In addition, recent developments and literature are discussed and categorized. This chapter can serve as a source of background information and provides many references regarding control-oriented modeling and control of wind farms.*

---

Parts of this chapter have been published in (Boersma et al., 2017).

## 2.1. INTRODUCTION

This chapter is, with respect to the literature overview presented in (Knudsen et al., 2015), focused on the corresponding flow control problem and discusses recent wind farm research developments and field test experiments in more detail. It is organized as follows. In §2.2, a brief introduction to wind and wind turbines will be given. At the end of this section, the concept of a wake will be introduced. In §2.3, wind farm control objectives in terms of performance indicators will be presented. Typically, controllers are designed and evaluated according to these indicators. In §2.4, control-oriented wind farm modeling will be discussed. These models can be used for designing and/or testing a controller. In §2.5, control of wind farms will be introduced and typical wind farm sensors and actuators will be discussed. In §2.6, a categorization of wind farm control strategies will be presented. In §2.7, a number of field tests for model validation are briefly discussed. In §2.8, conclusions and an outlook will be provided.

## 2.2. WIND AND WIND TURBINES

This section briefly introduces wind energy and single wind turbine control as it pertains to the challenge of larger wind farm control. A more complete and detailed description can be found in (Burton et al., 2001; Bianchi et al., 2007; Tong, 2010; Hansen, 2015). This section will end by introducing the concept of a wake and its essential characteristics relevant for wind farm control-oriented modeling and control.

### 2.2.1. WIND

Wind is the source of energy exploited by a wind turbine. Wind flows are mainly caused by the Earth's rotation and thermal heating of the Earth's surface by the sun, hence wind is ubiquitous. However, its force is not everywhere equivalent. The behavior of wind at a specific location and for a certain time instant can be characterized by a direction and magnitude. The process of energy extraction by turbine rotors can better be understood by looking at the energy extracted from the wind flowing through a thin disk (see Fig. 2.1), with this disk being equivalent to the rotor swept area.

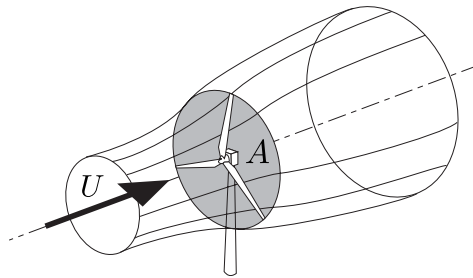


Figure 2.1: Flow with velocity  $U$  [m/s] through a rotor disk with rotor swept area  $A$  [m<sup>2</sup>]. Figure adapted from (Burton et al., 2001).

From the continuity equation of fluid mechanics, the mass flow of air is a function of air density  $\rho$  [kg/m<sup>3</sup>], surface area  $A$  [m<sup>2</sup>], and flow velocity  $U$  [m/s]. Assuming the latter

is uniform across the rotor swept area,  $A$ , the mass flow of air  $\frac{dm}{dt}$  through a rotor disk is defined as

$$\frac{dm}{dt} = \rho AU. \quad (2.1)$$

The instantaneous kinetic power of the wind available at surface  $A$ ,  $P_w$  [W], is calculated by

$$P_w = \frac{1}{2} \frac{dm}{dt} U^2 = \frac{1}{2} \rho AU^3. \quad (2.2)$$

Note that the power expression depends linearly on the rotor disk area,  $A$ , (and thus rotor radius squared), and on the wind velocity,  $U$ , cubed. This implies that relatively higher gains in power generation can be achieved by placing turbines at locations with high wind velocities.

However, a wind turbine cannot extract all this available power from the wind, as the flow is required to still have velocity behind the rotor. The theoretical limit for energy extraction by a rotor is determined by the Betz limit (Betz, 1920). This limit will be, *i.a.*, discussed in the following section.

### 2.2.2. WIND TURBINE

There are different types of vertical-axis and horizontal-axis wind turbines. The most commonly produced and used wind turbine is the upwind horizontal-axis wind turbine. One of its advantages can be explained by the fact that the blades are always facing fully into the wind, because incoming wind does not have to pass the turbine tower first (in contrast to downwind turbines) or other blades (in contrast to vertical-axis turbines). A horizontal-axis wind turbine consists of a rotor, most often with three rotor blades, that is attached to the generator through a drivetrain. The generator and drivetrain are housed in the nacelle, which is supported by a tower. See Fig. 2.2 for a schematic representation of the main wind turbine components.

The rotor blades convert the momentum of a wind field passing the rotor plane into aerodynamic forces that drive the rotor. The drivetrain transfers the aerodynamic torque from the rotor to the generator shaft, either directly (direct drive) or through a transmission (gearbox). The generator converts rotational kinetic power into electrical power by generating a reactive torque on the shaft. To control the power production and forces (torques) on the wind turbine, a number of degrees of freedom (control variables) are typically available:

- Blade pitch ( $\theta$ ) - The rotor blades can rotate, with their axis of rotation aligned with the blades, using hydraulic actuators or servo pitch motors. Pitch control can be used to influence the power capture (see, *e.g.*, (Hand and Balas, 2002)) and the loads (see, *e.g.*, (Bossanyi, 2003, 2005; Selvam et al., 2009; Ungurán and Kühn, 2016)) experienced by the wind turbine.
- Generator torque ( $\tau_g$ ) - The generator converts mechanical power into electricity. Torque control is used to control the power capture.
- Yaw ( $\gamma$ ) - The nacelle can rotate, with the axis of rotation aligned with the tower, using a yaw motor. The yaw angle is defined as the angle between the axial rotor axis and the incoming wind direction. In single turbine control, yaw control is



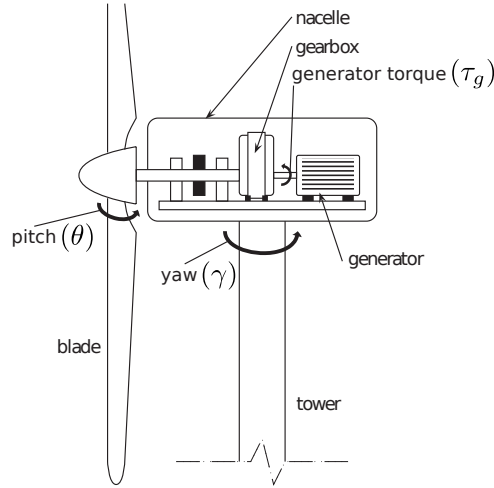


Figure 2.2: Horizontal-axis wind turbine with labeled main components and control variables. Figure adapted from (Bianchi et al., 2007).

2

often used to set the rotor plane perpendicular to the incoming wind direction to increase the turbine's power capture.

The control variables are shown in Fig. 2.2 with a number of basic components of a wind turbine. With these control variables we can optimize the performance of a single wind turbine, such as produced power,  $P$ , and turbine loading. An uncommon, and for now more scientifically interesting, control variable is the tilt angle of a turbine. This is defined as the difference of the wind angle of attack and the nacelle angle, with respect to the horizontal plane. In current wind turbines, this tilt angle is fixed.

A wind turbine exerts a force on the wind flowing through the rotor. This thrust force represents the amount of energy extracted from the flow and can be described by

$$F = C_T(\theta, \lambda, \gamma) \frac{1}{2} \rho A U_\infty^2, \quad (2.3)$$

with  $U_\infty$  [m/s] as the free-stream wind velocity and  $C_T(\theta, \lambda, \gamma)$  as the dimensionless thrust force coefficient, which is a function of the tip-speed ratio,  $\lambda$ , blade pitch,  $\theta$ , and yaw angle,  $\gamma$ . The tip-speed ratio is defined as the ratio of the tangential speed at the blade tip to free-stream wind velocity:

$$\lambda = \frac{\omega R}{U_\infty}, \quad (2.4)$$

with  $R$  the rotor radius and  $\omega$  the rotor rotational speed. The tip-speed ratio is directly influenced by the rotor speed, which is influenced by the generator torque or by changing the pitch angle to change the lift forces on the rotor blades. The generator torque control loop is relatively fast because the system is manipulated at the electrical level, though

changes in the rotor speed itself are not that fast due to inertia, especially for large rotors. Although the blade pitch control loop is slower than the torque loop, it is still relatively fast because of powerful motors that typically can achieve up to a 10 [deg/s] blade pitch rate for a utility-scale wind turbine.

The power in the wind across a rotor was given in (2.2). Although power production can be improved using control, not all the power in the wind can be extracted by a wind turbine. The wind power available for extraction by a turbine is given by:

$$P = C_P(\theta, \lambda, \gamma) \frac{1}{2} \rho A U_\infty^3, \quad (2.5)$$

where  $C_P(\theta, \lambda, \gamma) < 1$  is the dimensionless power coefficient and the ratio of generated power by the wind turbine to the available power in the wind (see (2.2) and (2.5)). There are many models in literature that provide expressions for the thrust and power coefficient. One popular way to get an expression for the force and power coefficients is by exploiting the momentum theory developed in the 19<sup>th</sup> century by W. J. M. Rankine, A. G. Greenhill, and R. E. Froude. R. E. Froude, D. W. Taylor, and S. Drzewiecki combined momentum theory with blade element theory, which resulted in the blade element model (BEM) for calculating the forces that a blade exerts on a flow. When these forces are then converted into a disk of distributed forces that model the rotor, this is referred to as the actuator disk model (ADM). In (Burton et al., 2001), it is explained that, by using momentum theory for an ideal rotor, the thrust coefficient,  $C_T$ , and power coefficient,  $C_P$ , can be written as:

$$C_T(a, \gamma) = 4a(\cos(\gamma) - a), \quad C_P(a, \gamma) = 4a(\cos(\gamma) - a)^2, \quad (2.6)$$

for  $0 \leq a \leq \frac{1}{2}$  and the yaw angle,  $\gamma$ . The parameter,  $a$ , is called the axial induction factor of a wind turbine. It is the ratio of the difference between  $U_\infty$  and the wind velocity at the rotor  $U_r$  to  $U_\infty$ , and is defined as:

$$a = \frac{U_\infty - U_r}{U_\infty}. \quad (2.7)$$

The axial induction factor is thus a measure of the decrease in wind velocity behind a wind turbine and provides a relatively simple expression for coordinated control of wind turbines. Note that this factor, or more precisely,  $U_r$ , can be controlled using the generator torque and blade pitch angle, but is also influenced by the yaw angle.

It was already stated that even a perfect wind turbine cannot fully capture all of the available power in the wind. There is a theoretical maximum that can be extracted by a turbine. This maximum can be obtained by calculating the supremum of  $C_P(a, \gamma)$ , given in (2.6), as a function of the axial induction factor and yaw angle. It can be found that for any wind turbine, the induction factor that results in the maximum power extraction is  $a^* = \cos(\gamma)/3$ , which translates to a theoretical limit of  $C_{P_{\max}} = 16/27 \cos^3(\gamma)$ , which is approximately 0.6 if  $\gamma = 0$ . This theoretical maximum is called the Betz limit. In a practical sense, the maximum power coefficient for horizontal-axis wind turbines lies around 0.45 according to (Bianchi et al., 2007). The maximum force can be found in a similar way: for  $a = 1/2$ , the wind exerts the maximum force on the wind turbine. Note that empirical data published in (Marshall and Buhl, 2005) revealed that the thrust coefficient

expression given in (2.6) is not accurate when  $a > 1/2$ . A possible correction based on empirical data has been proposed in that paper. This correction is based on the Glauert empirical relation between the thrust coefficient and axial induction.

A more detailed representation of the rotor than the ADM is the actuator line model (ALM), which represents each blade individually in the flow, as a distribution of forces along a rotating line.

### OPERATING REGIONS

For single wind turbines, different operating regions can be distinguished. Each region has its own control strategy and is typically determined based on a generator speed feedback signal. The ideal power curve for a variable pitch/speed wind turbine is shown in Fig. 2.3. In addition, a wind power curve is depicted and the ratio between this curve and

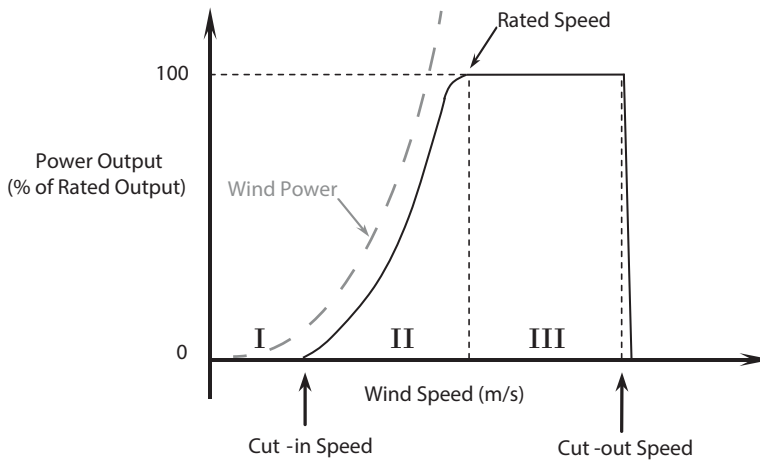


Figure 2.3: Typical wind turbine power curve. Figure adapted from (Tong, 2010).

the power curve is defined by the power coefficient. The ideal power curve exhibits three main regions with distinct control objectives. In Region II, the control problem can be seen as a tracking problem, whereas in Region III, the control problem can be seen as a disturbance rejection problem.

### 2.2.3. WAKE

As a wind turbine extracts energy from the wind, it causes a change in the wind flow downstream from the wind turbine. The altered flow is called the wake of a turbine. The wake characteristics are space-, time-, and parameter-dependent. A wake is space-dependent because, e.g., far downstream of a turbine, it is different from the wake closer downstream of the turbine. The wake is also time-dependent because the operation of a wind turbine changes over time as well as the surrounding flow. Finally, a wake is parameter-dependent, as the external variables (such as temperature) influence the behavior of the wake. It should be clear that studying and modeling a wake is a broad

research topic by itself and ongoing (Sanderse et al., 2011; Bartl and Sætran, 2016). Models range from low to high fidelity, where the latter describes the wake in more detail and tries to capture more of its characteristics than the former. However, this increase in precision will result in higher computational costs. A more complete discussion on different wake models is presented in § 2.4.

Typical characteristics of a wake and its main causes are:

- Wind velocity deficit, as a result of the turbine's energy extraction.
- Increased turbulence intensity, as a result of *i.a.*, the turbine blade's rotation.
- Wake recovery, which is the phenomenon that downwind a wind turbine, *i.a.*, the wind velocity recovers to the free-stream velocity due to mixing.
- Wake meandering, which is a large-scale stochastic phenomenon of a wake in which the entire wake structure will show horizontal and vertical oscillations over time, rather than maintaining a certain fixed position and shape (España et al., 2011; Medici and Alfredsson, 2006).
- Wake expansion, which occurs with distance from the turbine and can be explained using the law of mass conservation and the assumption of flow incompressibility. It can be shown that a decrease in velocity means a proportional increase in the wake's cross-sectional area (see *e.g.*, (Hansen, 2015)).
- Wake deflection, which is the phenomenon that the complete wake is diverging in the latitudinal direction from the rotor center because of blade rotations (Fleming et al., 2014a) or the fact that the rotor is not oriented perpendicular with respect to the incoming wind, *i.e.*, a yawed or tilted turbine.
- Wake skewing, as a result of veer (Gebraad et al., 2016a).
- Vertical wind shear, which is the change of wake properties with height, typically an increase of wind speed with height because of ground friction.
- A kidney-shaped wake, as a result of a yawed turbine (Howland et al., 2016).
- Wake rotation due to the rotating turbine blades.

Note that the external atmospheric properties also have a critical impact on wakes and their propagation, and thus, *i.e.*, land-based and offshore wind turbines develop different wakes. Fig. 2.4 illustrates a horizontal slice of the wake at turbine hub height with  $\gamma = 30^\circ$ . The contour plot with normalized velocities is obtained from wind tunnel data.

Using momentum theory and assuming  $\gamma = 0$ , a lower bound on the wind velocity,  $U_-$ , and a wind velocity at the rotor,  $U_r$ , can be estimated as

$$U_- = U_\infty(1 - 2a), \quad U_r = U_\infty(1 - a). \quad (2.8)$$

As stated before, it is through the wake that an upwind turbine can influence the performance of downwind turbines. The key objective of wind farm modeling and control is to take these interactions into account and use control variables to ensure a specific level

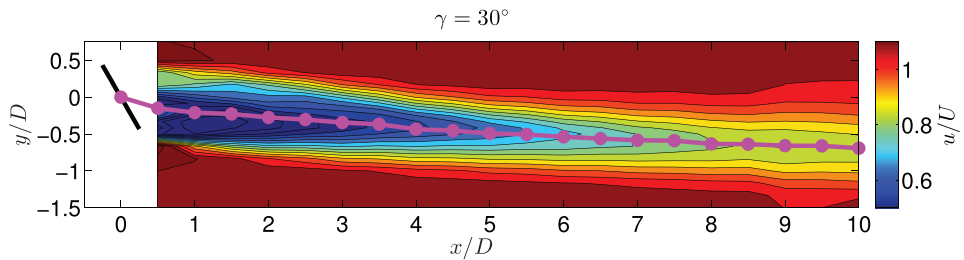


Figure 2.4: A time-averaged, stream-wise wind velocity contour plot at hub height obtained from wind tunnel data. The center of the wake is shown in filled magenta circles. Figure taken from (Howland et al., 2016).

of performance. One option is to capture the nonlinear stochastic behavior in a mathematical model and then use this model to design a controller that guarantees a performance. The assumption is that, when applying this controller to the real wind farm, equivalent performance will be achieved as predicted by the model used for controller design. This assumption is based on the validity of the used model. In this approach lies one of the main challenges in wind farm modeling and control: understanding wake behavior and capturing the important dynamics of wake interactions. An open question is: which wake dynamics are important for a control-oriented wind farm model. A subsequent challenge is controller design for the identified model. Most standard controller synthesis methods known in literature are based on linear state-space models. When dealing with nonlinear and stochastic systems, control design techniques are less available, and optimal performance can (in these cases) not be ensured because of possible local minima.

Another option is to find an optimal control policy following a model-free approach. Both model-based and model-free approaches will be discussed later in this chapter. In §2.3, an introduction to wind farms will be given. This chapter will then discuss control-oriented modeling and control of a wind farm in §2.4 and §2.5, respectively.

### 2.3. WIND FARM: MOTIVATION AND CHALLENGES

The previous section gave a brief introduction on wind energy and single turbine control and ended by introducing the concept of a wake. This was defined as the changed downstream flow caused by a wind turbine (see Fig. 1.3) and can result in interactions between wind turbines. It was stated that wind farm control aims to take these interactions into account while ensuring wind farm performance. This section follows by discussing reasons why it is interesting to study wind farms, and also the related challenges.

Placing turbines together has a number of benefits, which are, *i.a.*:

- Reduced deployment costs of the turbines.
- Reduced deployment costs of the electricity grid.
- Reduced operation and maintenance costs.

Especially in densely populated countries such as the Netherlands, deploying turbines



Figure 2.5: Part of the Gemini offshore wind farm located in the Netherlands. Picture taken from <http://geminiwindpark.nl/foto-s.html>.

individually is unfeasible, with governments often investing in both land-based and offshore wind farms. However, grouping turbines together in farms also introduces a number of complications that often significantly affect their performance. These complications can impact downstream turbines as follows:

- Because of the wind velocity deficit in the wakes of upstream turbines, the downstream turbine will capture less power than when operated in free-stream conditions (Steinbuch et al., 1988; Johnson and Thomas, 2009).
- As a result of increased turbulence in the wake, fatigue loads on the downstream turbine can increase (see, e.g., (Hahm and Wußow, 2006; Bossuyt et al., 2017)), thereby shortening its lifetime in the absence of control algorithms that take this turbulence increase into account.
- In most cases, the center of the wake will not coincide with the center of a downstream rotor. This can be caused by wake meandering, deflection, and wind direction (mostly). Because of this, there is more thrust on one side of the rotor, leading to large cyclic variations as the blades pass in and out of the wake (van Dijk et al., 2017; Zalkind and Pao, 2016). This imbalance can contribute to an accelerated structural degradation of waked turbines.

Wind farm control consists of finding control inputs using measurements to increase the performance of a wind farm, thus improving quality or minimizing the cost of wind energy. The latter can of course be carried out by increasing the spacing between turbines, though this may have a negative impact on the aforementioned advantages, such as reduced deployment costs of the electricity grid. Also, obtaining the required spacing is an increasing challenge as rotor sizes grow with the newer turbines. Next, the objectives and corresponding challenges in wind farm control will be discussed.

### 2.3.1. OBJECTIVES OF WIND FARM CONTROL

In this section, the two most common wind farm performance indicators will be discussed. In general, the goal of wind farm control is to minimize the cost of wind en-

ergy. This can be translated into a number of technical objectives, namely maximizing power production, minimizing structural degradation, and active power control (APC). APC provides grid services, such as frequency control and power reference tracking, and its objective is to improve the quality of wind energy. It will not be discussed in this chapter, though interested readers can find related information in (Aho et al., 2012; Ela et al., 2014; Fleming et al., 2016a; Göçmen et al., 2016a; van Wingerden et al., 2017; Shapiro et al., 2017a; Vali et al., 2018b; Boersma et al., 2018a) and Chapter 4. The power production and load performance indicators will be discussed in this section.

#### POWER PRODUCTION MAXIMIZATION

Wind turbines extract momentum from the flow, which results in the previously explained velocity deficit in the wake. The amount of this deficit limits the power production of downwind turbines, but can be controlled using the wind farm control variables that will be discussed in §2.5.1. In (Fletcher and Brown, 2010), the authors show that, when considering a perfectly aligned two-turbine case, the power loss of the downwind turbine scales approximately linearly with the spacing. Losses range from around 25% for radially aligned turbines spaced 16 rotor diameters apart to 80% when the aligned turbines are placed 4 rotor diameters apart. The study in (Barthelmie et al., 2009) reports a power production loss of 12%, averaged over different wind directions, in an offshore wind farm as a result of wake effects.

It is important to note that results like these are in general obtained using a specific mathematical model trying to capture the wake dynamics for specific atmospheric conditions. Outcomes can differ according to the model and method used. However, wake loss predictions have also been measured in real wind farms. Wind farm control can mitigate part of the wake losses, although given the variable nature of a wake, it is still a point of research to quantify how much wind farm control can reduce wake losses exactly.

#### LOAD MINIMIZATION

A wind turbine structure has been designed to withstand steady loads several times larger than nominal loads (Spudic et al., 2010), and so it is necessary to study fatigue loading with respect to the lifetime of a wind turbine. In (Sutherland and Herbert, 1999), it is stated that modern wind turbines are fatigue-critical machines, *i.e.*, the design of many of their components is dictated by fatigue considerations. The authors in (Soleimanzadeh et al., 2012) also conclude that mostly dynamic loads are responsible for fatigue and reduced lifetime of wind turbines in wind farms. In these papers, different loading models were used, hence it is important to first investigate which type of loading occurs. The three most important sources for the loading of an upwind horizontal-axis wind turbine are (Hansen, 2015):

- Gravitational loading.
- Inertial loading.
- Aerodynamical loading.

The first type of loading is caused by the gravitational field of the Earth and rotation of the blades. It is clear that a blade rotating downward experiences different forces than a blade rotating upward. It causes a sinusoidal loading on the blades with a frequency

corresponding to the rotor rotation of once per revolution (1P). Inertial loading occurs when the wind turbine changes the rotation speed. Certain parts on the blades experience different changes that will result in inertial loading. Another source is the centrifugal force acting on the blades. Aerodynamical loading is caused by the flow passing the wind turbine and varies in space and time. For example, a wind field contains a velocity profile with a bigger magnitude that is relatively high from the ground because of shear effects, whereas the turbulent effects introduce time-varying behaviour in a wind field. Also, according to (Hansen, 2015), the yaw (and tilt) angle of a wind turbine causes additional aerodynamical periodical forces on a wind turbine. In a wind farm, a wind field will also be perturbed by wind turbines causing changes in a wind field as highlighted at the end of §2.2. Downwind turbines in a wind farm can then experience a changing wind field over the rotor that can introduce additional aerodynamical loading. Loading can, in the end, lead to fatigue damage and breakdowns. There are different measures of fatigue loading, such as the rainflow counting, spectral, stochastic, and hysteresis operator method. This chapter does not cover these methods, but the interested reader is referred to (Berglind and Wisniewski, 2014).

The purpose of single turbine control is to mitigate the effects of gravitational, inertial, and aerodynamical loading. On a wind farm control level, it is more important to focus on the effects of the changed aerodynamical loading caused by the upwind wind turbines in the farm. Damage equivalent load (DEL) is a measure that is commonly used in literature to quantify loading, and allows for direct quantitative comparisons of different loading types on the turbine structure. DEL defines the equivalent fatigue damage caused by a load, taking into account the fatigue properties of the material.

In this section, two wind farm performance indicators were introduced. Wind farm control aims to optimize these indicators. For synthesis and evaluation of controllers, wind farm models are typically used. This will therefore be the topic of the following section.

## 2.4. CONTROL-ORIENTED WIND FARM MODELING

The advancements in wind farm control have gone hand in hand with advancements in wind farm modeling, as typically modern control algorithms rely on an internal model. These models are often simple and relatively computationally inexpensive. We refer to these types of models as low fidelity (possibly parametric) models. High fidelity simulation models are typically used to assess a controller's performance as the last step before being put to the test on an actual wind farm. These models are more accurate, but also significantly more computationally time consuming, and can therefore not be employed for real-time control. Although wind farm models are different, two main components can always be distinguished:

- Turbine model: These models predict the interaction between the flow and the turbine structure. Additionally, structural loads on the turbine given the incoming flow field may be predicted, which can include extreme loading, vibrational modes, and fatigue.
- Flow model: A model that predicts the flow properties in a wake or of the total flow field in a wind farm.



A turbine model gets a flow field from a flow model as an input, whereas the turbine loadings are inputs to a flow model that indicates the unavoidable interconnection between the two submodels. The two types are described next.

### 2.4.1. TURBINE MODEL

Wind turbine models describe the flow effect on the turbine structure, including loading and vibrations. A flow field serves as an input with which the turbine model evaluates the resulting loading. Two models traditionally used for estimating aerodynamic loading are the ADM and ALM, both introduced in §2.2. These models can predict turbine flow interactions and provide estimations of the turbine's power capture and forces exerted on the flow. A more elaborate turbine model is FAST (Jonkman and Buhl, 2005), developed by the National Renewable Energy Laboratory (NREL). It contains, *i.a.*, the ALM and takes into account, given an incoming flow field, all of the three types of loading discussed in §2.3.1. DEL values can be determined and the lifetime of a turbine can be assessed. Other turbine models exist, such as HAWC (Larsen et al., 2012), but will not be further discussed in this chapter. By using models such as these, accurate predictions can be made on the (extreme and fatigue) forces, moments, and vibrations of a turbine structure for given wind conditions. Also, these models provide accurate predictions of power capture of the turbine at given inflow conditions. It should be clear that more advanced turbine models require relatively more computation time. An overview of the components generally present in such turbine models can be found in (Moriarty and Butterfield, 2009).

### 2.4.2. FLOW MODEL

It was previously stated that the dynamical behaviour of a wake (or more general, a flow) is governed by the three-dimensional (3-D) unsteady Navier-Stokes equations. These equations are mathematically defined as a nonlinear infinite dimensional system with equality constraint. Under boundary conditions (inflow conditions) and forcing terms (the wind turbines) typically used in a wind farm model, and without making significant assumptions, no analytic solution has been found yet for these equations. Hence, in such a case, it is impossible to solve the governing equations directly. Computational fluid dynamics (CFD) is a branch of fluid mechanics that uses numerical analysis and algorithms to solve and analyze this type of problem.

Spatial discretization is a method that is applied to obtain a set of solvable equations. Because turbulence exists on many different temporal and spatial scales in a wind farm, the most accurate way to simulate turbulent flows is to directly solve the obtained set of equations on a very dense grid, capturing all eddy scales. This method is referred to as direct numerical simulation (DNS). It is computationally expensive because, after spatially discretizing, the dimensionality of the obtained set of equations is huge as a result of the fact that every cell in the wind farm has its own Navier-Stokes equations. Large-eddy simulations (LES), on the other hand, resolve the governing equations (after spatially or temporally filtering the Navier-Stokes equations) on a coarser mesh (capturing only the large-scale eddies), but can approximate the smaller-scale eddies with subgrid models. Small-scale turbulence is then calculated within each coarse cell using this subgrid model. Most wind farm flow solvers that are considered as high fidelity models employ

this method.

Less computationally expensive models are also present in literature. Most of these models consider a two-dimensional (2-D) space to reduce the model complexity and assume incompressibility of the flow, and only have a simplified turbulence model to induce wake recovery. In addition, parametric models exist that only estimate specific characteristics of a wake, such as velocity deficit and wake deflection. This chapter will continue giving a brief overview of some wind farm models that exist.

### 2.4.3. EXAMPLES

Wind farm models that use LES flow models include Simulator fOr Wind Farm Applications (SOWFA) (Churchfield et al., 2012) and UTD Wind Farm (UTDWF) (Martinez-Tossas et al., 2014), a wind farm model developed at UT Dallas, and SP-Wind (Leuven) (Meyers and Meneveau, 2010), and PARallelized LES Model (PALM) (Maronga et al., 2015). These 3-D, high fidelity flow solvers contain, in general, sophisticated wind turbine models and  $10^6$  or more states. The resulting computation time can be on the order of days or weeks using distributed computation. It should be clear that these types of models are not useful for online control, wherein measurements are fed into a controller that calculates optimal actuator settings based on an internal model in real time. However, these models can serve as analysis tools. The cost of doing simulation experiments using these solvers is significantly less than the cost of doing experiments on a real wind farm. Moreover, simulation experiments can be done in controlled atmospheric conditions, which is important for one-to-one quantitative comparisons after, *e.g.*, changing a control policy.

The authors in (Soleimanzadeh et al., 2014; Boersma et al., 2016b, 2018b) present more control-oriented and relatively less computationally expensive wind farm models based on the unsteady 2-D Navier-Stokes equations following a LES approach. It is attempted to solve the set of discretized equations governing the wake and wind turbines directly, without model reduction nor any assumptions other than incompressibility. The number of states in these models can easily be  $10^3$  or more, which makes it challenging to use them for controller design. A second challenge using this approach is the choice of a (relatively simple) turbulence model, which should be included to account for wake recovery. In (Boersma et al., 2018b), the authors include a simplified mixing-length turbulence model to create wake recovery behind a turbine, whereas in (Soleimanzadeh et al., 2014), no turbulence model is included. In these dynamic wind farm models, the turbines are modeled using the ADM. The cost of solving these wind farm models is relatively low because of the exploitation of sparsity and structure in the system's matrices.

Another approach is using simplified versions of the governing equations. For example, in the 2-D Ainslie (Ainslie, 1988) and 2-D dynamic wake meandering (DWM) model (also called the Larsen model) (Larsen et al., 2007), assumptions are made such that the Navier-Stokes equations can be approximated with a thin shear layer approximation that is less computationally expensive. Currently, NREL is developing FAST.Farm, which extends the DWM model to include more control-relevant dynamics (Jonkman et al., 2017). WakeFarm (also referred to as Farmflow), developed at Energy research Centre of the Netherlands (ECN), simulates the wind turbine wakes by solving the steady parabolized

Navier-Stokes equations in perturbation form in three dimensions (Crespo et al., 1988; Özdemir et al., 2013). When applying time averaging on the Navier-Stokes equations, the Reynolds Averaged Navier-Stokes (RANS) equations can be obtained. With this approach used in, e.g., (Annoni and Seiler, 2015), a time-averaged (mean) flow is computed and the effects of turbulence are implemented using the mixing-length hypothesis. The computational cost for using RANS equations in a wind farm model will also be computationally less expensive than for high fidelity flow solvers. A combination is presented in (Lungo et al., 2015b), in which the authors present a RANS wind farm model for which model parameters are updated online using the high fidelity flow solver UTDWE. The authors in (Bastankhah and Porté-Agel, 2016) present a, with wind tunnel experiment data validated, wind farm model based on simplified RANS equations. The simplification results in the approximate governing equations upon which an inexpensive analytical model is built. A completely different dynamic wind farm model is presented in (Rott et al., 2017) where the Navier-Stokes equations are solved using a semi-Lagrangian approach. The interested reader is referred to (McDonough, 2004; Blazek, 2001) for more background information on the Navier-Stokes equations and its varieties.

One way to circumvent the complexity of wake modeling is by using 2-D parametric models. The idea is to capture only the most dominant wake characteristics. Most of these parametric wake models estimate a steady-state situation for, *i.a.*, a given inflow direction. If the wind farm is large, this inflow direction should then hold for the whole farm, which can be an unrealistic assumption. Examples are the Frandsen model (Frandsen et al., 2006), the model presented in (Porté-Agel and Niayifar, 2016), and the Jensen Park model (Jensen, 1983; Katic et al., 1986), which predict a linearly expanding wake with a velocity deficit that only depends on the distance behind the rotor. Extending Jensen's model resulted in the parametric model called FLOW Redirection and Induction in Steady-state (FLORIS) (Gebraad et al., 2014). A dynamical version named FLOW Redirection and Induction Dynamics (FLORIDyn) of this is presented in (Gebraad and van Wingerden, 2014) and a similar model is SimWindFarm (Grunnet et al., 2010), wherein relatively simple dynamical equations are used to estimate the velocity deficit in a wake. Interestingly, recent findings have shown that these simple parametric models, such as the Jensen model and models based on the Jensen model like FLORIS, can in some cases predict wake losses accurately, if uncertainty is included in the calculation (Rostampour et al., 2013; Gaumond et al., 2014; Peña et al., 2015). Inclusion of uncertainty in wake models, and evaluating controllers based on uncertain wake models, is an active field of research.

Note that never all flow behaviour will be captured when simulating a wind farm using a model, especially when employing a 2-D model. For example, in the latter case, the inflow from above and below is not taken into account, even though it influences wake properties. In addition, the underlying assumption of infinitely tall turbines in 2-D models that are based on the unsteady Navier-Stokes equations results in flow speedup effects on the right and left downwind the turbines. Interestingly, the model presented in (Boersma et al., 2017) includes information on the third dimension in the 2-D unsteady Navier-Stokes equations, effectively reducing this undesired effect. However, for some specific cases, 2-D wind farm models have been validated with high fidelity 3-D models, which hints to the fact that the assumption could be reasonable. It is the time-

reducing property that makes 2-D models attractive for wind farm control.

In addition to the above, the authors in (Sanderse et al., 2011; Sanderse, 2009; Crespo et al., 1999; Vermeer et al., 2003; Göçmen et al., 2016b; Annoni et al., 2014) provide overviews of rotor blade models and wake models. In Table 2.1, a classification of previously described models is given, noting that in this table the term "fidelity" is mainly used to describe the amount of detail described by the model. This does not automatically imply that more detailed models are more suitable for (online) control purposes, as discussed before. In addition, it has been shown in several wind farm simulation cases that medium and low fidelity models are able to estimate wind velocity and power data from a high fidelity model. The acronym NS stands for the Navier-Stokes equations.

Table 2.1: A classification and properties of different models.

	Low fidelity		Medium fidelity	High fidelity
Model type	Kinematic models		Flow field models	Flow field models
Fundamentals	Parametric		2D NS	3D NS
Models	Jensen, FLORIS, Frandsen, ...	FLORI-Dyn,...	DWM, WFSim, Ainslie...	SOWFA, WakeFarm, UTDWF, SP-Wind,...
Flow dimension	2D		2D	3D
Dy-namic/Static	Static	Dynamic	Dynamic	
Turbine model	ADM		ADM/ALM and/or an aerodynamic package (e.g., FAST)	
Comp. effort	Order of seconds on a desktop PC		Order of minutes on a desktop PC	Order of days on a cluster of $10^2$ CPUs
Model accuracy	Low – medium		Medium – high	High – very high

### REDUCED ORDER MODELS

Performing model order reduction techniques, such as proper orthogonal decomposition and dynamic mode decomposition on high fidelity flow solver data, is another method to obtain a model. The authors in (Annoni et al., 2016b; Fortes-Plaza et al., 2018) illustrate that it is possible to apply proper orthogonal decomposition and compare the flow fields obtained with the low-order model with that of a high fidelity flow solver. Other articles that deal with proper orthogonal decomposition applied to a wind farm model are (Hamilton et al., 2015; Bastine et al., 2015). In (Hamilton et al., 2015) and (Iungo et al., 2015a), the authors illustrate that by using data from a high fidelity flow solver and dynamic mode decomposition, a low-order, two-turbine wind farm model can be obtained in which states retain a physical interpretation.

Note that model order reduction techniques rely on specific operating conditions, *i.e.*, they provide linear models for a specific operating point and are only valid within

small deviation from this point. These reduced-order linear models can be defined at, *e.g.*, specific wind speeds and directions. However, techniques in parameter-varying control exist that can help link these models together (Annoni and Seiler, 2016). Also, reduced-order models could be data-driven in a more system identification approach (see *e.g.*, (Schmid, 2010)) or model-based considering, *e.g.*, the Navier-Stokes equations. Examples of the latter are balanced proper orthogonal decomposition and the Galerkin projection (see *e.g.*, (Rowley et al., 2004)). This chapter will not discuss these different techniques.

A note for this section is that a model's accuracy and applicability are highly dependent on the atmospheric conditions of the relevant wind site. It is shown in, *e.g.*, (Abkar and Porté-Agel, 2016) that wake characteristics change a lot relatively when the atmosphere is stable or not. In addition, in unstable atmospheric conditions, often wakes are extremely hard to control, and no significant improvements can be yielded by active wind farm control. In stable conditions, wakes are less difficult to control; however, the problem is still challenging.

In this section, two main components of a wind farm model were discussed and examples of wind farm models were given. These models can be used to conduct wind farm analysis or control. The latter will be the topic of the following section.

## 2

## 2.5. WIND FARM CONTROL

It was stated earlier that wind farm control is aimed at optimizing the previously presented objectives: minimization of power losses and structural loading. More precisely, wind farm control aims to find control actions that increase the wind farm performance by taking measurements (and possibly an internal model) into account. By (partially) relying on measurements, a controller can cope with changing environments. In this section, wind farm actuators and sensors will first be discussed, followed by the discussion of two wind farm actuation methods. The categorization of different control strategies will be covered in §2.6.

### 2.5.1. ACTUATORS AND SENSORS

In wind farm control, measurements from sensors and/or possibly an internal model are used to compute control settings. These control settings are assigned to the turbine's actuators, which can be considered the degrees of freedom in the wind farm control problem. In this section, typical wind farm actuators and sensors will be discussed.

#### ACTUATORS

For a single turbine, actuators were defined as turbine yaw,  $\gamma$ , generator torque,  $\tau_g$ , and blade pitch angles,  $\theta$ . Tilting the turbine's rotor provides an additional actuator for control, though this approach has only been used in simulations until now (Fleming et al., 2014a,b; Guntur et al., 2012; Annoni et al., 2017). In a real wind farm and some wind farm models, the control variables are  $(\gamma_i, \tau_{g_i}, \theta_i)$  for  $i = 1, 2, \dots, \aleph$ , with  $\aleph$  the number of turbines in the farm. However, it is common in wind farm modeling to define the axial induction (see (2.7)) or similarly the thrust force coefficient (see (2.6)), and the yaw angles as actuators. Although this approach neglects the dynamics between the physical turbine actuators  $\tau_{g_i}, \theta_i$  and the axial induction or thrust force coefficient, it simpli-

fies the modeling and control problem. Some studies (see *e.g.*, (Knudsen and Bak, 2013; Boersma et al., 2018c)) include a first-order time filter to circumvent sudden unrealistic axial induction changes in simulations. The following wind farm actuators can be defined for models employing the ADM:

- $\gamma_i$  for  $i = 1, 2, \dots, \aleph$ ,
- $a_i$  (or  $C_{T_i}, C'_{T_i}$ ) for  $i = 1, 2, \dots, \aleph$ .

Note that by changing  $a_i$ , the thrust force, *i.e.*, the amount of energy the turbine extracts from the flow, will change. These two variables are illustrated for one turbine in Fig. 2.6.

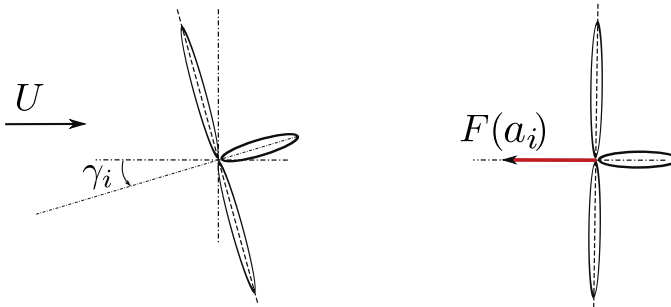


Figure 2.6: A schematic representation of wind farm actuators typically used in simulations. The thrust force,  $F(a_i)$ , is determined by the axial induction  $a_i$  of turbine  $i$ .

## SENSORS

Proper placement and choice of sensors is key to the success of wind farm control. Examples of wind turbine sensors include:

- Anemometers and wind vanes. These devices are mounted on the nacelle to locally determine the wind speed and direction at the rotor plane. However, note that when a turbine is in operation, these measurements are disturbed because of the interactions between the flow and turbine rotor, especially at small distances around the rotor plane (Pao and Johnson, 2009).
- Power sensors.
- Strain sensors, which measure structural deformations.
- Accelerometers, which measure the turbine's acceleration.
- Generator shaft-speed sensors.
- Torque sensors.
- Temperature sensors, which are used for anti- and de-icing techniques (Parent and Ilinca, 2011).

These turbine sensors are also useful for wind farm control. Examples of sensors on a wind farm level are:

- Separate meteorological measurement masts, which are located in the farm, and provide information on the flow velocity for their respective positions.
- Remote-sensing (RS) technologies, which measure the flow field at different positions upstream or downstream of turbines, without the need for repositioning the sensor. RS can use sodar, lidar, or radar technology, or satellite scatterometry.

According to (Peña et al., 2013), sodar systems use sound waves and are deemed too slow and of too low accuracy for wind farm applications, although they are capable of wind field monitoring (Anderson et al., 2005; Barthelmie et al., 2003). More recently, lidar technology has been applied, which relies on the same principle as sodar but using laser instead of sound waves (Rettenmeier et al., 2014). The authors in (Goossens, 2015) show that sodar and lidar can achieve similar accuracy in field tests on one of the Vattenfall wind farms. However, theoretically, lidar is able to achieve higher measurement accuracy because of the nature of light (Peña et al., 2013). Furthermore, both (Rettenmeier et al., 2014; Schlipf et al., 2011a) show that lidar has real potential to improve the accuracy of current wind speed measurements above the resolution of a mast. Also, a lidar device can be placed on top of a wind turbine to measure upwind or downwind. Because a lidar device is relatively expensive, it is interesting to investigate how to use it in an optimal way such that expenses can be minimized. The authors in (Mirzaei and Mann, 2016) present such a study. Interestingly, lidar technology was initially applied for single-turbine control, incorporating feed-forward control (see, e.g., (Schlipf et al., 2011a, 2013, 2014; Schlipf, 2016; Scholbrock et al., 2016; Mirzaei et al., 2013)). At this moment, radar devices are relatively expensive and large regarding dimension.

The main challenges in RS technology are data outliers because of hard targets and interference with the turbine blades, and problematic wind field reconstruction due to the cyclops dilemma. For example, a single lidar system measures the wind from only one angle of view. Thus, with a single lidar system, it is not possible to reconstruct the full 3-D wind field without making any assumptions (Schlipf et al., 2011b). An example of this can be found in (Raach et al., 2014), which shows that it is possible to estimate a 3-D wind field using lidar.

Given the actuators and sensors, the next question is which actuation methods can be used to optimize performance within the wind farm. This will be the topic of the following section.

### 2.5.2. ACTUATION METHODS FOR WAKE CONTROL

Currently, most wind farms are operated using individually optimal wind turbine control settings referred to as greedy control. As stated before, wind farm control consists of finding control inputs using measurements (and possibly an internal model) to increase the performance of a wind farm, thus minimizing the cost of wind energy. It has been an active research topic since the 1990s and relies on the assumption that the performance of a wind farm can be increased by operating turbines in the farm at configurations different from their individual optimal settings. Two general control methods exist for this purpose: axial induction control (AIC) and wake redirection control (WRC). Simulation studies such as (Horvat et al., 2012; Fleming et al., 2013), illustrated that both methods have a potential to increase the power production and can influence structural loading.

Another possible future method is to actively reconfigure the wind turbines in a wind farm with floating turbines. Wind farm layout optimization can be considered as initial work towards such a strategy. This will, however, not be discussed further in this chapter though the interested reader is referred to (Stevens, 2015; Fleming et al., 2015; King et al., 2016; Mittal et al., 2017). AIC and WRC will be topics of the remainder of this section.

### AXIAL INDUCTION CONTROL

The idea of AIC is to reduce the power production of upwind turbines by changing the axial induction so that downwind turbines can generate more. The axial induction is changed by adjusting the blade pitch angles and generator torque away from individually optimal settings. AIC is worthwhile if the reduced power production of the upwind turbines can be compensated for by the downwind turbines, and if performance of a turbine is significantly impacted by an upstream turbine through its wake, e.g., in situations with little wake recovery, dense turbine spacing, and relatively high wake-rotor overlap. Fig. 2.7 illustrates an aligned two-turbine situation in which this is not completely the case.

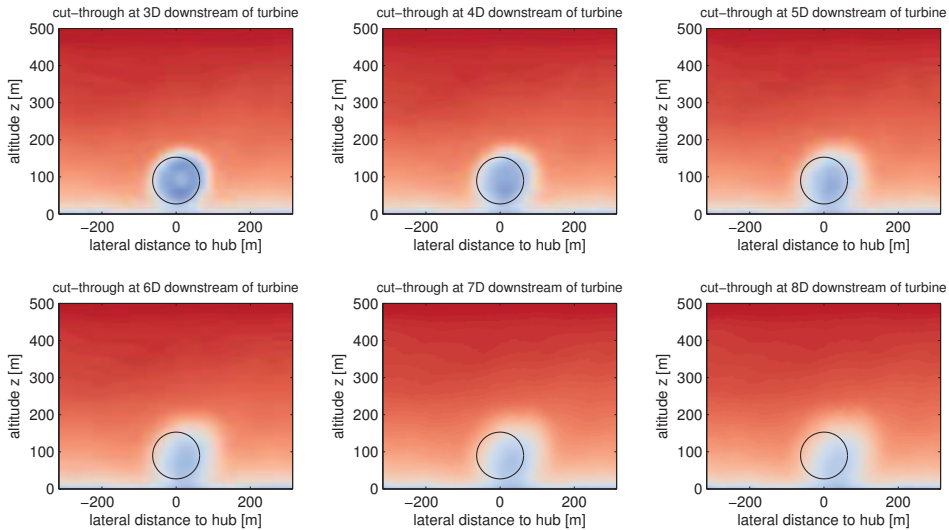


Figure 2.7: A cut-through at different distances of a wake from SOWFA data (red colored area contains higher wind velocity than the blue colored area). Figure taken from (Gebraad, 2014). It can be seen that more downwind, the wake is less overlapping the virtual downwind rotor.

Typically, in a wind farm, the distance between up and downwind turbines is around  $7D$ , meaning seven times the rotor diameter. Hence, the power that is purposely not captured by the upwind turbine will not be captured completely by the downwind turbines for the case in Fig. 2.7. It is the deviation of the upwind turbine wake which, according to the authors in (Annoni et al., 2016a), is, *i.a.*, determined by:

- Wind direction.



- Relative position of turbines.
- Wake meandering.
- Atmospheric conditions.
- Wake expansion.

Wind direction is important in two ways. First, changes in the wind direction in the farm contribute to deflection and skewing of the wake, which causes the wake to overlap less with the downwind rotor. Second, the wind direction is never exactly perpendicular to the rotor, and hence there will always be a deviation of the upwind turbine wake from the downwind rotor. Note that especially the latter could be captured using uncertainties in the model. Importance of wake expansion is emphasized because the authors in (Annoni et al., 2016a) show that, when using pitch offsets, most power passed by the upwind turbine is located in the outer ring of the wake. This complicates AIC, as it becomes more difficult for the downstream to capture this energy because of wake expansion. Note that this specific spatial distribution of the power cannot be modeled using the standard ADM, but can be captured using ALM.

Another interesting point regarding AIC is that, when the thrust force is reduced, the turbulent wake mixing and thereby wake recovery will be reduced. There are thus two counteracting effects: increased velocity in the near wake, but reduced recovery downstream (effectively decreasing velocity of the far wake). In (Annoni et al., 2016a), it is shown that including this effect in an engineering model reduces the expected power production increase from AIC.

Research of AIC is done quite extensively, showing inconclusive results on its feasibility. Most work in recent literature only takes power production into account, whereas loading is neglected. An example is the LES simulation results presented in (Goit and Meyers, 2015), wherein power production is increased using AIC by enforcing quick variations in the thrust force. These variations will increase turbulence in the wake and mixing with the upper boundary layer containing a higher flow velocity, which is beneficial for the power production. Subsequent work (Munters and Meyers, 2016, 2017) shows that by constraining thrust force variations, the power gain will again be reduced. Theoretically, it can be possible to increase power, but of course quick variation of thrust force will have implications on loads and these should be taken into account. Differentiation of the results can be made with respect to the used models: steady-state (Horvat et al., 2012; Mirzaei et al., 2015; Gebraad and Wingerden, 2015; Marden et al., 2013) or dynamical (Goit and Meyers, 2015; Schepers and van der Pijl, 2007; Vali et al., 2018a). In general, early results based on relatively simple steady-state parametric models illustrate increases in wind farm power production. The simplified models in mentioned studies might not represent the relevant wake phenomena in AIC, and thus it is questionable if the optimized control settings would work for the atmospheric conditions under consideration. High fidelity studies such as (Annoni et al., 2016a) and wind tunnel experiments such as (Campagnolo et al., 2016b) show that it is not always possible to increase power by AIC, and this can be explained by phenomena mentioned earlier. Interestingly, the authors in (Santoni et al., 2015) show that, although it seems that the power production cannot be increased, it can be interesting to employ AIC to reduce turbine loading while maintaining equivalent power production. In addition, AIC can possibly be used in APC.

It is still difficult to make conclusive statements on AIC. Perhaps a solution lies in adjusting the structural design of wind turbines in a farm according to previously described phenomena, but this is beyond the scope of this chapter. In conclusion, although the concept of AIC is promising, recent advances in wind farm modeling and wind tunnel and field tests have shown that possible production gains may be smaller and more difficult to harvest than initially expected based on static control strategies and more simplified models. Further research is needed to conclude whether it is possible to find a wind farm controller that will use AIC to reduce loads and/or increase production by dynamically adjusting pitch and torque settings to atmospheric conditions.

### WAKE REDIRECTION CONTROL

In this approach, the rotor of the upstream turbine is purposely misaligned with the incoming flow to deflect the wake downstream so that it will not at all or partially overlap a downwind turbine. The deflection can be done using:

- Tilt actuation.
- Individual pitch control (IPC).
- Yaw actuation.

Tilt actuation will not be further discussed in this chapter, but the reader is referred to (Fleming et al., 2014a,b; Guntur et al., 2012; Annoni et al., 2017). In simulation studies, IPC is shown to be effective at inducing wake redirection, though this results in a large increase in loads (Fleming et al., 2014a). Fig. 2.8 depicts a schematic illustration of yaw actuation.

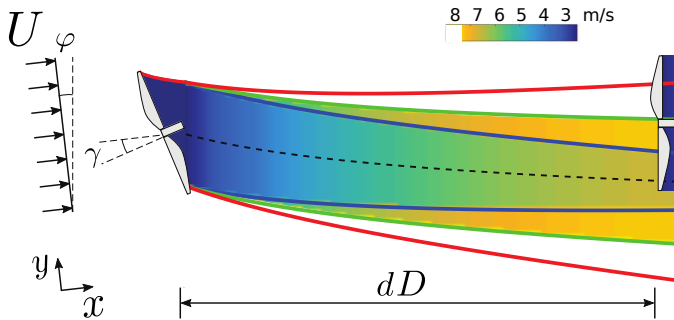


Figure 2.8: An illustration of wake redirection control with inflow angle  $\varphi$  and a second turbine placed  $d$  rotor diameters  $D$  downstream of the first turbine. Figure taken from (Zalkind and Pao, 2016).

Wake redirection promises significant improvements in simulation with power production increases on the order of 4%-7% (Knudsen et al., 2015) and an annual energy production increase on the order of 3%-4% (Gebraad et al., 2016b). In (Gebraad et al., 2015), a similar simulation is done as previously presented in Fig. 2.7, but instead of changing the axial induction of the first turbine, it is actuated with a yaw angle of 25 degrees. The authors conclude that the induced velocity increase caused by yaw actuation

is better concentrated within the rotor area of a downwind turbine placed more than  $3D$  behind the upwind turbine. Wake behavior as a result of yaw actuation is an actively researched topic (Howland et al., 2016; Vollmer et al., 2016; Bastankhah and Porté-Agel, 2016). The developments in WRC as an actuation method go hand in hand with these studies and more details regarding this method need to be investigated using simulation and field studies.

An interesting but rarely seen approach is to use both AIC and WRC (Park and Law, 2015; Munters and Meyers, 2018a). In the former, a relatively simple engineering model to capture wake dynamics is used, but its parameters are calibrated using one data set from a high fidelity flow solver. The AIC and WRC analysis is done for different wind directions. It is shown that a power increase is achieved for all studied wind directions using the proposed approach. The obtained control settings are not tested on a real wind farm nor a high fidelity flow solver. The wind farm controller presented in Munters and Meyers (2018a) provides plant wide power maximization by utilizing AIC and WRC in an adjoint based model predictive controller.

In this section, we discussed the most common wind farm actuation methods. Possible control strategies are discussed in the following section.

## 2

## 2.6. WIND FARM CONTROL STRATEGIES

In wind farm control, a supervisory controller determines a collective control policy using measurements (and possibly an internal model) so that performance (as defined in §2.3.1) is achieved. According to this control policy, the supervisory controller assigns individual control settings as defined in §2.5.1 to each turbine in the farm. Then, relatively simple internal controllers enforce the tracking of this assigned turbine setting. In this closed-loop approach, not only the atmospheric conditions but also quantities such as power production and a turbine's structural loading can be defined as measurements. Hence, control actions can adapt to the changing wind farm and atmospheric properties, which has the potential to lead to robust control solutions. Controllers are evaluated using an internal model, which can be dynamic or static. For a dynamical model, the model states can have a physical meaning, such as wind flow velocity, but it can also be a nonvariable. No system states are present with (parametric) steady-state models.

A distinction between closed-loop controllers can be made with respect to the measurements used. In closed-loop state-feedback, all the states of the model (e.g., flow velocity vectors or power signals from the turbines) are assumed to be measured and fed back to the controller. This assumption can be unrealistic, because measuring each system state can be impractical and often impossible depending on the used model. In closed-loop output feedback, only the measurements, e.g., a subset of the states, are fed back to the controller and used to evaluate control actions. State estimators (observers) can be used to estimate the system states using only measurements. For example, the state of a model can contain all flow velocities (or a linear combination of these velocities) in a wind farm, whereas the output may be only the flow velocity at hub height of the rotors. An observer (discussed in § 2.6.3) can estimate all flow velocities using only these few measured flow velocities at the rotors. Different closed-loop control strategies and their applications to wind farms will be discussed next.

### 2.6.1. OPTIMIZATION-BASED CLOSED-LOOP CONTROL

In this strategy, wind farm measurements are fed into a controller. Here, an optimization procedure evaluates, using an internal model, optimal control inputs such as yaw angles, pitch angles, and generator torque (or axial induction) values for the turbines in the farm. In addition, the model parameters can be updated using the wind farm measurements. Then, optimal control inputs are sent to the turbines in the farm and new measurements are taken.

An algorithm that can be used for finding optimal inputs is game theory (GT). Here, favorable actions lead to high rewards and unfavorable actions to low rewards. The algorithm tries to find the most rewarding action according to the used model. The reward can, *e.g.*, be the amount of power or the experienced loading. Because of the random search actions, the algorithm needs time to converge to optimal control settings. The duration depends on the complexity of the internal model, but even if the model is a simple parametric steady-state model and consequences of certain control actions can be evaluated quickly, GT needs many iterations to converge to an optimal solution. If atmospheric conditions in a wind farm change during the search for optimal control settings, the algorithm has to start again finding optimal settings for these new atmospheric conditions. Literature such as (Marden et al., 2012, 2013) illustrate AIC using GT. For specific conditions, power production improvements are shown with respect to a baseline controller. However, relatively simple engineering wake models are used, and the found optimal inputs are not applied on a wind farm nor a high fidelity model. It is therefore not clear how these results would apply to real wind farms. The authors in (Jinkyoo Park et al., 2013) illustrate AIC and WRC using GT to optimize the power production. Using their approach on an engineering model results in improvements, though again the control settings are not tested on a more realistic situation. The authors in (Gebraad et al., 2014) apply WRC using GT with FLORIS, a steady-state model introduced in §2.4. The optimal inputs are then applied to a high fidelity model SOWFA. An increase in power with respect to a baseline controller is presented.

Another approach is extremum seeking control (ESC), an optimization approach that can work for nonlinear, time-varying systems. ESC algorithms estimate the gradient of the cost function (*e.g.*, the total power of a wind farm) using measurements. In literature such as (Johnson and Fritsch, 2012; Yang et al., 2015; Menon and Baras, 2014), AIC using ESC and a greedy controller are applied on a relatively simple wind farm model and the results are compared. The found optimal values are not sent to a high fidelity model or real wind farm to validate the results. The authors show that, for different cases, power production can increase with respect to greedy control. In (Ciri et al., 2016), AIC using ESC is applied on the high fidelity model UTDWF and power production improvements with respect to a baseline controller are presented. In (Gebraad and Wingerden, 2015), AIC using gradient-based ESC (therein defined as maximum power-point tracking (MPPT)) while having information only from neighboring turbines is applied to maximize the power output of a wind farm for different atmospheric conditions. An extended Jensen Park wind farm model is used and a benchmark power production is obtained using GT. The results illustrate that, by using gradient-based ESC, the power production can be improved with respect to the benchmark results. The optimal control inputs are not tested on a wind farm nor a high fidelity model, hence results depend

on the validity of the model used. In this case study, the information for the individual wind turbines is also limited, hence a global optimum cannot be guaranteed, but the computation time is reduced. In (Campagnolo et al., 2016b), AIC and WRC using a similar gradient-based ESC algorithm as (Gebraad and Wingerden, 2015) is applied in a wind tunnel with power maximization as an objective. The case study includes three turbines with limited information for the individual turbines. Hence, again, it is observed that a global optimum cannot be guaranteed though a power production increase with respect to a baseline controller is presented. In (Park and Law, 2016), AIC and WRC using a Bayesian Ascent method is presented. Simulation and wind tunnel test results are shown for a four-turbine case. Dynamic programming is another algorithm also applied to wind farm models (see, e.g., (Tang et al., 2014; Rotea, 2014; Dar et al., 2017)). The latter aims at optimizing the power production among the yaw angles employing an extended Jensen Park model. These results will not be discussed further in this chapter.

Note that the optimization-based closed-loop control results presented so far, except for (Gebraad et al., 2014; Ciri et al., 2016, 2017, 2018; Campagnolo et al., 2016b; Park and Law, 2016), are obtained using a relatively simple model. The control actions are not tested in high fidelity simulations nor a real or scaled wind farm, and the question is if similar results will be obtained when doing so. It is also important to note that GT and ESC are, in essence, model-free approaches, hence they could be applied directly on a wind farm. However, this is due to, i.a., wake traveling delays, challenging hence these methods are applied on relatively simple (fast) models. With ESC as well as MPPT, only information from neighboring turbines is used, which decreases the necessary wake traveling time. The computation time these optimization algorithms need to converge remains a critical issue because of the time-varying conditions in a wind farm, though not enough data is available to make conclusive statements on these methods. We therefore encourage researching methods that can increase the convergence rate of these optimization algorithms.

Closed-loop control based on a dynamic model has potential to find a temporally optimal solution. An example of this is presented in (Goit and Meyers, 2015; Munters and Meyers, 2016, 2018a). Here, model-predictive control is applied using the high fidelity model SP-Wind. Knowledge of all the flow velocities and wind turbine power signals is assumed and the algorithm maximizes the total power production among axial induction factors for a given time horizon. Computationally, this is a heavy task, but the results give insights into the possibilities of AIC. The authors in (Spudic et al., 2010; Soleimanzadeh et al., 2012; Vali et al., 2016) also present AIC using MPC via a medium fidelity flow model to reduce the computational effort. Power increase (and load reduction in (Spudic et al., 2010; Soleimanzadeh et al., 2012)) with respect to a baseline controller are presented, though the controller is not tested in a high fidelity model. In all the MPC examples, full state knowledge is assumed. As stated before, this is in general not realistic.

### 2.6.2. LINEAR DYNAMIC CLOSED-LOOP CONTROL

Examples of these approaches are PID,  $\mathcal{H}_2$ , and  $\mathcal{H}_\infty$  controllers. These controllers are defined as dynamic controllers and can be designed using (mostly) linear models. Tracking behavior and disturbance rejection are time-domain specifications that can be imposed

relatively easily on closed-loop systems.

The authors in (Soleimanzadeh et al., 2013) did implement a  $\mathcal{H}_2$  controller using a medium fidelity wind farm model that neglects turbulence. The controller is tested on a nonlinear model and the authors conclude that the controller provides a distribution of power references between wind turbines so that demanded wind farm power is ensured and structural loading is minimized. The authors claim that their method can also be used to evaluate a  $\mathcal{H}_\infty$  controller. Unfortunately, the controller is not evaluated on a high fidelity model.

In (Raach et al., 2016), the authors designed a PID controller for wake tracking. The controller is applied in SimWindFarm, a model discussed in §2.4. In (Raach et al., 2017a, 2018) and (Raach et al., 2017b), a  $\mathcal{H}_\infty$  and a robust  $\mathcal{H}_\infty$  controller are designed, respectively, to steer the wake while employing a dynamic wind farm model based on the 2-D Navier-Stokes equations. Perfect knowledge of the center of the wake using lidar is assumed in both papers. The concept of steering the wake to a certain position makes the work in these papers unique. However, the question remains as to which position the wake should be steered to increase wind farm performance as discussed in §2.3.1.

### 2.6.3. OBSERVER

An observer is able to estimate the full state (and possibly update model parameters) based on specific measurements. A closed-loop control scheme using an observer is depicted in Fig. 2.9.

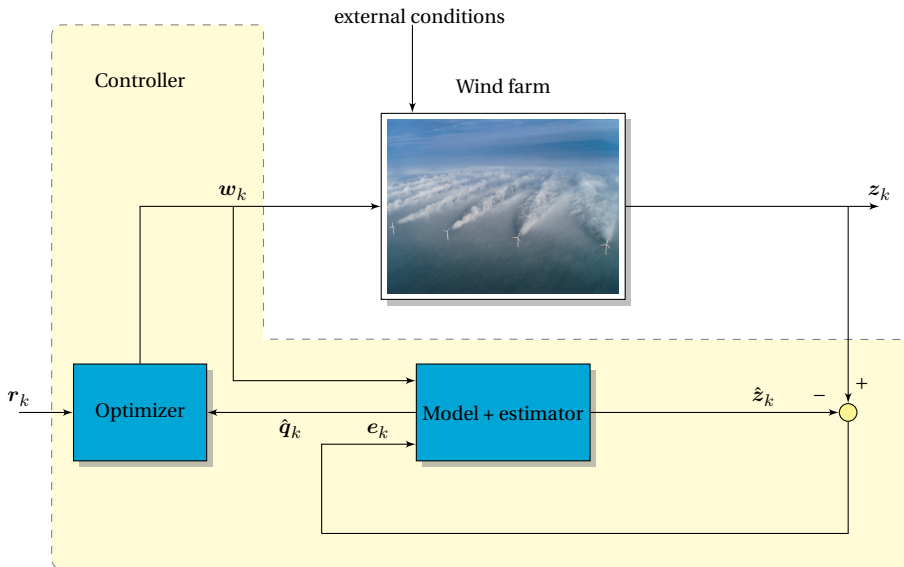


Figure 2.9: General dynamical closed-loop control framework with measurements  $z_k$  and its estimation  $\hat{z}_k$  and state estimation  $\hat{q}_k$ . The signals  $r_k$  and  $w_k$  are reference and control signals, respectively. The observer is the model and estimator combined. Note that this figure is similar as Fig. 1.5, but repeated for completeness of this chapter.

For example, given only rotor velocities, an observer can, when containing a proper model, estimate the flow velocity vectors in the complete farm assuming observability. The latter holds true if initial conditions can be inferred from measurements (see, e.g., (Aström and Murray, 2008) for more information on this topic). Observers (also called estimators) contain a dynamical model and can be used in combination with, e.g., a model-predictive controller. Observer properties include the ability to:

- Estimate states from specific measurements.
- Deal with noise in measurements and may act as a low-pass filter in estimating the system states.
- Enrich the state estimation with small-scale flow behavior in which a control-oriented model is able to estimate the large-scale flow behavior.

The latter property is especially interesting because model mismatches are most likely to occur as a result of the dynamic complexity in a wind farm. In (Doekemeijer et al., 2016, 2017, 2018), the authors implement a type of observer called the Ensemble Kalman filter using a medium fidelity flow model. Although the initial results are promising in simulation with LES data, no real closed-loop simulations have yet been performed with a controller and state observer. The authors show that the flow estimations can be improved using an observer, and flow fields can better approximate high fidelity flow data when applying an observer.

In (Shapiro et al., 2016), the authors use a relatively simple dynamic wake model in an observer while taking measurements from the LESGO flow solver. The objective of the control framework is power reference tracking, and AIC using a MPC controller is applied. The results look promising. Another example of applying an observer in a wind farm simulation can be found in (Shapiro et al., 2017b).

Open questions regarding the application of an observer in wind farms are 1) what are the optimal sensor locations and 2) how many sensors should be used such that state reconstruction is still possible and qualitatively acceptable. The first question relates to increasing the information density from each sensor. Minimizing the number of sensors is from an economical perspective important. These questions are not easy to be answered due to the time-varying behaviour a wind farm exhibits.

In §2.6.1, 2.6.2 and 2.6.3, a summary of wind farm control strategies has been given. It can be concluded that most of these strategies are optimization-based and evaluate optimal control settings by optimizing a cost function. However, most controllers in literature are not implemented in a wind farm or a high fidelity flow solver to validate their true performance. Less research has been done regarding the application of modern control strategies in wind farms, thereby making this a relatively undiscovered research area. Applying observers in wind farms shows promising results, though more research is necessary.

## 2.7. FIELD TESTS

From §2.4, it can be concluded that there are many wind farm models that predict flow fields, power capture, and/or loading in a wind farm. Parametric and medium fidelity models are sometimes validated using flow data from high fidelity wind farm models.

However, validation of these solvers using real wind farm data is still ongoing. Although it is expensive to do field testing, it is essential for further development. Field tests are not only used to validate high fidelity flow models, but also to obtain results that show that wind farm control can be worthwhile in general. For example, field tests are described in (Barthelmie et al., 2007, 2010; Wagenaar and Schepers, 2012; Hirth et al., 2014; Fleming et al., 2016b; Sakagami et al., 2015; Fleming et al., 2017a,b). A less expensive approach is doing wind tunnel experiments (see *e.g.*, (Howland et al., 2016; Bossuyt et al., 2017; Bastankhah and Porté-Agel, 2016; Campagnolo et al., 2016b,a)). Although wind tunnel tests can provide interesting data, the experiment environment remains a scaled conditioned one. This prevents a one-to-one comparison to real wind farms. In addition, it appears to be challenging to have realistic turbines and flow characteristics at a smaller scale. However, the advantage of this is that a more idealized experiment can be performed, which can better be represented in simulation, and thus provide a better comparison between a simulation and an experiment.

## 2.8. CONCLUSIONS

In this chapter, basic wind farm control-oriented modeling and control concepts have been explained and literature has been categorized and discussed. The following summarizing conclusions can be drawn:

- High fidelity models are suitable for flow and wind farm controller analysis. They are also suitable for exploring the possibilities of wind farm control. However, more validation of high fidelity models with field test data is necessary to improve their quality. Because high fidelity models are computationally complex, they are not suitable for online control.
- The use of medium fidelity dynamical models can, *e.g.*, be employed to predict the available power and/or flow fields in a wind farm. In addition, they can deal with changing atmospheric conditions over space and time. However, current medium fidelity dynamical models based on the Navier-Stokes equations are still computationally complex, hence studying simple dynamical and parametric steady-state models could be helpful. The question is if a sufficient amount of dynamics can still be captured with these models so that they can be used for wind farm control resulting in realistic results. In some specific cases, medium fidelity dynamical and low fidelity steady-state models have shown similar simulation results with respect to high fidelity models, though no conclusive statement can be made yet.
- Reduced-order models can provide information on important wake farm dynamics with limited computational complexity. However, these models are valid for one specific atmospheric condition, and applicability in real wind farms is yet to be proven. Still, the use of techniques in parameter-varying control that can help link multiple linear reduced-order models is promising.
- Dynamic feedback control is a relatively open and interesting area that still can be explored in wind farm control.
- Current literature tells us that axial induction control based on steady-state models will most likely not result in power production increases without increasing struc-



tural loading. Open questions are if axial induction control can be used to minimize the turbine's structural loading while maintaining power production and if it is applicable in active power control.

- Wake redirection control is a promising actuation method for wake control. Additional field tests are required to provide more information on the true potential of this actuation method. Furthermore, it could be beneficial to study the combination of axial-induction and wake redirection control in greater detail.
- Designed controllers should be tested on real wind farms, or at least in a high fidelity wind farm simulator for different test cases, to get a better idea of their effectiveness in realistic wind farm scenarios.
- Remote-sensing technologies, or other measurement devices used in wind farms, should be researched further. These methods are critical for control algorithms to obtain reliable measurements of wake dynamics used for determining a certain control policy and to update an internal model.
- The application of an observer including model parameter estimation in a wind farm is promising. It provides the ability to take a few measurements and thereby estimate the full state space of the model. From a practical point of view, this is much more realistic than assuming full state knowledge. An observer is based on a dynamical model and can be used in combination with, e.g., a model-predictive controller. However, relatively little research has been done regarding this topic, and its true potential is still a question.
- More field experiments should be conducted to further investigate if wind farm control can improve the performance of a real wind farm and to obtain data to validate existing models.
- For long-term research challenges in wind energy, see ([van Kuik and Peinke, 2016](#)).

# 3

## THE WINDFARMSIMULATOR MODEL

*Wind turbines are often sited together in wind farms as it is economically advantageous. Controlling the flow within wind farms to reduce the fatigue loads, maximize energy production and provide ancillary services is a challenging control problem due to the underlying time-varying nonlinear wake dynamics. In this chapter, we present a control-oriented dynamical wind farm model called the WindFarmSimulator (WFSim) that can be used in closed-loop wind farm control algorithms. The three-dimensional Navier-Stokes equations were the starting point for deriving the control-oriented dynamic wind farm model. Then, in order to reduce computational complexity, terms involving the vertical dimension were either neglected or estimated in order to partially compensate for neglecting the vertical dimension. Sparsity of and structure in the system matrices make this model relatively computational inexpensive. We showed that by taking the vertical dimension partially into account, the estimation of flow data generated with a high-fidelity wind farm model is improved relative to when the vertical dimension is completely neglected in WFSim. Moreover we showed that, for the study cases considered in this work, WFSim is potentially fast enough to be used in an online closed-loop control framework including model parameter updates. Finally we showed that the proposed wind farm model is able to estimate flow and power signals generated by two different 3D high-fidelity wind farm models.*

---

Parts of this chapter have been published in (Boersma et al., 2018b).

### 3.1. INTRODUCTION

Optimizing the control of wind turbines in a farm is challenging due to the aerodynamic interactions among turbines. These interactions come from the fact that downwind turbines are often operating in the wakes of upwind ones (Barthelmie et al., 2009). Two important wake characteristics are 1) a flow velocity deficit and 2) an increase in turbulence intensity. The former reduces power production of the farm while the latter leads to a higher dynamic loading on downstream turbines, but also induces wake recovery. Individual turbine control variables can influence the wake's flow velocity, turbulence intensity and also location. Hence, by changing the control variables of individual turbines, power production of and loading on these controlled turbines and the downwind turbines can be manipulated. Wind farm control aims to find control variables under changing atmospheric conditions such that demanded power production and/or a minimization of the loading can be guaranteed, improving the cost and quality of wind energy. State-of-the-art closed-loop dynamic wind farm controllers are based on computationally expensive wind farm models, which make these methods suitable for analysis though unsuitable for online control. The latter is important, because it allows for model adaptation to the time-varying atmospheric conditions using supervisory control and data acquisition (SCADA) measurements. As a consequence, more reliable control settings can be evaluated. A survey on wind farm control can be found in (Knudsen et al., 2015) and (Boersma et al., 2017), for example. In the latter, a clear distinction is made between model-based and model-free control algorithms. This chapter is focussed on the former in which it is assumed that controllers are based on a mathematical model of the system, which is done because there is knowledge on the system under consideration. Consequently, the controller performance depends highly on the model quality. Modelling is therefore a crucial step towards successful implementation of model-based wind farm control.

Overviews on wind farm models can be found in (Crespo et al., 1999; Vermeer et al., 2003; Sanderse, 2009; Sanderse et al., 2011; Annoni et al., 2014; Göçmen et al., 2016b; Boersma et al., 2017). The spectrum of these models ranges from low-fidelity to high-fidelity. The latter tries to capture relatively precise wind farm flow and turbine dynamics, while the former tries to capture only the dominant characteristics (dynamic or static) in a wind farm. Examples of high-fidelity wind farm models are Simulator fOr Wind Farm Applications (SOWFA) (Churchfield et al., 2012), UTD Wind Farm (UT-DWF) (Martinez-Tossas et al., 2014), SP-Wind (Meyers and Meneveau, 2010) and PARallelized LES Model (PALM) (Maronga et al., 2015). These three dimensional (3D) high-fidelity wind farm models can easily have  $10^6$  or more states. The resulting computation time can be of the order of days or weeks using distributed computation for simulation times less than the computation time. In other words, the computation time needed for large-eddy-simulation (LES) is in general more than the total time that is simulated. Clearly, these types of models are not applicable for online model-based control. Rather, these models serve as analysis or validation tools.

One way to reduce the high complexity of wake modeling is by using two-dimensional (2D) heuristic models that only capture specific wake and turbine characteristics in a wind farm in the horizontal plane at hub height. These types of models are found on the low-fidelity side of the spectrum. Most of these wake models exclusively estimate a

steady state situation for given atmospheric conditions. Examples of static models are the Frandsen model (Frandsen et al., 2006) and the Jensen/Park model (Jensen, 1983) and (Katic et al., 1986). One extension of the Jensen model resulted in the parametric model called FLOW Redirection and Induction in Steady-state (FLORIS) (Gebraad et al., 2014). Two examples of low-fidelity dynamic models are SimWindFarm (Grunnet et al., 2010) and the model used in (Shapiro et al., 2017a), in which relatively simple approximations of the flow deficit are computed using heuristic expressions.

Medium-fidelity models can be found in the middle of the spectrum as they trade off the accuracy of high-fidelity models, with the computational complexity of low-fidelity models. These are in general based on simplified versions of the Navier-Stokes equations. For example, in the 2D dynamic wake meandering (DWM) model (Larsen et al., 2007), assumptions are made regarding the thin shear layer such that the Navier-Stokes equations can be approximated using less computational effort. The authors in (Trabucchi et al., 2016) present a model, which is also based on the thin shear layer approximation, but according to the authors applicable for non-axisymmetric wind turbine wakes. WakeFarm (also referred to as FarmFlow) simulates the wind turbine wakes by solving the steady parabolized Navier-Stokes equations in three dimensions (Crespo et al., 1988) and (Özdemir et al., 2013). Other wind farm models based on the 3D Reynolds averaged Navier-Stokes (RANS) equations are (Avila et al., 2013) and (van der Laan et al., 2015). In (Annoni and Seiler, 2015), time averaging is applied to the Navier-Stokes equations, resulting in the 2D RANS equations. The number of states is then reduced by employing a state reduction technique.

Also considered as medium-fidelity models are the ones presented in (Boersma et al., 2016b) and (Soleimanzadeh et al., 2014). These wind farm models are based on the discretized 2D Navier-Stokes equations. However, these models do not contain a turbulence model that allows for wake recovery. In addition, these 2D models do not take any neglected 3D effects into account and no yaw actuation of the individual turbines is included.

In this chapter, a model will be presented that can be considered as a building block for the closed-loop control framework as illustrated in Fig. 3.1.

In current practice, signals such as power can be measured from a wind farm, but current research is also focussing on estimating wake characteristics using a lidar device (Raach et al., 2017a). These and other wind farm measurements are called SCADA data and can be used by an estimator that is able to adapt the model parameters to current atmospheric conditions and/or estimate the full state space, *e.g.* all the flow velocities at hub height in the farm. The work presented in (Doekemeijer et al., 2016) illustrates the latter and employs the dynamic wind farm model presented in this chapter. Subsequently, the estimation can then be used to compute optimal control variables using a model predictive controller. The work presented in (Vali et al., 2016) illustrates the application of such a model predictive wind farm controller using the dynamic model presented in this work.

The online closed-loop control paradigm as depicted in Fig. 3.1 demands for a control-oriented dynamic wind farm model that will be presented in this chapter.

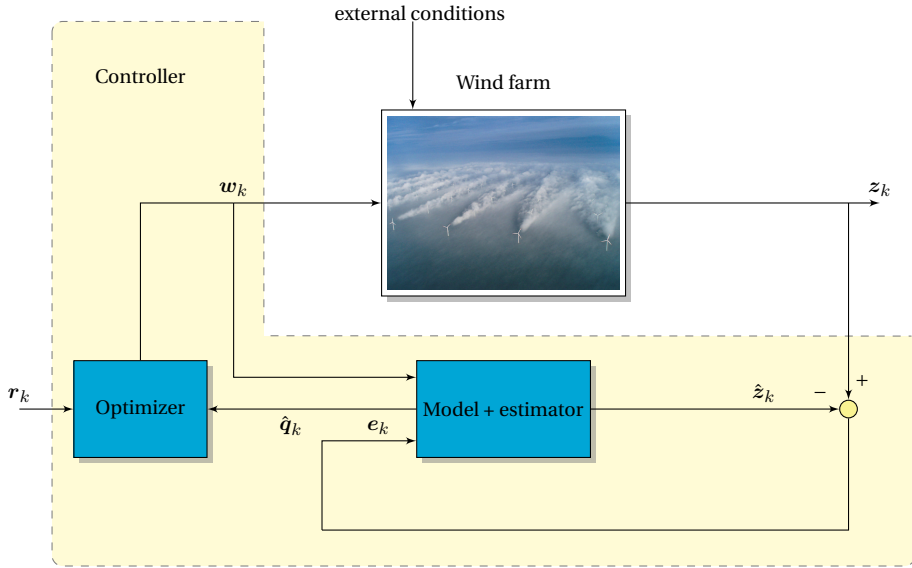


Figure 3.1: General dynamical closed-loop control framework with measurements  $z_k$  and its estimation  $\hat{z}_k$  and state estimation  $\hat{q}_k$  at time index  $k$ . The signals  $r_k$  and  $w_k$  are reference and control signals, respectively. In this chapter we present a dynamic model that is compatible with this framework. Note that this figure is similar as Fig. 1.5, but repeated for completeness of this chapter.

Characteristics of such control-oriented models are:

1. low computational cost such that online model update, state estimation and control signal evaluation is possible;
2. dynamical such that they can deal with varying atmospheric conditions within relatively small timescales.

The dynamic control-oriented wind farm model presented in this chapter, referred to as WindFarmSimulator (WFSim), is applicable in the framework discussed above and satisfies the two points above. It is based on corrected 2D Navier-Stokes equations and contains a heuristic turbulence model. The Navier-Stokes equations are modified in order to partially correct for the neglected vertical dimension. Each turbine is modelled using the actuator disk model (ADM) and features yaw and axial induction actuation. An important model feature is the exploitation of the sparse system matrices, leading to computational efficiency. WFSim will be compared to high-fidelity flow data and used in a practical control application.

The remainder of this chapter is organized as follows. In Section 3.2, the mathematical background of the medium-fidelity wind farm model will be explained including a discussion on the rotor and turbulence model. This section ends with an analysis regarding the wind farm model's computation time. In Section 3.4, WFSim will be validated in two cases using flow velocities in the longitudinal and lateral directions at hub height and turbine power signals computed with two different LES-based wind farm models.

The first case considered is a two-turbine wind farm with turbines modelled using the ADM. The second case is a nine-turbine wind farm with turbines modelled employing Fatigue, Aerodynamics, Structures and Turbulence (FAST) (Jonkman and Buhl, 2005). This chapter is concluded in Section 3.5.

### 3.2. FORMULATION OF A DYNAMICAL CONTROL-ORIENTED WIND FARM MODEL

In the current section, a simplified wind farm model is formulated that is sufficiently fast for online control but retains some of the elemental features of three-dimensional turbulent flows. In order for the model to be fast, we envisage a 2D-like model, but adapted to account for three-dimensional flow relaxation. We will dub the resulting model WFSim (WindFarmSimulator).

As starting point we use the standard incompressible three-dimensional filtered Navier-Stokes equations, as used in LES, *i.e.*

$$\begin{aligned} \frac{\partial \tilde{\mathbf{v}}}{\partial t} + (\tilde{\mathbf{v}} \cdot \nabla) \tilde{\mathbf{v}} + \nabla \cdot \boldsymbol{\tau}_M + \frac{1}{\rho} \nabla \tilde{p} - \mathbf{f} &= 0, & \text{momentum equations,} \\ \nabla \cdot \tilde{\mathbf{v}} &= 0, & \text{continuity equation.} \end{aligned} \quad (3.1)$$

The velocity field  $\tilde{\mathbf{v}} = (\tilde{v}_1, \tilde{v}_2, \tilde{v}_3)^T$  and pressure field  $\tilde{p}$  represent filtered variables,  $\nabla = (\partial/\partial x, \partial/\partial y, \partial/\partial z)^T$ , the air density  $\rho$ , which is assumed to be constant, and  $\boldsymbol{\tau}_M$  represents the subgrid-scale model, which will be defined in §3.2.1. As is common in LES of high-Reynolds number atmospheric simulations with grid resolutions in the meter range, direct effects of viscous stresses on the filtered fields are negligible, so that these terms are left out. Finally, the term  $\mathbf{f}$  represents the effect of turbines on the flow, as further detailed in §3.2.2.

Although LES filters are usually implicitly tied to the LES grid and filter length scale in the subgrid-scale model, we presume here that  $\tilde{\mathbf{v}}$  corresponds to a top-hat filtered velocity field, with filter width  $D$ , where  $D$  is the turbine diameter. Thus,

$$\tilde{\mathbf{v}}(x, y, z) = \frac{1}{D^3} \int_{z-D/2}^{z+D/2} \int_{y-D/2}^{y+D/2} \int_{x-D/2}^{x+D/2} \mathbf{v}(x', y', z') \, dx' dy' dz'. \quad (3.2)$$

From a wind farm simulation perspective, we are mainly interested in the flow velocity field at hub height  $z_h$ , *i.e.*  $\tilde{\mathbf{v}}(x, y, z_h)$ . Moreover, to evaluate turbine forces and power, it suffices to know the velocity at turbine locations  $\mathbf{t}_n = (x_n, y_n)^T$  (with  $n = 1 \dots \aleph$  and  $\aleph$  the number of turbines in the farm), since  $\tilde{\mathbf{v}}(x_n, y_n, z_h)$  is a reasonable representation of the turbine disk-averaged velocity.

Therefore, we focus on formulating a 2D-like set of equations for  $\tilde{\mathbf{v}}(x, y, z_h)$ . To this end we define

$$\mathbf{u} = (\tilde{v}_1(x, y, z_h) \quad \tilde{v}_2(x, y, z_h))^T, \quad (3.3)$$

$$= (u \quad v)^T, \quad (3.4)$$

and  $w = \tilde{v}_3(x, y, z_h)$  and  $p = \tilde{p}(x, y, z_h)/\rho$ . Moreover, we assume that  $w \approx 0$ , so that the LES equations given in (3.1) can be reformulated in terms of  $\mathbf{u}$  as

$$\frac{\partial \mathbf{u}}{\partial t} + (\mathbf{u} \cdot \nabla_H) \mathbf{u} + \nabla_H \cdot \boldsymbol{\tau}_H + \nabla_H p - \mathbf{f} = -\frac{\partial(uw + \tau_{M,13})}{\partial z} \mathbf{e}_1 - \frac{\partial(vw + \tau_{M,23})}{\partial z} \mathbf{e}_2, \quad (3.5)$$

$$\nabla_H \cdot \mathbf{u} = -\frac{\partial w}{\partial z}, \quad (3.6)$$

with  $\nabla_H = (\partial/\partial x, \partial/\partial y)^T$ ,  $\boldsymbol{\tau}_H$  a 2D tensor containing the horizontal components of the subgrid stresses  $\boldsymbol{\tau}_M$ , and  $\mathbf{e}_1$  and  $\mathbf{e}_2$  the unit vectors in the  $x$  and  $y$  directions, respectively.

Finally, we further simplify the equations above using two additional assumptions. First of all, we presume  $\partial w/\partial z \approx \partial v/\partial y$ . When centred at the turbine axis, this is one of the conditions required for axial symmetry, though axial symmetry also requires further conditions on  $\partial v/\partial z$  and  $\partial w/\partial y$ , which are not imposed. In general,  $\partial w/\partial z \approx \partial v/\partial y$  implies equal divergence/convergence of streamlines in  $y$  and  $z$  directions. Although this is a very simple condition, we presume it to be good enough to resolve the lack of relaxation of purely 2D models. If necessary, a more general form ( $w \approx 0$  and  $\partial w/\partial z \approx c \cdot \partial v/\partial y$ ), with  $c$  a tuning parameter (*e.g.*, obtained through state estimation) could be considered, but results in the current work indicate that this may not be necessary. Secondly, we simply neglect the right-hand side of (3.5). Though this is a rather crude assumption, the rationale is that the modelling term  $\boldsymbol{\tau}_H$  will suffice in the context of a control model, where model coefficients can be updated online based on feedback (see also the discussion in §3.2.1). Hence our final 2D-like model corresponds to

$$\frac{\partial \mathbf{u}}{\partial t} + (\mathbf{u} \cdot \nabla_H) \mathbf{u} + \nabla_H \cdot \boldsymbol{\tau}_H + \nabla_H p - \mathbf{f} = 0, \quad (3.7)$$

$$\nabla_H \cdot \mathbf{u} = -\frac{\partial v}{\partial y}. \quad (3.8)$$

We emphasize here that the model above is not a classical 2D model due to the difference in formulation of the continuity equation. In contrast to a standard 2D model, this allows for flow relaxation in the third direction when, *e.g.*, encountering slow down by a wind turbine. This can be seen in Fig. 3.2, in which simulation results obtained with the model above, a standard 2D dynamic wind farm model and LES are shown. The simulation case itself will be discussed in more detailed in §3.4.2. Here we depict the normalised flow deficit in the wake at 5D downstream of the turbine along the cross-stream axis. The figure illustrates that the standard 2D Navier-Stokes equations lead to a significant speed up at the wake edges. This is a result from conservation of mass in two dimensions and the flow deceleration in front of the turbine, pushing part of the air around the turbine. In the WFSim model, this speed up is smaller, as mass can also flow around the turbine in the third dimension. In Fig. 3.2 it can be seen that LES data are better estimated when imposing flow relaxation in the third dimension. Finally, note that partially modelling the missing vertical dimension as proposed above is novel with respect to the work presented in (Boersma et al., 2016a).

This section is further organized as follows. First, in §3.2.1, the subgrid-scale model will be introduced. Then, in §3.2.2, the turbine model will be explained. The discretization of the equations is presented in §3.2.3, and boundary and initial conditions are discussed in §3.2.4.

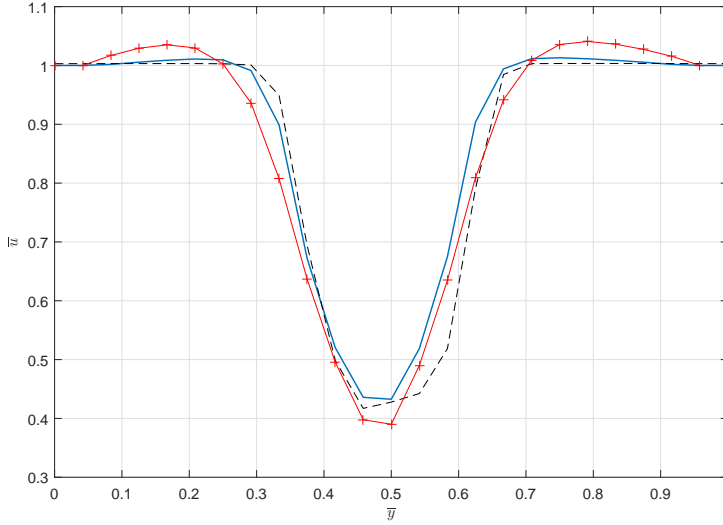


Figure 3.2: Results of two-turbine simulations. Normalised time-averaged wake deficit ( $\bar{w}$ ) at hub height  $5D$  downwind from the downwind turbine using standard 2D Navier-Stokes equations (red crossed), our model with the adapted continuity equation (blue), and LES data (black dashed) as a function of the normalized y-axis ( $\bar{y}$ ).

### 3.2.1. TURBULENCE MODEL

In the literature, many subgrid-scale models are documented, and to date, model accuracy remains a challenge in LES research (see *e.g.*, (Sagaut, 2006)). However, in the current work, an important factor in the selection of a model is simplicity and computational efficiency, rather than accuracy. In fact, in contrast to conventional modelling, in a control-oriented model completeness of the turbulence model is not a major issue since unknown model coefficients can be calibrated online using measurements and feedback (Shapiro et al., 2017b), thus also controlling the overall error. Therefore, in this work we fall back to one of the simplest and first known turbulence models, Prandtl's mixing length model.

We formulate the stress tensor  $\tau_H$  using an eddy-viscosity assumption, *i.e.*

$$\tau_H = -\nu_t \mathbf{S}, \quad (3.9)$$

with  $\mathbf{S} = \frac{1}{2}(\nabla_H \mathbf{u} + (\nabla_H \mathbf{u})^T)$  the 2D rate-of-strain tensor, and  $\nu_t$  the eddy viscosity. The latter is further modelled as in (Prandtl, 1925):

$$\nu_t = l_u(x, y)^2 \left| \frac{\partial u}{\partial y} \right|, \quad (3.10)$$

where  $l_u(x, y)$  is the mixing length. It could be interesting to define the mixing length for each position in the wind farm separately, but this will lead to too many tuning variables. Moreover, in (Jungo et al., 2015b), the authors illustrate that in a turbine's near wake



the mixing length is roughly invariant for different downstream locations, but in the far wake, the mixing length increases linearly with downstream distance. We use this to formulate a simple heuristic parametrization for the mixing length model so that the number of decision variables will be reduced drastically. From now on we assume that the wind is coming from the east, but can have a direction defined by  $\varphi$ . Then, the wind farm will be divided in segments as illustrated in Fig. 3.3.

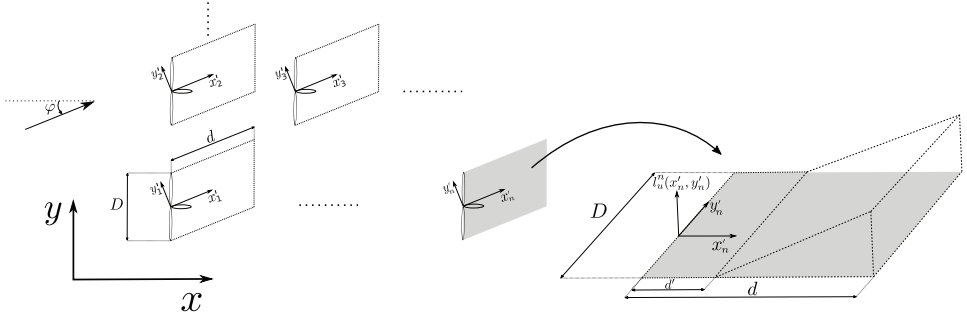


Figure 3.3: Schematic illustration of the mixing length.

Each segments has its own  $(x'_n, y'_n)$  coordinate system located in the global  $(x, y)$  coordinate system. Now we propose the following mixing length parametrization:

$$l_u(x, y) = \begin{cases} G(x'_n, y'_n) * l_u^n(x'_n, y'_n), & \text{if } x \in \mathcal{X} \text{ and } y \in \mathcal{Y}. \\ 0, & \text{otherwise,} \end{cases} \quad (3.11)$$

with  $G(x, y)$  a (smoothing) pillbox filter with radius 3,  $*$  the 2D spatial convolution operator,  $\mathcal{X} = \{x : x'_n \leq x \leq x'_n + \cos(\varphi)d\}$ ,  $\mathcal{Y} = \{y : y'_n - \frac{D}{2} + \sin(\varphi)x'_n \leq y \leq y'_n + \frac{D}{2} + \sin(\varphi)x'_n\}$  and  $\varphi$  defined as the mean wind direction (see Fig. 3.3), which we bound by  $|\varphi| \leq 45^\circ$ . In addition we constraint  $d$  by  $\cos(\varphi)d \leq |x_q - x_n|$ , with  $x_n$  a turbine x-coordinate and  $x_q$  its downwind turbines x-coordinate. We can see  $l_u^n(x'_n, y'_n)$  as the local mixing length that belongs to turbine  $n$  and denote it as:

$$l_u^n(x'_n, y'_n) = \begin{cases} (x'_n - d')l_s, & \text{if } x'_n \in \mathcal{X}'_n \text{ and } y'_n \in \mathcal{Y}'_n. \\ 0, & \text{otherwise.} \end{cases} \quad (3.12)$$

with  $\mathcal{X}'_n = \{x'_n : d' \leq x'_n \leq d\}$  and  $\mathcal{Y}'_n = \{y'_n : |y'_n| \leq D\}$  and tuning parameter  $l_s$  that defines the slope of the (linearly increasing) local mixing length parameter. In fact, this parameter could be related to turbulence intensity, *i.e.*, the amount of wake recovery. In this work we will not investigate this relation further. With the formulation above, the number of tuning variables that belong to the turbulence model ( $l_s, d, d'$ ) is reduced to 3. Additionally, we assume that  $l_s, d$  and  $d'$  are equal for each turbine in the farm, which reduces the number of tuning variables that belong to the turbulence model to three, a quantity that could be dealt with by an online estimator. However, in order to have only three tuning variables, the included turbulence model is defined as a simplified mixing length model found heuristically using and adapting information from (Jungo et al., 2015b).

### 3.2.2. TURBINE MODEL

Turbines are modelled using a classical non-rotating actuator disk model (ADM). In this method, each wind turbine is represented by a uniformly distributed force acting on the grid points where the rotor disk is located. Figure 3.4 depicts a schematic top-view representation of a turbine with yaw angle  $\gamma$ .

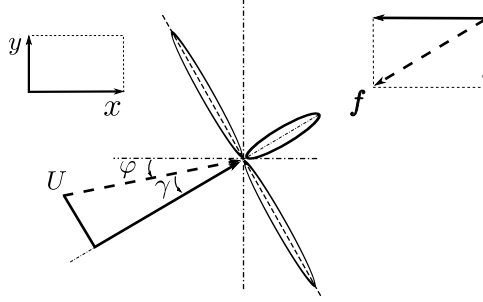


Figure 3.4: Schematic representation of a turbine with yaw angle  $\gamma_n$  and flow velocity  $U = ([u(x_n, y_n)]^2 + [v(x_n, y_n)]^2)^{1/2}$  at the rotor. Figure adapted from (Jiménez et al., 2010).

Using such an approach, the force exerted by the turbines can be expressed as

$$\mathbf{f} = \sum_{n=1}^N \mathbf{f}_n, \quad \text{with}$$

$$\mathbf{f}_n = \frac{c_f}{2} C'_{T_n} [U_n \cos(\gamma_n)]^2 \begin{pmatrix} \cos(\gamma_n + \varphi) \\ \sin(\gamma_n + \varphi) \end{pmatrix} \mathbb{H} \left[ \frac{D}{2} - \|\mathbf{s} - \mathbf{t}_n\|_2 \right] \delta[(\mathbf{s} - \mathbf{t}_n) \cdot \mathbf{e}_{\perp, n}], \quad (3.13)$$

with  $\mathbf{s} = (x, y)^T$ ,  $\mathbb{H}[\cdot]$  the Heaviside function and  $\delta[\cdot]$  the Dirac delta function,  $\mathbf{e}_{\perp, n}$  the unit vector perpendicular to the  $n^{\text{th}}$  rotor disk with position  $\mathbf{t}_n$ . Furthermore, we have  $C'_{T_n}$  the disk-based thrust coefficient following (Meyers and Meneveau, 2010), which can be expressed in terms of the classical thrust coefficient  $C_{T_n}$  using the following relation:  $C'_{T_n} = C_{T_n} / (1 - a_n)^2$ , with  $a_n$  the axial induction factor of the  $n^{\text{th}}$  turbine. Interestingly, the coefficient  $C'_{T_n}$  can be directly related to the turbine set point in terms of blade pitch angle and rotational speed (see, e.g. Appendix A in (Goit and Meyers, 2015)). In the WFSim model,  $C'_{T_n}$  and yaw angle  $\gamma_n$  are considered as the control variables and can thus be used to regulate the wakes and hence wind farm performance. Furthermore, the scalar  $c_f$  in (3.13) can be regarded as a tuning variable and will in this work be set equal for all turbines in the farm.

### POWER

From the resolved flow velocity components, the power generated by the farm is computed as

$$P = \sum_{n=1}^N \frac{1}{2} \rho A C'_{P_n} [U_n \cos(\gamma_n)]^3. \quad (3.14)$$

It is stated in (Goit and Meyers, 2015) (Appendix A) that when there is no drag and swirl is added to the wake,  $C'_{T_n} = C'_{P_n}$ . Since this is an idealized situation, a loss factor will

be introduced such that  $C'_{P_n} = c_p C'_{T_n}$ . The scalar  $c_p$  can be seen as a tuning variable and will be set equal for all turbines in the farm. In the power expression above, we have the factor  $\cos(\gamma_n)^3$  with exponent 3. In literature such as (Gebraad and van Wingerden, 2014) and (Medici and Alfredsson, 2006) (page 37), numerical values for the exponent were given according to LES and wind tunnel data, respectively. However, to date, the exact value for it is still under research and since this is outside the scope of this study, the value of the exponent will be 3.

This concludes the formulation of the WFSim model. In order to resolve for flow velocity components and wind farm power, the governing equations given in (3.7) and (3.8) need to be discretized, a topic that will be discussed in the following section.

### 3.2.3. DISCRETIZATION

The set of equations are spatially discretized over a staggered grid following (Versteeg and Malalasekera, 2007). This is carried out by employing the finite volume method and the hybrid differencing scheme. Temporal discretization is performed using the implicit method that is unconditionally stable (Versteeg and Malalasekera, 2007). This comes down to deriving the integrals:

$$\begin{aligned} \int_{\Delta t} \int_{\Delta V} \left[ \frac{\partial \mathbf{u}}{\partial t} + (\mathbf{u} \cdot \nabla_H) \mathbf{u} + \nabla_H \cdot \boldsymbol{\tau}_H + \nabla_H p - \mathbf{f} \right] dV dt = 0, \\ \int_{\Delta t} \int_{\Delta V} \left[ \nabla_H \cdot \mathbf{u} + \frac{\partial v}{\partial y} \right] dV dt = 0, \end{aligned} \quad (3.15)$$

with  $\Delta V$  the volume of one cell (see Fig. 3.5) and  $\Delta t$  the sample period. One obtains, for each cell, the following fully discretized Navier-Stokes equations (for detailed derivation we refer to Appendix 3.A):

– x-momentum equation for the  $(i, J)^{\text{th}}$  cell (black in Fig. 3.5):

$$\begin{aligned} a_{i,J}^{px} u_{i,J} = & \left( a_{i,J}^{nx} \quad a_{i,J}^{sx} \quad a_{i,J}^{wx} \quad a_{i,J}^{ex} \right) (u_{i,J+1} \quad u_{i,J-1} \quad u_{i-1,J} \quad u_{i+1,J})^T \\ & \dots + \left( a_{i,J}^{nwx} \quad a_{i,J}^{swx} \quad a_{i,J}^{nex} \quad a_{i,J}^{sex} \right) (v_{I-1,j+1} \quad v_{I-1,j} \quad v_{I,j+1} \quad v_{I,j})^T \\ & \dots - \delta y_{j,j+1} (p_{I,J} - p_{I-1,J}) + f_{i,J}^x \end{aligned} \quad (3.16)$$

– y-momentum equation for the  $(I, j)^{\text{th}}$  cell (yellow in Fig. 3.5):

$$\begin{aligned} a_{I,j}^{py} v_{I,j} = & \left( a_{I,j}^{ny} \quad a_{I,j}^{sy} \quad a_{I,j}^{wy} \quad a_{I,j}^{ey} \right) (v_{I,j+1} \quad v_{I,j-1} \quad v_{I-1,j} \quad v_{I+1,j})^T \\ & \dots + \left( a_{i,J}^{nwy} \quad a_{i,J}^{swy} \quad a_{i,J}^{ney} \quad a_{i,J}^{sey} \right) (u_{i,J} \quad u_{i,J-1} \quad u_{i+1,J} \quad u_{i+1,J-1})^T \\ & \dots - \delta x_{i,i+1} (p_{I,J} - p_{I,J-1}) + f_{I,j}^y \end{aligned} \quad (3.17)$$

– continuity equation for the  $(I, J)^{\text{th}}$  cell (pink in Fig. 3.5):

$$0 = \delta y_{j,j+1} (u_{i+1,J} - u_{i,J}) + 2\delta x_{i,i+1} (v_{I,j+1} - v_{I,j}), \quad (3.18)$$

The states  $u_{\bullet,\bullet}, v_{\bullet,\bullet}, p_{\bullet,\bullet}$  are defined for the time  $k+1$  while the coefficients  $a_{\bullet,\bullet}$  and the forcing terms  $f_{\bullet,\bullet}$  depend on the state at time  $k$ . Detailed definitions of these coefficients

are given in Appendix 3.A, Table 3.4. Note the appearance of the previously explained factor 2 (see (3.8)) in (3.18).

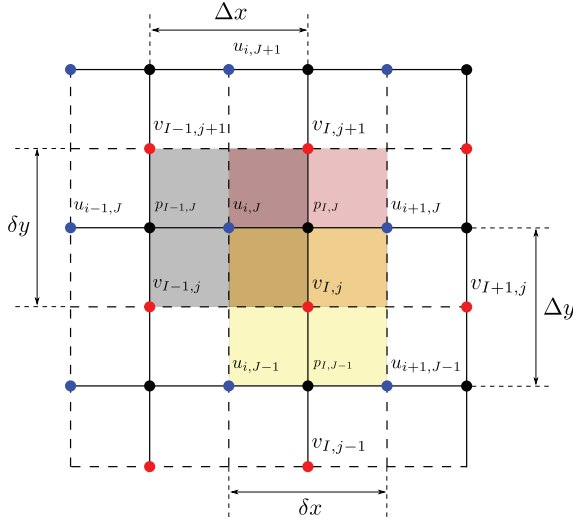


Figure 3.5: One cell for the x-momentum equation (grey with in its centre  $u_{i,j}$ ), one for the y-momentum equation (yellow with in its centre  $v_{I,j}$ ) and one for the continuity equation (pink with in its centre  $p_{I,j}$ ). All three cells have equal dimensions and overlap.

Next, the state vectors  $\mathbf{u}_k$ ,  $\mathbf{v}_k$ , and  $\mathbf{p}_k$  and control variable vectors  $\boldsymbol{\nu}_k$  and  $\boldsymbol{\gamma}_k$  at time step  $k$  will be defined:

$$\mathbf{u}_k = \begin{pmatrix} u_{3,2} \\ \vdots \\ u_{3,N_y-1} \\ u_{4,2} \\ \vdots \\ u_{4,N_y-1} \\ \vdots \\ u_{N_x-1,2} \\ \vdots \\ u_{N_x-1,N_y-1} \end{pmatrix}, \quad \mathbf{v}_k = \begin{pmatrix} v_{2,3} \\ \vdots \\ v_{2,N_y-1} \\ v_{3,3} \\ \vdots \\ v_{3,N_y-1} \\ \vdots \\ v_{N_x-1,3} \\ \vdots \\ v_{N_x-1,N_y-1} \end{pmatrix}, \quad \mathbf{p}_k = \begin{pmatrix} p_{2,2} \\ \vdots \\ p_{2,N_y-1} \\ p_{3,2} \\ \vdots \\ p_{3,N_y-1} \\ \vdots \\ p_{N_x-1,3} \\ \vdots \\ p_{N_x-1,N_y-2} \end{pmatrix}, \quad (3.19)$$

$$\boldsymbol{\nu}_k = \left( C'_{T_1} \quad C'_{T_2} \quad \dots \quad C'_{T_{\aleph}} \right)^T, \quad \boldsymbol{\gamma}_k = (\gamma_1 \quad \gamma_2 \quad \dots \quad \gamma_{\aleph})^T, \quad (3.20)$$

with  $N_x$  and  $N_y$  the number of cells in the x and y directions, respectively, and  $\aleph$  the number of turbines in the wind farm. Each component in  $\mathbf{u}_k$ ,  $\mathbf{v}_k$  and  $\mathbf{p}_k$  represents a flow velocity and pressure at a point in the field defined by the subscript. For clarity reasons, an example of a staggered grid is depicted in Fig. 3.6.

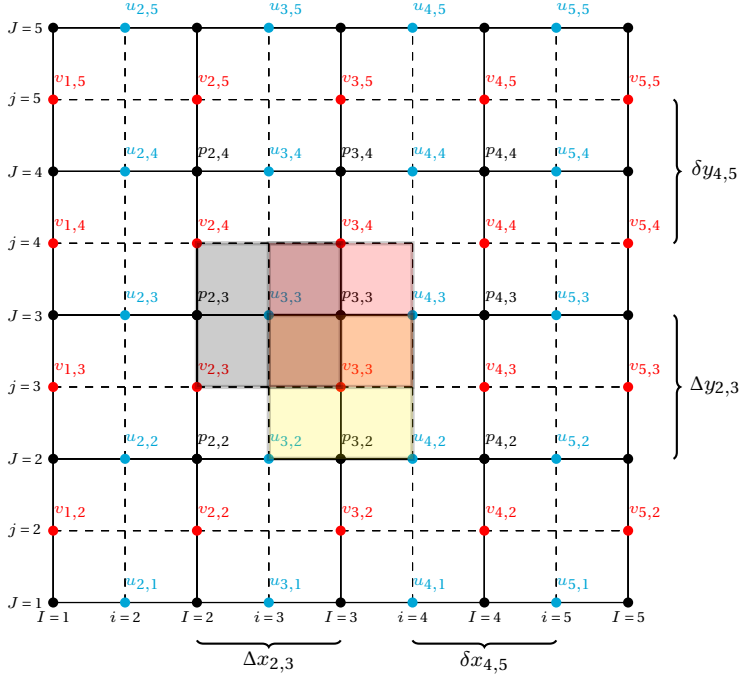


Figure 3.6: Example of a staggered grid with cells each having volume  $\Delta V$ . In the WFSim model, the grid is quadrilateral.

### 3.2.4. BOUNDARY AND INITIAL CONDITIONS

All the components that are not contained in the vector,  $\mathbf{u}_k, \mathbf{v}_k$  and  $\mathbf{p}_k$ , but do appear in the staggered grid need to be defined. For the flow velocity components, first-order conditions on the west side of the grid are prescribed assuming the wind is coming from the east. These Dirichlet inflow boundary conditions are related to the ambient inflow defined as  $u_b$  and  $v_b$  and can vary over time. Zero stress (also referred to as Neumann) boundary conditions are prescribed on the other boundaries. Therefore, for the flow velocity components on the boundaries we define:

$$\begin{aligned}
 u_{2,J} &= u_b & \text{for } J = 1, 2, \dots, N_y, & & v_{1,j} &= v_b & \text{for } j = 2, 3, \dots, N_y, \\
 u_{i,N_y} &= u_{i,N_y-1} & \text{for } i = 3, 4, \dots, N_x, & & v_{I,N_y} &= v_{I,N_y-1} & \text{for } I = 2, 3, \dots, N_x, \\
 u_{i,1} &= u_{i,2} & \text{for } i = 3, 4, \dots, N_x, & & v_{I,2} &= v_{I,3} & \text{for } I = 2, 3, \dots, N_x, \\
 u_{N_x,J} &= u_{N_x-1,J} & \text{for } J = 2, 3, \dots, N_y-1, & & v_{N_x,j} &= v_{N_x-1,j} & \text{for } j = 3, 4, \dots, N_y-1.
 \end{aligned}$$

For the initial conditions, we define all longitudinal and lateral flow velocity components in the field as  $u_b$  and  $v_b$ , respectively, which are the boundary velocity values. The initial pressure field is set to zero. Note that by defining the boundary conditions as given above, the assumption is that the wind is coming from the east in Fig. 3.6, which coincides with the definition of the mixing length (see §3.2.1). Finally, the equations given

in (3.7) and (3.8) can be transformed to the difference algebraic equation <sup>1</sup>:

$$\underbrace{\begin{pmatrix} \mathbf{A}_x(\mathbf{u}_k, \mathbf{v}_k) & \mathbf{A}_{xy}(\mathbf{u}_k) & \mathbf{B}_1 \\ \mathbf{A}_{yx}(\mathbf{u}_k) & \mathbf{A}_y(\mathbf{u}_k, \mathbf{v}_k) & \mathbf{B}_2 \\ \mathbf{B}_1^T & 2\mathbf{B}_2^T & 0 \end{pmatrix}}_{\mathbf{E}(\mathbf{q}_k)} \underbrace{\begin{pmatrix} \mathbf{u}_{k+1} \\ \mathbf{v}_{k+1} \\ \mathbf{p}_{k+1} \end{pmatrix}}_{\mathbf{q}_{k+1}} = \underbrace{\begin{pmatrix} \mathbf{A}_{11} & 0 & 0 \\ 0 & \mathbf{A}_{22} & 0 \\ 0 & 0 & 0 \end{pmatrix}}_{\mathbf{A}} \underbrace{\begin{pmatrix} \mathbf{u}_k \\ \mathbf{v}_k \\ \mathbf{p}_k \end{pmatrix}}_{\mathbf{q}_k} + \dots \\ \dots + \underbrace{\begin{pmatrix} \mathbf{b}_1(\mathbf{u}_k, \mathbf{v}_k, \boldsymbol{\nu}_k, \boldsymbol{\gamma}_k) \\ \mathbf{b}_2(\mathbf{u}_k, \mathbf{v}_k, \boldsymbol{\nu}_k, \boldsymbol{\gamma}_k) \\ \mathbf{b}_3 \end{pmatrix}}_{\mathbf{b}(\mathbf{q}_k, \mathbf{w}_k)}, \quad (3.21)$$

with  $n_q = n_u + n_v + n_p$  and  $\mathbf{u}_k \in \mathbb{R}^{n_u}$ ,  $\mathbf{v}_k \in \mathbb{R}^{n_v}$ ,  $\mathbf{p}_k \in \mathbb{R}^{n_p}$  containing all flow velocities in the longitudinal and lateral direction and the pressure vector at time  $k$  and control variable  $\mathbf{w}_k^T = (\boldsymbol{\nu}_k \quad \boldsymbol{\gamma}_k)^T \in \mathbb{R}^{2N}$ . The non-singular square descriptor matrix  $\mathbf{E}(\mathbf{q}_k)$  contains the coefficients  $a_{\bullet, \bullet}^*$ , appearing in (3.16) and (3.17), that depend on the state at time  $k$ . The square constant matrix  $\mathbf{A}$  solely depends on grid spacing and sample period  $\Delta t$ . Note that the state vector contains three states for every cell hence an increase in grid resolution results in an increase in matrix dimensions. However, the system matrices that occur in (3.21) are sparse and efficient numerical solvers are available for these types of problems. This will be demonstrated in § 3.3. The vector  $\mathbf{b}(\mathbf{q}_k, \mathbf{w}_k)$  contains the forcing terms (turbines) and boundary conditions.

By defining  $N_x, N_y, \Delta x_{I, I+1}, \Delta y_{J, J+1}$ , and the turbine positions, a wind farm topology is determined. Next, ambient flow conditions  $u_b$  and  $v_b$ , tuning parameters  $c_f, c_p, d, d', l_s$  and the control variable  $\mathbf{w}_k$  need to be specified. The system given in (3.21) is then fully defined and can be solved.

### 3.3. COMPUTATION TIME

When discretizing partial differential equations, a trade-off has to be made between the computation time and grid resolution. Typically, a higher resolution results in more precise computation of the variables but also increasing computation time. In WFSim, computational cost is reduced by exploiting sparsity and by applying the reverse Cuthill-McKee algorithm (Cuthill and McKee, 1969).<sup>2</sup> The latter is applicable due to the fact that the matrix structure is fixed. The interested reader is referred to (Doekemeijer et al., 2016) for more information on the Cuthill-McKee algorithm in WFSim.

In this section, the mean computation time needed for one time step  $\Delta t^{\text{CPU}}$  will be analysed. The presented results are obtained on a regular notebook with an Intel Core i7-4600U 2.7 GHz processor employing one core and MATLAB. Since the objective is to do online control, *i.e.*, it is desired to reduce computational complexity, this section introduces a second WFSim representation. The first representation was given in (3.21)

<sup>1</sup>This type of system can also be referred to as a quasi-linear parameter-varying model or descriptor model.

<sup>2</sup>The sparse toolbox and reverse Cuthill-McKee algorithm are both utilised in MATLAB.

while the second is defined as:

$$\underbrace{\begin{pmatrix} \mathbf{A}_x(\mathbf{u}_k, \mathbf{v}_k) & 0 & \mathbf{B}_1 \\ 0 & \mathbf{A}_y(\mathbf{u}_k, \mathbf{v}_k) & \mathbf{B}_2 \\ \mathbf{B}_1^T & 2\mathbf{B}_2^T & 0 \end{pmatrix}}_{\mathbf{E}(\mathbf{q}_k)} \underbrace{\begin{pmatrix} \mathbf{u}_{k+1} \\ \mathbf{v}_{k+1} \\ \mathbf{p}_{k+1} \end{pmatrix}}_{\mathbf{q}_{k+1}} = \underbrace{\begin{pmatrix} \mathbf{A}_{11} & 0 & 0 \\ 0 & \mathbf{A}_{22} & 0 \\ 0 & 0 & 0 \end{pmatrix}}_{\mathbf{A}} \underbrace{\begin{pmatrix} \mathbf{u}_k \\ \mathbf{v}_k \\ \mathbf{p}_k \end{pmatrix}}_{\mathbf{q}_k} + \dots \\ \dots + \underbrace{\begin{pmatrix} \mathbf{b}_1(\mathbf{u}_k, \mathbf{v}_k, \boldsymbol{\nu}_k, \gamma_k) \\ \mathbf{b}_2(\mathbf{u}_k, \mathbf{v}_k, \boldsymbol{\nu}_k, \gamma_k) \\ \mathbf{b}_3 \end{pmatrix}}_{\mathbf{b}(\mathbf{q}_k, \mathbf{w}_k)}. \quad (3.22)$$

The difference can be found in the descriptor matrix. In the representation above, the elements  $\mathbf{A}_{xy}(\mathbf{u}_k), \mathbf{A}_{yx}(\mathbf{u}_k)$  that occur in (3.21) are set to zero. This can be justified by the fact that their contribution is negligible since these matrices contain elements that, for our case studies, are of the order of  $\mathcal{O}(1)$  while the elements in  $\mathbf{A}_x(\mathbf{u}_k, \mathbf{v}_k)$  and  $\mathbf{A}_y(\mathbf{u}_k, \mathbf{v}_k)$  are of the order of  $\mathcal{O}(3)$ . Consequently, no significant change in the com-

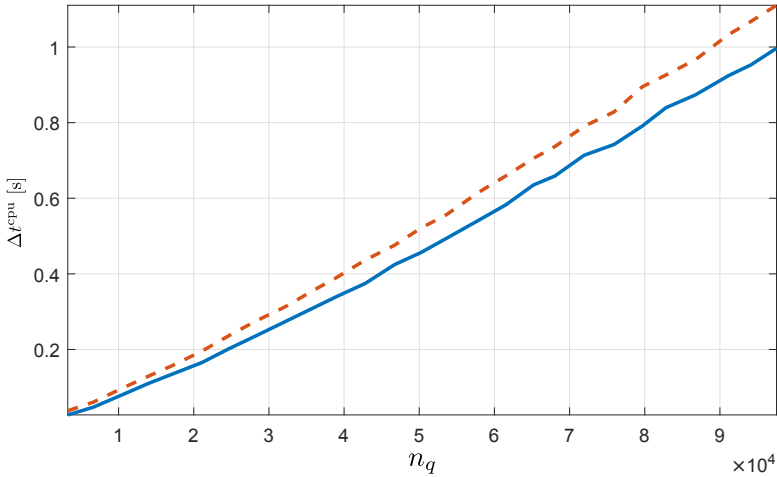


Figure 3.7: Mean computation time per simulation time step  $\Delta t^{\text{cpu}}$  versus number of states  $n_q$ . The red dashed line is WFSim as presented in (3.21) and blue is WFSim as presented in (3.22). Note that the number of cells is approximately  $n_q/3$  with  $n_q$  the number of states.

puted flow field has been observed, but a decrease in  $\Delta t^{\text{cpu}}$  has (see Fig. 3.7). Therefore, the remainder of this chapter will continue with the WFSim representation given in (3.22). Table 3.1 depicts more numerical values of  $\Delta t^{\text{cpu}}$  for this WFSim representation.

From Table 3.1 we can conclude that  $\Delta t^{\text{cpu}}$  increases between quadratic and linear with respect to the number of states  $n_q$  for  $n_q < 221 \cdot 10^3$ . It depends on the computer properties how much you can increase the number of states until the CPU is out of memory.

Table 3.1: Mean computation time per simulation time step  $\Delta t^{\text{cpu}}$  versus number of states  $n_q$  for the WFSim representation as given in (3.22). Computations are performed on a regular notebook with one core.

$n_q$	$\Delta t^{\text{cpu}}$ [s]	$n_q$	$\Delta t^{\text{cpu}}$ [s]	$n_q$	$\Delta t^{\text{cpu}}$ [s]	$n_q$	$\Delta t^{\text{cpu}}$ [s]
$3 \cdot 10^3$	0.02	$27 \cdot 10^3$	0.22	$115 \cdot 10^3$	1.19	$239 \cdot 10^3$	3.1
$6 \cdot 10^3$	0.04	$43 \cdot 10^3$	0.37	$147 \cdot 10^3$	1.66	$258 \cdot 10^3$	3.5
$9 \cdot 10^3$	0.06	$64 \cdot 10^3$	0.60	$182 \cdot 10^3$	2.12	$268 \cdot 10^3$	3.7
$14 \cdot 10^3$	0.10	$88 \cdot 10^3$	0.88	$221 \cdot 10^3$	2.50	$276 \cdot 10^3$	3.8

### 3.4. SIMULATION RESULTS

In this section, WFSim flow and power data will be compared with LES data and it is organised as follows. In §3.4.1, quality measures are introduced. In §3.4.2, WFSim data are compared with PALM data, and WFSim is validated against SOWFA data. In both simulation cases (PALM and SOWFA), the thrust coefficients  $C'_T$  are varied while the yaw angles are set to zero.

#### 3.4.1. QUALITY MEASURES

Suppose we have at time  $k$  a measurement of one quantity  $z_k \in \mathbb{R}^N$  and its estimation  $\hat{z}_k \in \mathbb{R}^N$ . Define the prediction error  $e_k = \hat{z}_k - z_k$ . The quality measure RMSE is, for time step  $k$ , defined as

$$\text{RMSE}(z_k, \hat{z}_k) = \sqrt{\frac{1}{N} e_k^T e_k}. \quad (3.23)$$

This measure is used to compare the flow centreline velocity  $U_k^c(x)$  and power signals from LES and WFSim data for different model parameters. The flow centreline is, for one time step, defined as the laterally averaged longitudinal flow velocity throughout the simulation domain across the rotor diameter. Mathematically this can, for LES data at time step  $k$  at longitudinal position  $x_i$ , be defined as:

$$U_k^c(x_i) = \frac{1}{N_{\bar{y}}} \sum_{s=1}^{N_{\bar{y}}} u_k(x_i, y_s), \quad (3.24)$$

with  $y_s$  the y-coordinate of one cell across the line  $\bar{y} \subset y$ , which contains  $N_{\bar{y}}$  number of cells and has a length equal to the rotor diameter. From WFSim data, the flow velocity component at the rotor centre will be taken across the position  $x$ .

In this work we compare lateral and longitudinal flow velocity components at hub height and power signals calculated with LES with lateral and longitudinal flow velocity components and power signals calculated with WFSim.<sup>3</sup>

#### 3.4.2. AXIAL INDUCTION ACTUATION

Studies such as (Shapiro et al., 2017a; Munters and Meyers, 2017; Vali et al., 2017) and (van Wingerden et al., 2017) illustrate that axial induction actuation can be used in active power control where the objective is to provide grid facilities. In order to utilize

<sup>3</sup>The LES flow data are mapped onto the grid of WFSim using bilinear interpolation techniques.



the WFSim model in active power control, it is important to first validate it when exciting the thrust coefficient.

In the following, WFSim is compared with simulation data from PALM (Maronga et al., 2015) and SOWFA (Churchfield et al., 2012), both high-fidelity wind farm models that were briefly discussed in Section 3.1. The latter includes the actuator line model (ALM) while the former employs the ADM.<sup>4</sup>

### PARALLELIZED LES MODEL (PALM) AND WFSIM

PALM predicts the 3D flow velocity vectors and turbine power signals in a wind farm using LES and is based on the 3D incompressible Navier-Stokes equations.<sup>5</sup> Table 3.2 gives a summary of the two-turbine wind farm simulated in WFSim. A summary of the PALM simulation set-up can be found in Appendix 3.B (including a  $C_P/C_T$ -curve). The applied control signals are depicted in Fig. 3.8 and are chosen such that different system dynamics are excited. The final values for the tuning parameters are obtained using a grid search. Figure 3.9 and Fig. 3.10 show a comparison of the mean flow centreline and the wind farm power, respectively. A flow field evaluated with both the WFSim model and PALM can be found in Appendix 3.B.

Table 3.2: Summary of the WFSim simulation set-up.

Domain size $L_x \times L_y$	$2 \times 0.63$ [km <sup>2</sup> ]	Turbine rotor diameter $D$	126.4 [m]
Grid size $N_x \times N_y$	$50 \times 25$	Turbine arrangement	$2 \times 1$
Cell size $\Delta x \times \Delta y$	$40 \times 23$ [m <sup>2</sup> ]	Turbine spacing	$5D$
Times	$\Delta t = 1, \Delta t^{\text{CPU}} = 0.02$ [s]	Atmospheric conditions	$u_b = 8, v_b = 0$ [m/s], $\rho = 1.2$ [kg/m <sup>3</sup> ]
Force and power factor	$c_f = 1.7, c_p = 0.95$	Turbulence model	$d = 530, d' = 122$ [m] $l_s = 0.06$

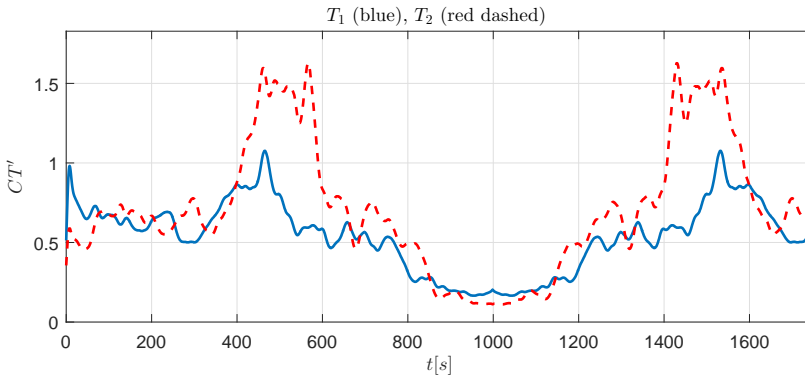


Figure 3.8: Excitation signals for the 2-turbine simulation case. The yaw angles are set to zero.

In Fig. 3.9, the mean flow centrelines through the farms of WFSim and PALM are relatively similar. The PALM data exhibit more turbulent fluctuations due to the presence of a more sophisticated turbulence model, which allows for better capturing small-scale

<sup>4</sup>PALM also includes the rotating ADM, but in our case study the ADM is employed.

<sup>5</sup>In this work we consider PALM as a wind farm model since PALM is simulated with turbine models. However, PALM is also applicable for simulating oceanic behaviour.

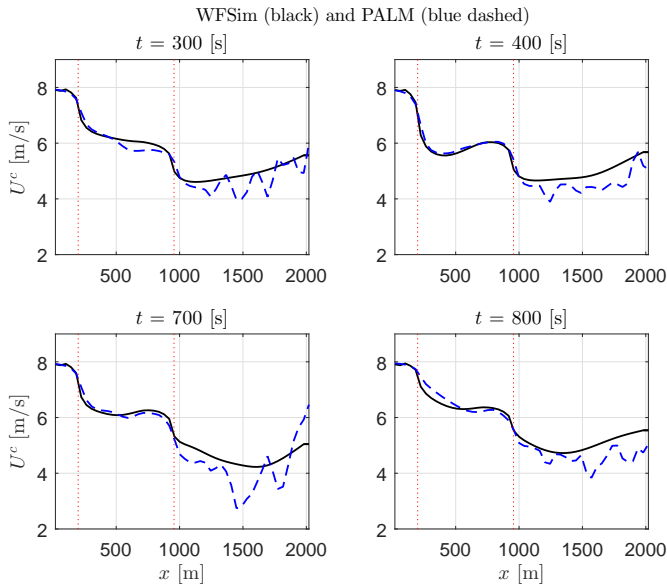


Figure 3.9: Mean flow centreline at four time instances through the farm. The vertical red dashed lines indicate the positions of the turbines.

dynamics such as turbine-induced turbulence. However, the WFSim model is capable of estimating wake recovery similar to the PALM model. The recovery in the WFSim model is due to the turbulence model as presented in §3.2.1. It is in fact the slope of the local mixing length parameters that can determine the amount of wake recovery, or more precisely, the larger this slope, the higher the wake recovery. It is therefore interesting to link this tuning variable to the turbulence intensity in the farm. Furthermore, it can be seen in Fig. 3.10 that the WFSim model is capable of estimating the wind farm power. Since both the WFSim model and PALM employ the ADM, fast fluctuations in the power signal can be observed. This is due to the lack of rotor inertia in both simulation cases. The simulation case presented in this section illustrates that the WFSim model, in which the third dimension is partially neglected, is able to estimate wind farm flow and power signals computed with a 3D LES wind farm model. In the following, a SOWFA case study will be presented, an LES model that includes turbine dynamics.

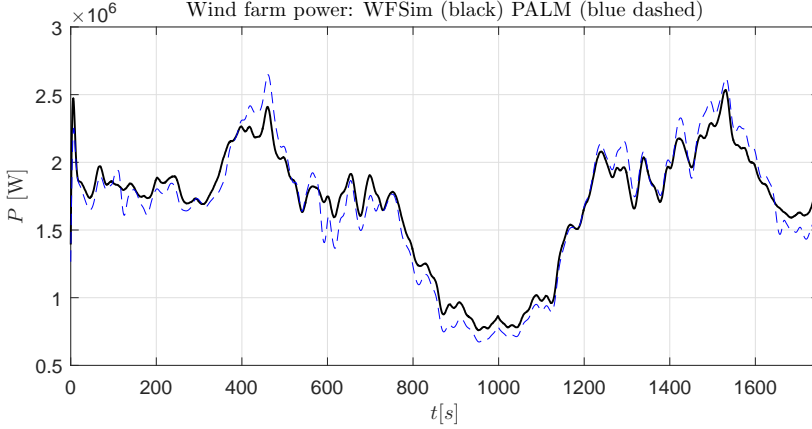


Figure 3.10: Wind farm power from PALM (blue dashed) and WFSim (black).

### SIMULATOR FOR WIND FARM APPLICATIONS (SOWFA) AND WFSIM

SOWFA predicts the 3D flow velocity vectors in a wind farm using LES and is based on the 3D incompressible Navier-Stokes equations. For turbine modeling it employs the ALM, which is a more sophisticated model than the ADM (Sanderse et al., 2011). In addition, the FAST model from the National Renewable Energy Laboratory (NREL) is implemented (Jonkman and Buhl, 2005). This model calculates turbine power production, blade forces on the flow and structural loading on the turbine. In the SOWFA simulation presented, the NREL 5-MW wind turbine is simulated (Jonkman et al., 2009).

The SOWFA data set used in this work for validation is equivalent to the set used in (van Wingerden et al., 2017). The thrust coefficient  $C'_T$  is not a control variable in SOWFA due to the employment of the ALM and therefore has to be estimated. This will be discussed in the following paragraph.

### TURBINE OPERATING SETTINGS

For estimating the control signals  $C'_{T_n}$ , the turbine's fore-aft bending moment  $M_k^{\text{sowfa}}$  calculated with FAST is exploited. Using the relation  $M_k^{\text{sowfa}} = \mathbf{F}_k^{\text{sowfa}} z_h$  with  $z_h$  the hub height, the (indirect) measured thrust force  $\mathbf{F}_k^{\text{sowfa}}$  can be derived. An estimation from SOWFA data of the rotor flow velocity  $U_k^{\text{sowfa}}$  is obtained by averaging the flow velocity components across the rotor. Using the standard ADM yields for each turbine:

$$\mathbf{F}_k^{\text{sowfa}} = \frac{1}{2} A \rho C'_T \left[ U_k^{\text{sowfa}} \right]^2 \begin{pmatrix} \cos(\gamma_k + \varphi_k) \\ \sin(\gamma_k + \varphi_k) \end{pmatrix}. \quad (3.25)$$

Since  $\mathbf{F}_k^{\text{sowfa}}$ ,  $U_k^{\text{sowfa}}$  and  $\rho$  can be obtained from SOWFA data and the yaw angles are given, all the variables in (3.25) are known hence the control variable  $C'_T$  can be estimated from SOWFA data for each turbine.<sup>6</sup> It will be used, together with the yaw angles, as an input to the WFSim model.

<sup>6</sup>The estimated  $C'_T$  from SOWFA data is relatively noisy and hence filtered.

In the following, flow data at hub height from a nine-turbine SOWFA simulation case will be compared with WFSim data. See Fig. 3.12 (a) for the simulated wind farm topology. The turbines are excited with thrust coefficients as depicted in Fig. 3.11. These excitation signals are estimated from SOWFA data using the relation defined in (3.25). Table 3.3 presents the WFSim parameters used during simulations. The tuning variables of the WFSim model are found using a grid search and the inflow conditions  $u_b, v_b$  are estimated from SOWFA data.

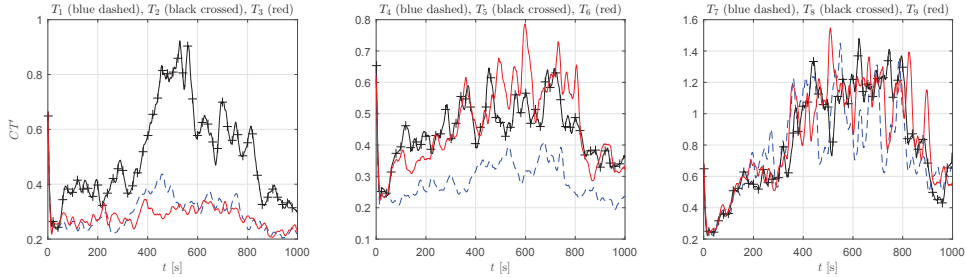


Figure 3.11: Excitation signals for the nine-turbine simulation case. The yaw angles are set to zero. See (van Wingerden et al., 2017) for more information on the simulation case study and turbine excitation signals.

Table 3.3: Summary of the WFSim simulation set-up.

Domain size $L_x \times L_y$	$2.5 \times 1.5$ [km <sup>2</sup> ]	Turbine rotor diameter $D$	126.4 [m]
Grid size $N_x \times N_y$	$100 \times 42$	Turbine arrangement	$3 \times 3$
Cell size $\Delta x \times \Delta y$	$25 \times 15$ [m <sup>2</sup> ]	Turbine spacing	$5D \times 3D$
Times	$\Delta t = 1, \Delta t^{\text{cpu}} = 0.1$ [s]	Atmospheric conditions	$u_b = 12, v_b = 0$ [m/s], $\rho = 1.2$ [kg/m <sup>3</sup> ]
Force and power factor	$c_f = \frac{1}{2}, c_p = 1.1$	Turbulence model	$d = 635, d' = 76.2$ [m] $l_s = 0.17$

Figure 3.12 (b) and Fig. 3.13 depict a mean flow centreline (see (3.24)) comparison for each row at four time instances. It can be concluded that the mean flow centreline derived from WFSim data approximates the mean flow centreline derived from SOWFA data. In Fig. 3.14, time series of the power signals from SOWFA and WFSim are depicted. The signals from the latter are more oscillating than the power signals from SOWFA. This is due to the fact that the power expression in WFSim is a nonlinear static map depending on the  $C'_T$ . Thus, no turbine dynamics are taken into account, which is contrary to SOWFA in which the FAST turbine model is simulated. However, important characteristics can be captured with WFSim. A flow field evaluated with both the WFSim model and SOWFA can be found in Appendix 3.C.

WFSim is capable of estimating dominant wake dynamics, the objective of the control-oriented model WFSim. Smaller-scale and stochastic effects can be measured by sensors and incorporated using an estimator based on WFSim, as has been shown in (Doekemeijer et al., 2016, 2017, 2018).

### 3.5. CONCLUSIONS

Current literature on wind farm control can be categorized into model-free and model-based methods. This chapter focused on the latter category. Here, a distinction can be

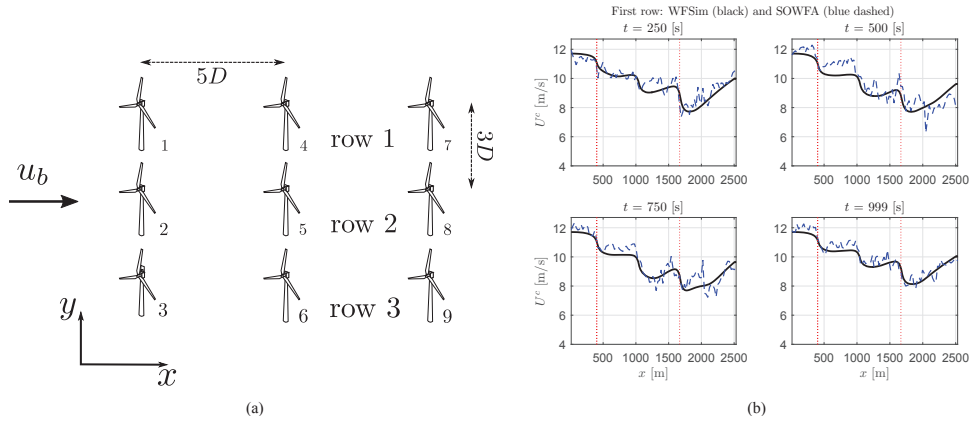


Figure 3.12: Topology simulated wind farm (a) and mean flow centreline at four time instances through the first row (b).

made between type of model employed, a steady-state or dynamic wind farm model. In order to use the closed-loop control paradigm, and account for model uncertainties, we think it is important to utilize a dynamic wind farm model for controller design and possible online wind farm control. In this chapter, such a control-oriented dynamic wind farm model, referred to as WFSim, has been presented.<sup>7</sup> It is a wind farm model that can predict flow fields and power production and includes turbines that are modelled using actuator disk theory and is based on modified two-dimensional Navier-Stokes equations. Completely neglecting the third (vertical) dimension is a too crude assumption to describe the flow in a wind farm accurately enough for control purposes. In this chapter, we included a correction term in the continuity equation. It has been illustrated that the inclusion of this factor reduces the effect of neglecting the third (vertical) dimension. More precisely, it has been shown that the speed-up effect of the flow on the right and left downwind of a turbine will be reduced when solving for the corrected Navier-Stokes equations compared to the standard two-dimensional Navier-Stokes equations. It has been shown that this resulted in a better approximation of LES data.

In addition, a turbulence model was included taking into account the desired wake recovery. The heuristically found turbulence model is based on Prandtl's mixing length hypotheses, where the mixing length parameter is made dependent on the downstream distance from the turbine rotors and also dependent on the mean wind direction. After theoretically formulating the WFSim model, this chapter followed by illustrating that the computed flow velocities and power signals from the 2D-like WFSim model can estimate flow velocity data and power signals from the 3D high-fidelity wind farm models PALM and SOWFA. The necessary computation time of the WFSim model is however a fraction of what is needed to do LES making the WFSim model potentially suitable for online control. More precisely, in the 9-turbine case, the controller model's computational time<sup>8</sup> is 0.1 [s] meaning that it takes 0.1 [s] to propagate one sample forward in time. However,

<sup>7</sup>The WFSim repository can be found in (Boersma, 2018b).

<sup>8</sup>All mentioned CPU times are obtained using a regular notebook and one single i7 core.

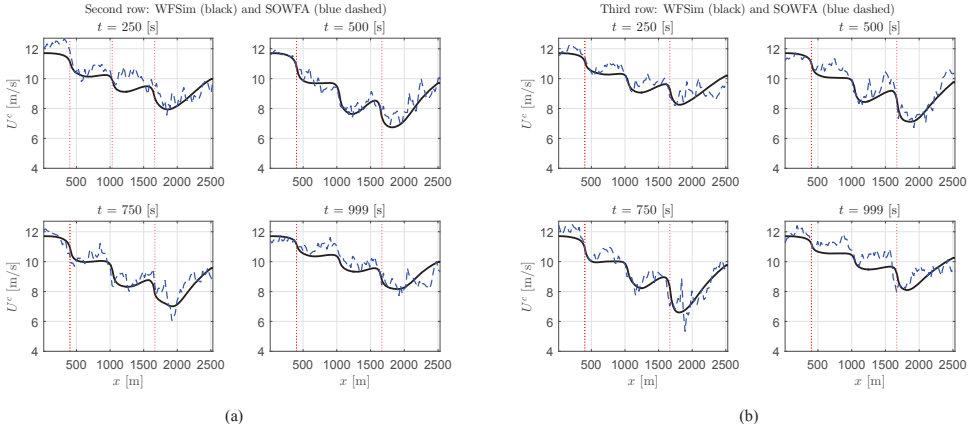


Figure 3.13: Mean flow centreline at four time instances through the second row (a) and third row (b) of turbines. The vertical red dashed lines indicate the positions of the turbines.

for a 80-turbine case, the computational time increases to approximately 8 [s] per time step<sup>8</sup>. In both cases, the sample period was set to 1 [s] indicating that in the 80-turbine case, no online control can be done if control signals are updated every second. It is still an open question if control signals need to be updated every second. Nevertheless, the developed WFSim model allows for varying the temporal and spatial resolution, and thus the required model fidelity. This work focussed on axial induction actuation, but future work will also include the validation of yaw actuation and wind direction changes. For the simulation cases presented, no grid convergence studies have been performed, but future work should entail this. Other work entails the online update of some of the the tuning variables  $c_f, c_p, d, d', l_s$  by an observer (Doekemeijer et al., 2018) and the employment of the presented dynamic wind farm model in an online closed-loop control scheme (Vali et al., 2018a).

### 3.A. DISCRETIZING THE NAVIER-STOKES EQUATIONS.

This section will present the necessary derivations to go from (3.15) to (3.21), *i.e.*, it will elaborate on the discretization of the NS equations. In the following subsections, all terms in the NS equations will subsequently be dealt with.

#### DISCRETIZING THE CONVECTION (NONLINEAR) TERMS

The nonlinear term that occurs in the momentum equations can be spatially discretized by deriving:

$$\int_{\Delta V} \rho (\mathbf{u} \cdot \nabla) \mathbf{u} \, dV = \int_{\Delta V} \rho \left( \frac{\partial u^2}{\partial x} + \frac{\partial uv}{\partial y} \right) dV.$$

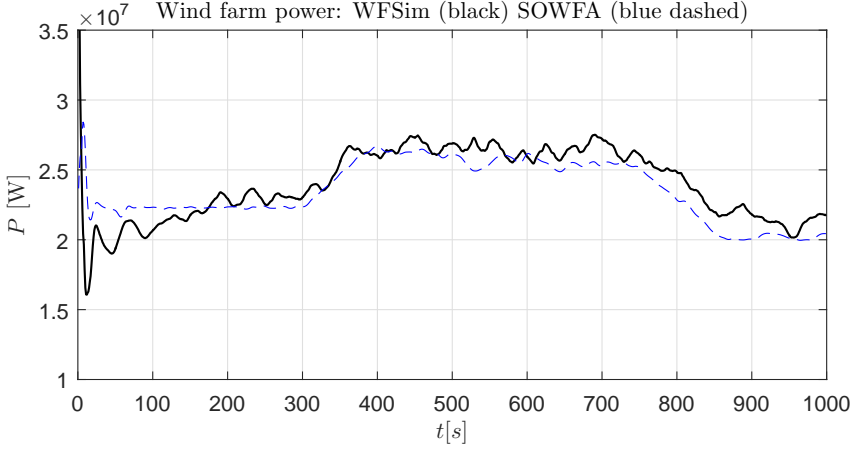


Figure 3.14: Wind farm power from SOWFA (blue dashed) and WFSim (black).

### X-MOMENTUM EQUATION

Deriving the term in the x-momentum equation (first element in the vector above) yields

$$\int_{\Delta V} \rho \left[ \frac{\partial u^2}{\partial x} + \frac{\partial uv}{\partial y} \right] dV = \rho [(u^2 \delta y)_e - (u^2 \delta y)_w + (uv \Delta x)_n - (uv \Delta x)_s],$$

where  $(u^2 \delta y)_e, (u^2 \delta y)_w$  are the quantities  $u^2$  at the east and west sides of the cell with surface  $\delta y_e, \delta y_w$ , respectively. Similarly,  $(uv \Delta x)_n, (uv \Delta x)_s$  are the quantities  $uv$  at the north and south sides of the cell with surface  $\Delta x_n, \Delta x_s$ , respectively. Assuming  $\delta y_e = \delta y_w = \delta y$  and  $\Delta x = \Delta x_n = \Delta x_s$ , the above can be written as

$$\int_{\Delta V} \rho \left[ \frac{\partial u^2}{\partial x} + \frac{\partial uv}{\partial y} \right] dV = \rho [(u^2)_e \delta y - (u^2)_w \delta y + (uv)_n \Delta x - (uv)_s \Delta x],$$

Define:  $F^{ex} = \rho u_e \delta y, F^{wx} = \rho u_w \delta y, F^{nx} = \rho v_n \Delta x, F^{sx} = \rho v_s \Delta x$ . This is in (Versteeg and Malalasekera, 2007) referred to as a convective mass flux approximation. The above can then be written as

$$\int_{\Delta V} \rho \left[ \frac{\partial u^2}{\partial x} + \frac{\partial uv}{\partial y} \right] dV = F^{ex} u_e - F^{wx} u_w + F^{nx} u_n - F^{sx} u_s,$$

In Fig. 3.5 we observe that  $u_e, u_w, u_n, u_s, v_n, v_s$  are not defined for the black cell. Applying central differencing approximates the terms as follows

$$\begin{aligned} u_e &= \frac{u_{i+1,j} + u_{i,j}}{2}, & u_w &= \frac{u_{i-1,j} + u_{i,j}}{2}, & u_n &= \frac{u_{i,j+1} + u_{i,j}}{2}, & u_s &= \frac{u_{i,j-1} + u_{i,j}}{2}, \\ v_n &= \frac{v_{I-1,j+1} + v_{I,j+1}}{2}, & v_s &= \frac{v_{I-1,j} + v_{I,j}}{2}. \end{aligned} \quad (3.26)$$

We can now write

$$\int_{\Delta V} \rho \left[ \frac{\partial u^2}{\partial x} + \frac{\partial uv}{\partial y} \right] dV = F_{i,J}^{ex} u_{i+1,J} - F_{i,J}^{wx} u_{i-1,J} + F_{i,J}^{nx} u_{i,J+1} - F_{i,J}^{sx} u_{i,J-1} + \dots \\ \dots + \left( F_{i,J}^{ex} - F_{i,J}^{wx} + F_{i,J}^{nx} - F_{i,J}^{sx} \right) u_{i,J}.$$

In (3.26), central differencing is applied. A disadvantage of this method is that it does not use prior knowledge on the flow direction. The upwind differencing scheme, however, employs this prior knowledge as explained in (Versteeg and Malalasekera, 2007). A combination of the central and upwind differencing scheme is the hybrid differencing scheme. When applying this, the above can be written as:

$$\int_{\Delta V} \rho \left[ \frac{\partial u^2}{\partial x} + \frac{\partial uv}{\partial y} \right] dV = c_{i,J}^{ex} u_{i+1,J} - c_{i,J}^{wx} u_{i-1,J} + c_{i,J}^{nx} u_{i,J+1} - c_{i,J}^{sx} u_{i,J-1} + c_{i,J}^{px} u_{i,J},$$

with  $c_{i,J}^{ex} = \max[-F_{i,J}^{ex}, 0]$ ,  $c_{i,J}^{wx} = \max[F_{i,J}^{wx}, 0]$ ,  $c_{i,J}^{nx} = \max[-F_{i,J}^{nx}, 0]$ ,  $c_{i,J}^{sx} = \max[F_{i,J}^{sx}, 0]$  and  $c_{i,J}^{px} = c_{i,J}^{ex} + c_{i,J}^{wx} + c_{i,J}^{nx} + c_{i,J}^{sx} + F_{i,J}^{ex} - F_{i,J}^{wx} + F_{i,J}^{nx} - F_{i,J}^{sx}$ . In WFSim, the coefficients  $c_{i,J}^{\bullet}$  and  $F_{i,J}^{\bullet}$  are evaluated for time  $k$  while the other flow velocity components are computed for time  $k+1$ .

#### Y-MOMENTUM EQUATION

Deriving the nonlinear term in the y-momentum equation yields

$$\int_{\Delta V} \rho \left[ \frac{\partial v^2}{\partial y} + \frac{\partial vu}{\partial x} \right] dV = F_{I,j}^{ey} v_{I+1,j} - F_{I,j}^{wy} v_{I-1,j} + F_{I,j}^{ny} v_{I,j+1} - F_{I,j}^{sy} v_{I,j-1} + \dots \\ \dots + \left( F_{I,j}^{ey} - F_{I,j}^{wy} + F_{I,j}^{ny} - F_{I,j}^{sy} \right) v_{I,j},$$

with  $F_{I,j}^{ey} = \rho u_e \Delta y$ ,  $F_{I,j}^{wy} = \rho u_w \Delta y$ ,  $F_{I,j}^{ny} = \rho v_n \delta x$ ,  $F_{I,j}^{sy} = \rho v_s \delta x$  and:

$$v_e = \frac{v_{I+1,j} + v_{I,j}}{2}, \quad v_w = \frac{v_{I-1,j} + v_{I,j}}{2}, \quad v_n = \frac{v_{I,j+1} + v_{I,j}}{2}, \quad v_s = \frac{v_{I,j-1} + v_{I,j}}{2}, \\ u_e = \frac{u_{i+1,J} + u_{i+1,J-1}}{2}, \quad u_w = \frac{u_{i,J} + u_{i,J-1}}{2}.$$

The intermediate steps are omitted here since they are similar to the steps presented when handling the nonlinear term in the x-momentum equation. Note, however, that the discretization is evaluated using the yellow cell (see Fig. 3.5). When applying the hybrid differencing scheme, the above can be written as

$$\int_{\Delta V} \rho \left[ \frac{\partial v^2}{\partial y} + \frac{\partial vu}{\partial x} \right] dV = c_{I,j}^{ey} v_{I+1,j} - c_{I,j}^{wy} v_{I-1,j} + c_{I,j}^{ny} v_{I,j+1} - c_{I,j}^{sy} v_{I,j-1} + c_{I,j}^{py} v_{I,j},$$

with  $c_{I,j}^{ey} = \max[-F_{I,j}^{ey}, 0]$ ,  $c_{I,j}^{wy} = \max[F_{I,j}^{wy}, 0]$ ,  $c_{I,j}^{ny} = \max[-F_{I,j}^{ny}, 0]$ ,  $c_{I,j}^{sy} = \max[F_{I,j}^{sy}, 0]$  and  $c_{I,j}^{py} = c_{I,j}^{ey} + c_{I,j}^{wy} + c_{I,j}^{ny} + c_{I,j}^{sy} + F_{I,j}^{ey} - F_{I,j}^{wy} + F_{I,j}^{ny} - F_{I,j}^{sy}$ . Similar as before, the coefficients  $c_{I,j}^{\bullet}$  and  $F_{I,j}^{\bullet}$  are evaluated for time  $k$  while the other flow velocity components are computed for time  $k+1$ .



### DISCRETIZING THE PRESSURE GRADIENT

For the pressure gradient we evaluate

$$\int_{\Delta V} \left( \frac{\partial p}{\partial x} \right) dV = \left( (p_{I,J} - p_{I-1,J}) \delta y \right)$$

$$\int_{\Delta V} \left( \frac{\partial p}{\partial y} \right) dV = \left( (p_{I,J} - p_{I,J-1}) \delta x \right).$$

The pressure components are evaluated for time  $k + 1$ .

### DISCRETIZING THE STRESS TERM

Evaluate

$$\int_{\Delta V} \tau_{\nabla} dV = \int_{\Delta V} \left( \frac{\partial}{\partial x} \left[ l_u(x,y)^2 \left| \frac{\partial u}{\partial y} \right| \frac{\partial u}{\partial x} \right] + \frac{\partial}{\partial y} \frac{1}{2} \left[ l_u(x,y)^2 \left| \frac{\partial u}{\partial y} \right| \left( \frac{\partial u}{\partial y} + \frac{\partial v}{\partial x} \right) \right] \right) dV. \quad (3.27)$$

### X-MOMENTUM EQUATION

Considering the x-momentum equation we have to evaluate multiple terms. The first term evaluates as

$$\int_{\Delta V} \frac{\partial}{\partial x} \left[ l_u(x,y)^2 \left| \frac{\partial u}{\partial y} \right| \frac{\partial u}{\partial x} \right] dV = \left[ l_u(x,y)^2 \left| \frac{\partial u}{\partial y} \right| \frac{\partial u}{\partial x} \right]_e \delta y - \left[ l_u(x,y)^2 \left| \frac{\partial u}{\partial y} \right| \frac{\partial u}{\partial x} \right]_w \delta y.$$

Here we have:

$$\left. \frac{\partial u}{\partial y} \right|_e = \frac{u_{i,J+1} - u_{i,J}}{\Delta y_{J,J+1}}, \quad \left. \frac{\partial u}{\partial x} \right|_e = \frac{u_{i+1,J} - u_{i,J}}{\delta x_{i,i+1}},$$

$$\left. \frac{\partial u}{\partial y} \right|_w = \frac{u_{i,J} - u_{i,J-1}}{\Delta y_{J-1,J}}, \quad \left. \frac{\partial u}{\partial x} \right|_w = \frac{u_{i,J} - u_{i-1,J}}{\delta x_{i-1,i}},$$

and  $\delta y = \delta y_{j,j+1}$ . Substituting these expressions yields

$$\int_{\Delta V} \frac{\partial}{\partial x} \left[ l_u(x,y)^2 \left| \frac{\partial u}{\partial y} \right| \frac{\partial u}{\partial x} \right] dV = \underbrace{l_u(x_{I-1}, y_J)^2 \left| \frac{(u_{i,J+1} - u_{i,J}) \delta y_{j,j+1}}{\Delta y_{J,J+1} \delta x_{i,i+1}} \right|}_{T_{i,J}^{ex}} (u_{i+1,J} - u_{i,J}) \dots$$

$$\dots \underbrace{- l_u(x_I, y_J)^2 \left| \frac{(u_{i,J} - u_{i,J-1}) \delta y_{j,j+1}}{\Delta y_{J-1,J} \delta x_{i-1,i}} \right|}_{T_{i,J}^{wx}} (u_{i,J} - u_{i-1,J}). \quad (3.28)$$

The second term evaluates as

$$\int_{\Delta V} \frac{\partial}{\partial y} \frac{1}{2} \left[ l_u(x,y)^2 \left| \frac{\partial u}{\partial y} \right| \left( \frac{\partial u}{\partial y} + \frac{\partial v}{\partial x} \right) \right] dV = \dots$$

$$\dots \frac{1}{2} \left[ l_u(x,y)^2 \left| \frac{\partial u}{\partial y} \right| \left( \frac{\partial u}{\partial y} + \frac{\partial v}{\partial x} \right) \right]_n \Delta x - \frac{1}{2} \left[ l_u(x,y)^2 \left| \frac{\partial u}{\partial y} \right| \left( \frac{\partial u}{\partial y} + \frac{\partial v}{\partial x} \right) \right]_s \Delta x.$$

Here we have:

$$\begin{aligned} \left. \frac{\partial u}{\partial y} \right|_n &= \frac{u_{i,J+1} - u_{i,J}}{\Delta y_{J,J+1}}, & \left. \frac{\partial v}{\partial x} \right|_n &= \frac{v_{I,j+1} - v_{I-1,j+1}}{\Delta x_{I-1,I}}, \\ \left. \frac{\partial u}{\partial y} \right|_s &= \frac{u_{i,J} - u_{i,J-1}}{\Delta y_{J-1,J}}, & \left. \frac{\partial v}{\partial x} \right|_s &= \frac{v_{I,j} - v_{I-1,j}}{\Delta x_{I-1,I}}, \end{aligned}$$

and  $\Delta x = \Delta x_{I-1,I}$ . Substituting yields

$$\begin{aligned} \int_{\Delta V} \frac{\partial}{\partial y} \frac{1}{2} \left[ l_u(x,y)^2 \left| \frac{\partial u}{\partial y} \right| \left( \frac{\partial u}{\partial y} + \frac{\partial v}{\partial x} \right) \right] dV = \\ \dots \frac{1}{2} \left[ l_u(x_i, y_{j+1})^2 \left| \frac{u_{i,J+1} - u_{i,J}}{\Delta y_{J,J+1}} \right| \left( \frac{u_{i,J+1} - u_{i,J}}{\Delta y_{J,J+1}} + \frac{v_{I,j+1} - v_{I-1,j+1}}{\Delta x_{I-1,I}} \right) \right] \Delta x_{I-1,I} \dots \\ \dots - \frac{1}{2} \left[ l_u(x_i, y_j)^2 \left| \frac{u_{i,J} - u_{i,J-1}}{\Delta y_{J-1,J}} \right| \left( \frac{u_{i,J} - u_{i,J-1}}{\Delta y_{J-1,J}} + \frac{v_{I,j} - v_{I-1,j}}{\Delta x_{I-1,I}} \right) \right] \Delta x_{I-1,I}, \end{aligned}$$

which can be rearranged to

$$\begin{aligned} \int_{\Delta V} \frac{\partial}{\partial y} \frac{1}{2} \left[ l_u(x,y)^2 \left| \frac{\partial u}{\partial y} \right| \left( \frac{\partial u}{\partial y} + \frac{\partial v}{\partial x} \right) \right] dV = \dots \\ \dots \underbrace{\frac{1}{2} l_u(x_i, y_{j+1})^2 \left| \frac{(u_{i,J+1} - u_{i,J}) \Delta x_{I-1,I}}{\Delta y_{J,J+1}^2} \right|}_{T_{i,J}^{nx}} (u_{i,J+1} - u_{i,J}) \dots \\ \dots + \underbrace{\frac{1}{2} l_u(x_i, y_{j+1})^2 \left| \frac{(u_{i,J+1} - u_{i,J})}{\Delta y_{J,J+1}} \right|}_{T_{i,J}^{newx}} (v_{I,j+1} - v_{I-1,j+1}) \dots \\ \dots - \underbrace{\frac{1}{2} l_u(x_i, y_j)^2 \left| \frac{(u_{i,J} - u_{i,J-1}) \Delta x_{I-1,I}}{\Delta y_{J-1,J}^2} \right|}_{T_{i,J}^{sx}} (u_{i,J} - u_{i,J-1}) \dots \\ \dots - \underbrace{\frac{1}{2} l_u(x_i, y_j)^2 \left| \frac{(u_{i,J} - u_{i,J-1})}{\Delta y_{J-1,J}} \right|}_{T_{i,J}^{sewx}} (v_{I,j} - v_{I-1,j}). \end{aligned} \quad (3.29)$$

Summarizing the above

$$\begin{aligned} \frac{\partial}{\partial x} \left[ l_u(x,y)^2 \left| \frac{\partial u}{\partial y} \right| \frac{\partial u}{\partial x} \right] + \frac{\partial}{\partial y} \frac{1}{2} \left[ l_u(x,y)^2 \left| \frac{\partial u}{\partial y} \right| \left( \frac{\partial u}{\partial y} + \frac{\partial v}{\partial x} \right) \right] = \dots \\ \dots T_{i,J}^{ex} u_{i+1,J} + T_{i,J}^{wx} u_{i-1,J} + T_{i,J}^{nx} u_{i,J+1} + T_{i,J}^{sx} u_{i,J-1} + T_{i,J}^{px} u_{i,J} \dots \\ \dots + T_{i,J}^{newx} (v_{I,j+1} - v_{I-1,j+1}) + T_{i,J}^{sewx} (v_{I-1,j} - v_{I,j}), \end{aligned}$$

with  $T_{i,J}^{px} = T_{i,J}^{ex} + T_{i,J}^{wx} + T_{i,J}^{nx} + T_{i,J}^{sx}$ . The coefficients  $T_{i,J}^{\bullet}$  will be computed for time  $k$  while the flow components will be evaluated for time  $k+1$ .

## Y-MOMENTUM EQUATION

Considering the y-momentum equation, the first term evaluates as

$$\int_{\Delta V} \frac{\partial}{\partial y} \left[ l_u(x, y)^2 \left| \frac{\partial u}{\partial y} \right| \frac{\partial v}{\partial y} \right] dV = \left[ l_u(x, y)^2 \left| \frac{\partial u}{\partial y} \right| \frac{\partial v}{\partial y} \right]_n \Delta x - \left[ l_u(x, y)^2 \left| \frac{\partial u}{\partial y} \right| \frac{\partial v}{\partial y} \right]_s \Delta x.$$

Here we have:

$$\begin{aligned} \left. \frac{\partial u}{\partial y} \right|_n &= \frac{u_{i+1,J} - u_{i+1,J-1}}{\Delta y_{J-1,J}}, & \left. \frac{\partial v}{\partial y} \right|_n &= \frac{v_{I,j+1} - v_{I,j}}{\delta y_{j,j+1}}, \\ \left. \frac{\partial u}{\partial y} \right|_s &= \frac{u_{i,J} - u_{i,J-1}}{\Delta y_{J-1,J}}, & \left. \frac{\partial v}{\partial y} \right|_s &= \frac{v_{I,j} - v_{I,j-1}}{\delta y_{j-1,j}}, \end{aligned}$$

and  $\Delta x = \delta x_{i,i+1}$ . Substituting these expressions yields

$$\begin{aligned} \int_{\Delta V} \frac{\partial}{\partial y} \left[ l_u(x, y)^2 \left| \frac{\partial u}{\partial y} \right| \frac{\partial v}{\partial y} \right] dV = & \dots \\ & \underbrace{\dots l_u(x_{I,j})^2 \left| \frac{(u_{i+1,J} - u_{i+1,J-1}) \delta x_{i,i+1}}{\Delta y_{J-1,J} \delta y_{j,j+1}} \right| (v_{I,j+1} - v_{I,j}) \dots}_{T_{I,j}^{ny}} \\ & \dots \underbrace{- l_u(x_{I,j-1})^2 \left| \frac{(u_{i,J} - u_{i,J-1}) \delta x_{i,i+1}}{\Delta y_{J-1,J} \delta y_{j-1,j}} \right| (v_{I,j} - v_{I,j-1})}_{T_{I,j}^{sy}} \dots \end{aligned} \quad (3.30)$$

The second term evaluates as

$$\begin{aligned} \int_{\Delta V} \frac{\partial}{\partial x} \frac{1}{2} \left[ l_u(x, y)^2 \left| \frac{\partial u}{\partial y} \right| \left( \frac{\partial u}{\partial y} + \frac{\partial v}{\partial x} \right) \right] dV = & \dots \\ \dots \frac{1}{2} \left[ l_u(x, y)^2 \left| \frac{\partial u}{\partial y} \right| \left( \frac{\partial u}{\partial y} + \frac{\partial v}{\partial x} \right) \right]_e \Delta y - & \frac{1}{2} \left[ l_u(x, y)^2 \left| \frac{\partial u}{\partial y} \right| \left( \frac{\partial u}{\partial y} + \frac{\partial v}{\partial x} \right) \right]_w \Delta y. \end{aligned}$$

Here we have:

$$\begin{aligned} \left. \frac{\partial u}{\partial y} \right|_e &= \frac{u_{i+1,J} - u_{i+1,J-1}}{\Delta y_{J-1,J}}, & \left. \frac{\partial v}{\partial x} \right|_e &= \frac{v_{I+1,j} - v_{I,j}}{\Delta x_{I,I+1}}, \\ \left. \frac{\partial u}{\partial y} \right|_w &= \frac{u_{i,J} - u_{i,J-1}}{\Delta y_{J-1,J}}, & \left. \frac{\partial v}{\partial x} \right|_w &= \frac{v_{I,j} - v_{I-1,j}}{\Delta x_{I-1,I}}, \end{aligned}$$

and  $\Delta y = \Delta y_{J-1,J}$ . Substituting these expressions yields

$$\begin{aligned}
 \int_{\Delta V} \frac{\partial}{\partial x} \frac{1}{2} \left[ l_u(x,y)^2 \left| \frac{\partial u}{\partial y} \right| \left( \frac{\partial u}{\partial y} + \frac{\partial v}{\partial x} \right) \right] dV = \dots & \quad (3.31) \\
 \dots \underbrace{\frac{1}{2} l_u(x_i, y_j)^2 \left| \frac{u_{i+1,J} - u_{i+1,J-1}}{\Delta y_{J-1,J}} \right|}_{T_{I,J}^{ensy}} (u_{i+1,J} - u_{i+1,J-1}) \dots \\
 \dots + \underbrace{\frac{1}{2} l_u(x_i, y_j)^2 \left| \frac{u_{i+1,J} - u_{i+1,J-1}}{\Delta x_{I,I+1}} \right|}_{T_{I,J}^{ey}} (v_{I+1,j} - v_{I,j}) \dots \\
 \dots - \underbrace{\frac{1}{2} l_u(x_{i+1}, y_j)^2 \left| \frac{u_{i,J} - u_{i,J-1}}{\Delta y_{J-1,J}} \right|}_{T_{I,J}^{wnsy}} (u_{i,J} - u_{i,J-1}) \dots \\
 \dots - \underbrace{\frac{1}{2} l_u(x_{i+1}, y_j)^2 \left| \frac{u_{i,J} - u_{i,J-1}}{\Delta x_{I-1,I}} \right|}_{T_{I,J}^{wy}} (v_{I,j} - v_{I-1,j}). & \quad (3.32)
 \end{aligned}$$

Summarizing the above

$$\begin{aligned}
 \int_{\Delta V} \frac{\partial}{\partial y} \left[ l_u(x,y)^2 \left| \frac{\partial u}{\partial y} \right| \frac{\partial v}{\partial y} \right] dV = \left[ l_u(x,y)^2 \left| \frac{\partial u}{\partial y} \right| \frac{\partial v}{\partial y} \right]_n \Delta x - \left[ l_u(x,y)^2 \left| \frac{\partial u}{\partial y} \right| \frac{\partial v}{\partial y} \right]_s \Delta x = \dots \\
 \dots T_{I,j}^{ey} v_{I+1,j} + T_{I,j}^{wy} v_{I-1,j} + T_{I,j}^{ny} v_{I,j+1} + T_{I,j}^{sy} v_{I,j-1} + T_{I,j}^{py} v_{I,j} \dots \\
 \dots + T_{I,j}^{ensy} (u_{i+1,J} - u_{i+1,J-1}) + T_{i,J}^{wnsy} (u_{i,J} - u_{i,J-1}),
 \end{aligned}$$

with  $T_{I,j}^{py} = T_{I,j}^{ey} + T_{I,j}^{wy} + T_{I,j}^{ny} + T_{I,j}^{sy}$ . The coefficients  $T_{I,j}^{\bullet}$  will be computed for time  $k$  while the flow components will be evaluated for time  $k+1$ .

### DISCRETIZING THE FORCING TERM

$$\int_{\Delta V} \frac{1}{2} \rho C'_T [U \cos(\gamma)]^2 \begin{pmatrix} \cos(\gamma + \varphi) \\ \sin(\gamma + \varphi) \end{pmatrix} dV = \frac{1}{2} \rho C'_T [U \cos(\gamma)]^2 \begin{pmatrix} \cos(\gamma + \varphi) \\ \sin(\gamma + \varphi) \end{pmatrix} \Delta V$$

### DISCRETIZING THE UNSTEADY TERM

Evaluate:

$$\int_{\Delta V} \begin{pmatrix} \frac{\partial u}{\partial t} \\ \frac{\partial v}{\partial t} \end{pmatrix} dV = \begin{pmatrix} \frac{\partial u}{\partial t} \\ \frac{\partial v}{\partial t} \end{pmatrix} \Delta V$$

Temporal discretization yields:  $\frac{u_{k+1} - u_k}{\Delta t}$  and  $\frac{v_{k+1} - v_k}{\Delta t}$  and we define:

$$a_0^{px} = \frac{\Delta V}{\Delta t} \quad \text{and} \quad a_0^{py} = \frac{\Delta V}{\Delta t}$$

## DISCRETIZING THE CONTINUITY EQUATION

$$\begin{aligned} 0 &= \int_{\Delta V} \frac{\partial u}{\partial x} + 2 \frac{\partial v}{\partial y} dV \\ &= (u_{i+1,J} - u_{i,J}) \delta y_{j,j+1} + 2(v_{I,j+1} - v_{I,j}) \delta x_{i,i+1}. \end{aligned}$$

All the coefficients derived above are given in Table 3.4.

Table 3.4: Fully discretized Navier-Stokes equations and all its coefficients.

x-momentum equation:

$$a_{i,j}^{px} u_{i,j} = \left( a_{i,j}^{nx} \quad a_{i,j}^{sx} \quad a_{i,j}^{wx} \quad a_{i,j}^{ex} \right) \left( u_{i,j+1} \quad u_{i,j-1} \quad u_{i-1,j} \quad u_{i+1,j} \right)^T - \delta y_{j,j+1} \left( p_{I,J} \dots \right. \\ \left. - p_{I-1,J} \right) + f_{i,j}^x + \left( a_{i,j}^{nwx} \quad a_{i,j}^{s wx} \quad a_{i,j}^{n ex} \quad a_{i,j}^{s ex} \right) \left( v_{I-1,j+1} \quad v_{I-1,j} \quad v_{I,j+1} \quad v_{I,j} \right)^T$$

y-momentum equation:

$$a_{I,j}^{py} v_{I,j} = \left( a_{I,j}^{ny} \quad a_{I,j}^{sy} \quad a_{I,j}^{wy} \quad a_{I,j}^{ey} \right) \left( v_{I,j+1} \quad v_{I,j-1} \quad v_{I-1,j} \quad v_{I+1,j} \right)^T - \delta x_{i,i+1} \left( p_{I,J} \dots \right. \\ \left. - p_{I,J-1} \right) + f_{I,j}^y + \left( a_{i,j}^{nwy} \quad a_{i,j}^{s wy} \quad a_{i,j}^{n ey} \quad a_{i,j}^{s ey} \right) \left( u_{i,j} \quad u_{i,j-1} \quad u_{i+1,j} \quad u_{i+1,j-1} \right)^T$$

continuity equation:

$$0 = \delta y_{j,j+1} (u_{i+1,J} - u_{i,J}) + 2\delta x_{i,i+1} (v_{I,j+1} - v_{I,j}),$$

$$a_{i,j}^{ex} = \max \left[ -F_{i,j}^{ex}, 0 \right] + T_{i,j}^{ex}, \quad a_{i,j}^{wx} = \max \left[ F_{i,j}^{wx}, 0 \right] + T_{i,j}^{wx}, \\ a_{i,j}^{nx} = \max \left[ -F_{i,j}^{nx}, 0 \right] + T_{i,j}^{nx}, \quad a_{i,j}^{sx} = \max \left[ F_{i,j}^{sx}, 0 \right] + T_{i,j}^{sx}, \\ a_{I,j}^{ey} = \max \left[ -F_{I,j}^{ey}, 0 \right] + T_{I,j}^{ey}, \quad a_{I,j}^{wy} = \max \left[ F_{I,j}^{wy}, 0 \right] + T_{I,j}^{wy}, \\ a_{I,j}^{ny} = \max \left[ -F_{I,j}^{ny}, 0 \right] + T_{I,j}^{ny}, \quad a_{I,j}^{sy} = \max \left[ F_{I,j}^{sy}, 0 \right] + T_{I,j}^{sy},$$

$$a_{i,j}^{nex} = T_{i,j}^{newx}, \quad a_{i,j}^{nwx} = T_{i,j}^{newx}, \quad a_{i,j}^{sex} = T_{i,j}^{sewx}, \quad a_{i,j}^{s wx} = T_{i,j}^{sewx}, \\ a_{I,j}^{ney} = T_{I,j}^{ensy}, \quad a_{I,j}^{nwy} = T_{I,j}^{wnsy}, \quad a_{I,j}^{sey} = T_{I,j}^{ensy}, \quad a_{I,j}^{s wy} = T_{I,j}^{wnsy},$$

$$a_{i,j}^{px} = a_{i,j}^{nx} + a_{i,j}^{ex} + a_{i,j}^{sx} + a_{i,j}^{wx} + F_{i,j}^{nx} + F_{i,j}^{ex} - F_{i,j}^{sx} - F_{i,j}^{wx} + T_{i,j}^{px} + a_0^{px}, \\ a_{I,j}^{py} = a_{I,j}^{ny} + a_{I,j}^{ey} + a_{I,j}^{sy} + a_{I,j}^{wy} + F_{I,j}^{ny} + F_{I,j}^{ey} - F_{I,j}^{sy} - F_{I,j}^{wy} + T_{I,j}^{py} + a_0^{py},$$

in which:

$$F_{i,j}^{ex} = \frac{1}{2} \rho (u_{i+1,J} + u_{i,J}) \delta y_{j,j+1}, \quad F_{i,j}^{wx} = \frac{1}{2} \rho (u_{i,J} + u_{i-1,J}) \delta y_{j,j+1}, \\ F_{i,j}^{nx} = \frac{1}{2} \rho (v_{I,j+1} + v_{I-1,j+1}) \Delta x_{I-1,I}, \quad F_{i,j}^{sx} = \frac{1}{2} \rho (v_{I,j} + v_{I-1,j}) \Delta x_{I-1,I}, \\ F_{I,j}^{ey} = \frac{1}{2} \rho (u_{i+1,J} + u_{i+1,J-1}) \Delta y_{J-1,J}, \quad F_{I,j}^{wy} = \frac{1}{2} \rho (u_{i,J} + u_{i,J-1}) \Delta y_{J-1,J}, \\ F_{i,j}^{ny} = \frac{1}{2} \rho (v_{I,j+1} + v_{I-1,j+1}) \Delta x_{I-1,I}, \quad F_{i,j}^{sy} = \frac{1}{2} \rho (v_{I,j} + v_{I-1,j}) \Delta x_{I-1,I},$$

$$a_0^{px} = \frac{\Delta x_{I-1,I} \delta y_{j,j+1}}{\Delta t}, \quad a_0^{py} = \frac{\Delta y_{J-1,J} \delta x_{i,i+1}}{\Delta t}, \\ \Delta x_{I-1,I} = x_I - x_{I-1}, \quad \Delta y_{J-1,J} = y_J - y_{J-1},$$

$$T_{i,j}^{px} = T_{i,j}^{ex} + T_{i,j}^{wx} + T_{i,j}^{sx} + T_{i,j}^{nx}, \quad \text{with } T_{i,j}^{\bullet} \text{ given in (3.28) and (3.29),} \\ T_{i,j}^{py} = T_{I,j}^{ey} + T_{I,j}^{wy} + T_{I,j}^{sy} + T_{I,j}^{ny}, \quad \text{with } T_{I,j}^{\bullet} \text{ given (3.30) and (3.32),}$$

and:

$$f_{i,j}^x = \frac{1}{2} \delta y_{j,j+1} \rho C_T' [U_k \cos(\gamma_k)]^2 \cos(\gamma_k + \varphi_k), \\ f_{I,j}^y = \frac{1}{2} \delta y_{J-1,J} \rho C_T' [U_k \cos(\gamma_k)]^2 \sin(\gamma_k + \varphi_k), \quad U_k = \sqrt{u_{i,j}^2 + v_{I,j}^2} \cos(\gamma_k).$$

### 3.B. PALM CASE STUDY

In this appendix, a resolved flow field for an arbitrarily chosen time step is depicted in Fig. 3.15 for the PALM case study presented in §3.4.2. Table 3.5 gives a summary of the PALM simulation set-up and Fig. 3.16 depicts the  $C_P/C_T$ -curve of one turbine simulated in PALM.

Table 3.5: Summary of the simulation set-up.

Domain size $L_x \times L_y \times L_z$	$19.2 \times 2.56 \times 1.28$ [km <sup>3</sup> ]	Turbine dimensions	$D=126$ [m], $z_h=90$ [m]
Grid size $N_x \times N_y \times N_z$	$1920 \times 256 \times 1280$	Turbine arrangement	$2 \times 1$
Cell size $\Delta x \times \Delta y$	$10 \times 10 \times 15$ [m <sup>2</sup> ]	Turbine spacing	$6D$
Sample period $\Delta t$	1 [s]	Atmospheric conditions	$u_b = 8, v_b = 0, w_b = 0$ [m/s], $\rho = 1.2$ [kg/m <sup>3</sup> ]
Simulation time $t$	1750 [s]	Inflow	uniform

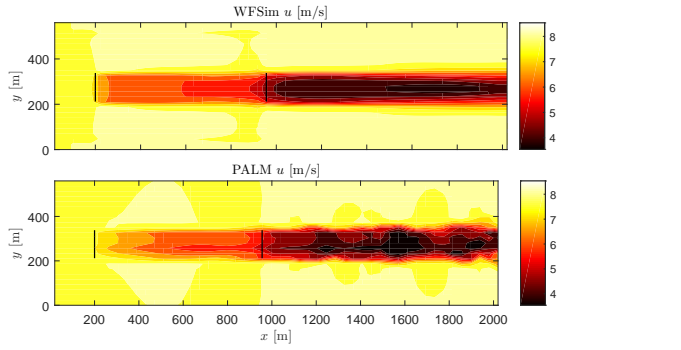


Figure 3.15: Flow field obtained with PALM (below) and WFSim at  $t = 750$  [s]. The black lines indicate the turbines.

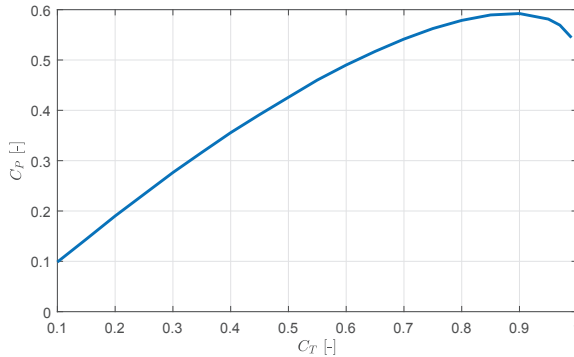


Figure 3.16:  $C_P/C_T$ -curve of one turbine simulated in PALM.

### 3.C. SOWFA CASE STUDY

In this appendix, a resolved flow field for an arbitrarily chosen time step is depicted for the SOWFA case study presented in §3.4.2. The SOWFA data set presented in (van Wingerden et al., 2017) is utilized.

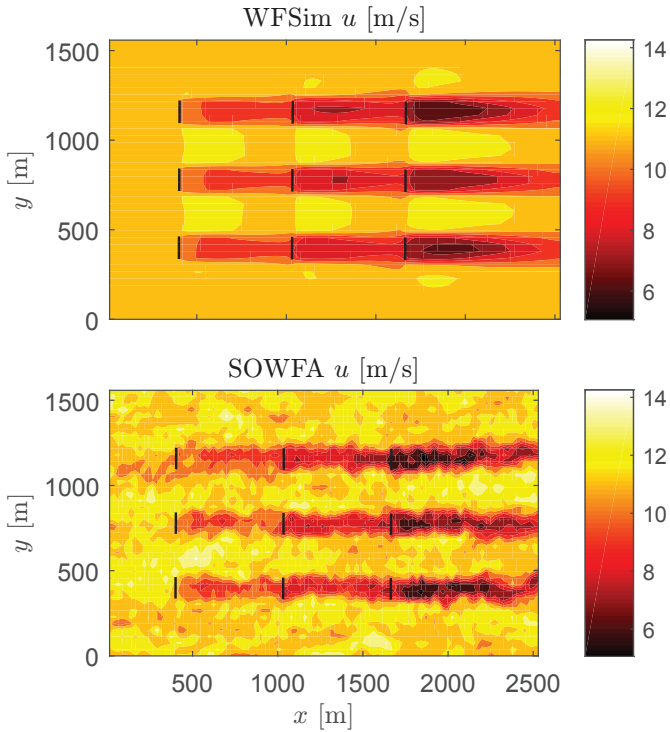


Figure 3.17: Flow field obtained with SOWFA (below) and WFSim at  $t = 250$  [s]. The black lines indicate the turbines.





# 4

## A CONSTRAINED WIND FARM CONTROLLER PROVIDING SECONDARY FREQUENCY REGULATION: AN LES STUDY

*Active power control for wind farms is needed to provide ancillary services. One of these services is to track a power reference signal with a wind farm by dynamically de- and up-rating the turbines. In this chapter we present a closed-loop wind farm controller that evaluates 1) thrust coefficients on a seconds-scale that provide power tracking and minimize dynamical loading on a farm level and 2) yaw settings on a minutes-scale that maximize the possible power that can be harvested by the farm. The controller is evaluated in a high-fidelity wind farm model. A six-turbine simulation case study is used to demonstrate the time-efficient controller for different controller settings. The results indicate that, with a power reference signal below the maximal possible power that can be harvested by the farm with non-yawed turbines, both tracking and reduction in dynamical loading can be ensured. In a second case study we illustrate that, when a wind farm power reference signal exceeds the maximal possible power that can be harvested with non-yawed turbines for a time period, it can not be tracked sufficiently. However, when solving for and applying optimized yaw settings, tracking can be ensured for the complete simulation horizon.*

## 4.1. INTRODUCTION

The trend towards clean energy is irreversible (Obama, 2017). A large part of the clean energy we are currently generating is harvested by wind farms that extract energy from the wind (WindEurope, 2018). A wind farm is a collection of wind turbines placed in each other's proximity to, *i.a.*, reduce maintenance and electricity cabling costs. However, a wake develops downstream of each turbine, which is a region that is characterized by a flow velocity deficit and an increased turbulence intensity (Barthelmie et al., 2007). Since wind turbines are placed together in a farm, the wakes of upstream turbines influence the performance of downstream turbines. For example, the flow velocity deficit influences the power production of downstream turbines (Barthelmie et al., 2010) while an increased turbulence intensity will increment the turbine's fatigue loads as suggested in (Rosen and Sheinman, 1995; Bossuyt et al., 2017), which possibly can reduce the turbine's lifetime. The objective of wind farm control is to reduce the levelized cost of wind energy by intelligently operating the turbines inside the farm. Subgoals may include the increase of the farm-wide power generation, the reduction of turbine fatigue, and the integration of energy from wind farms with the electricity grid. This integration is related to the provision of ancillary services. One example is secondary frequency regulation (a subclass of active power control) in which the objective is to have the wind farm's power generation track a power reference signal generated by transmission system operators, during a time span of several minutes (Ela et al., 2014). We call this power tracking and turbines need to increase and decrease their power output during this time span such that tracking at a farm level is ensured. Since the power reference signal is below the maximum possible power that can be harvested, the tracking problem has multiple solutions. For example, one could uprate the downstream turbines while derating the upstream turbines or the other way around while generating an equal amount of power with the farm. It is therefore possible and necessary to add, besides tracking, another performance measure, such as the decrease of load variations over time (dynamical loading) on the turbines and/or the increase of available power in the farm (see *e.g.*, (Siniscalchi-Minna et al., 2018a)). Two actuation methods to ensure these objectives are axial induction and wake redirection control. In the former, generator torques and pitch angles or thrust coefficients are utilized as control variables while in the latter, the yaw angles are utilized as control variables (Boersma et al., 2017).

Results that provide power tracking using axial induction actuation can be found in (Biegel et al., 2013; Spudić et al., 2014; Madjidian, 2016; Zhao et al., 2015; Siniscalchi-Minna et al., 2018b). More precisely, (Biegel et al., 2013) proposes a wind farm tracking solution that additionally reduces the turbine's tower and shaft bending moments. This controller utilizes turbine models to illustrate the controller's effectiveness, but is not tested in a wind farm simulation model. It is therefore uncertain whether the proposed solution works in a wind farm model. Then in (Spudić et al., 2014) and (Madjidian, 2016), the authors each propose a different wind farm power tracking solution while minimizing the axial force exerted by the flow on the turbines. However, as stated in (Bossuyt et al., 2017), the dynamical turbine loading is a better measure of fatigue than static turbine loading. In (Zhao et al., 2015), the authors propose a distributed controller providing tracking while minimizing variation in the axial force that is exerted by the turbine on the flow. In (Siniscalchi-Minna et al., 2018b), besides tracking, a power reference

distribution among the turbines is also found by the controller that maximizes the available power in the farm. The work presented in (Jensen et al., 2016) demonstrates an optimization algorithm that provides power tracking while minimizing the added turbulence intensity. However, all the above proposed controllers except for (Biegel et al., 2013) are tested in a simplified wind farm model (Grunnet et al., 2010), keeping the question open if similar results can be obtained when a more realistic dynamical wind farm model, such as a Large-Eddy Simulation (LES) based wind farm model, is utilized. The authors in (Bay et al., 2018) propose a tracking controller that contains a simplified wind farm model to evaluate control signals and the controller is tested in a simplified wind farm model. In this work, no additional objectives are considered and also, it remains questionable if the proposed controller will give similar results when tested in a more realistic simulation environment. A controller that is tested in an LES based wind farm model and employs axial induction actuation providing power tracking can be found in (Shapiro et al., 2017a). The therein solved optimization problem contains dynamical wake and turbine models, but the only objective is tracking and no constraint regarding, e.g., dynamical loading is included. Additionally, the authors state that it takes approximately 20 seconds to evaluate new control settings, which makes the proposed method not suitable for control on a seconds-scale. The controller presented in (van Wingerden et al., 2017) is also tested in an LES based simulator, but no wake model nor constraints were taken into account. The controller provides tracking and the wind farm power reference signal is distributed heuristically among the turbines without taking any measure of fatigue into account.

Time-varying yaw actuation has, to the best of our knowledge, yet to be employed in power tracking. However, this wake actuation method is utilized for the maximization of wind farm power generation in LES based simulations (Fleming et al., 2014a; Munters and Meyers, 2018a), a wind tunnel (Campagnolo et al., 2016b) and in a field test experiment (Fleming et al., 2017a).

From the above, we conclude that results obtained with a closed-loop controller that provides power tracking and dynamical load minimization in an LES based wind farm model and additionally increases the available wind farm power using yaw actuation are not yet available in current literature.

Therefore, in this work, a closed-loop reference power tracking solution is proposed in which 1) thrust coefficients that provide wind farm power tracking while minimizing dynamical turbine loading are evaluated for every second with a constrained model predictive controller (MPC) and 2) yaw settings that increase the available wind farm power can be evaluated every fifteen minutes in the situation where the farm's power generation has to be close to or above its upper limit, in order to increase the range of power reference signals that can be tracked. The MPC employs a dynamical wind farm model that is updated according to optimized yaw settings and rotor-averaged flow velocities, and solves for a constrained optimization problem that finds a distribution of the thrust coefficients among the turbines accordingly. This is different with respect to the previous work presented in (Boersma et al., 2018c) where a control signal distribution is imposed. When doing so, it is not possible to change controller settings to have the controller find a control signal distribution among the turbines that reduces, *i.e.*, dynamical turbine loading. In this work we investigate different controller settings and correspond-

ing control signal distributions that minimize dynamical turbine loading. Note that the dynamical wind farm model in this chapter is different from the model presented in Chapter 3. The latter includes wake dynamics, while it will be shown in this chapter that these dynamics are not necessary in the controller for providing power tracking. In addition to the MPC, if a reference will be above the maximum possible power extractable from the wind with zero yaw settings, the FLOW Redirection and Induction in Steady-state (FLORIS) tool (Gebraad et al., 2014) is employed to find optimal yaw settings that maximize the power that could be harvested from the wind with zero yaw settings. In addition to the proposed control strategy, another important contribution of this work is the controller evaluation in LES. For this, a software framework referred to as the PALM Supervisory Controller is developed that allows for programming controllers in a controller friendly software environment and their evaluation in the PARallelized Large-eddy simulation Model (PALM) (Maronga et al., 2015), an LES based wind farm model. Hence this work is more focused on controller evaluation in a more realistic wind farm flow model.

This chapter is organised as follows. In Section 4.2, the developed PALM Supervisory Controller is introduced and a brief explanation of the PALM itself is presented. Then in Section 4.3, a description of the employed surrogate models is given and in Section 4.4, the wind farm controller is formally introduced. Simulation results are presented in Section 4.5. More precisely, in §4.5.3, results obtained with different controller settings are compared and we show that these can influence the control signal distribution among the turbines. Consequences with respect to tracking behaviour and dynamical turbine loading are also presented. Then, in §4.5.4, we illustrate the potential of including yaw actuation when power generation has to be close to or above its upper limit. In §4.5.5 and §4.5.6, the proposed controller is tested against changes in the atmospheric conditions and an unexpected turbine shut down, respectively. The mean computation time of the controller as function of the number of turbines is investigated in §4.5.8 and this chapter is concluded in Section 4.6.

## 4.2. SIMULATION MODEL

The true wind farm is replaced by the high-fidelity “PARallelized Large-eddy simulation Model (PALM)” (Maronga et al., 2015), because 1) a wind farm is not available and 2) in a high-fidelity model, controller settings can be compared under exactly equivalent atmospheric conditions, which is not possible in a real wind farm. PALM is programmed in FORTRAN, while almost all academic wind farm control algorithms are implemented in MATLAB or Python. One of the contributions of this work is the development of the PALM Supervisory Controller, which provides a communication interface between PALM and wind farm controllers implemented in MATLAB. This allows the straightforward evaluation of such control algorithms in a high-fidelity simulation environment. In §4.2.1, a brief summary of PALM is given. Then in §4.2.2, the PALM Supervisory Controller is introduced and in §4.2.3, the specific controller implementation used throughout this work is given.

### 4.2.1. THE PARALLELIZED LARGE-EDDY SIMULATION MODEL

PALM is an meteorological model for atmospheric and oceanic boundary-layer flows. It has been developed as a turbulence-resolving large-eddy simulation (LES) model and is open source, available in the public domain (Leibniz Universität Hannover, 2018). In the LES approach, only the large eddies are simulated due to spatially filtering the Navier-Stokes equations. The dynamic influence of the small turbulent scales are consequently not resolved, but their influence is accounted for with a so called subgrid model. PALM is based on the unsteady, filtered, incompressible Navier-Stokes equations and the subgrid-scale turbulent kinetic energy (SGS-TKE) model (Deardorff, 1980). PALM can simulate the effect of the Coriolis forces and if non-cyclic boundary conditions are imposed, PALM can generate time-dependent turbulent inflow data by using a turbulence recycling method (see (Maronga et al., 2015)). The resolved equations are discretized using finite differences on a staggered grid. Examples of embedded models for PALM are a land surface model, canopy model, radiation models and wind turbine models. The latter is employed in this work. Two different turbine models are available in PALM. The actuator disk model (ADM) (Betz, 1926) and the rotating actuator disk model (ADM-R) (Dörenkämper et al., 2015). Both these turbine models can be utilized with the PALM Supervisory Controller that is discussed in the following section.

### 4.2.2. PALM SUPERVISORY CONTROLLER

The Supervisory Controller is a MATLAB/FORTRAN interface that allows for communicating with a wind farm controller implemented in MATLAB. This communication infrastructure is used for evaluating control signals by using measurements from PALM. A schematic representation is depicted in Fig. 4.1, where  $\mathcal{Y}$  is the set of available measurements and  $\mathcal{U}$  the set of control signals. The content of these sets depend on the employed turbine model, on the assumed measurements, and on the control signals sent from the wind farm controller. Table 4.1 gives all the possible options.

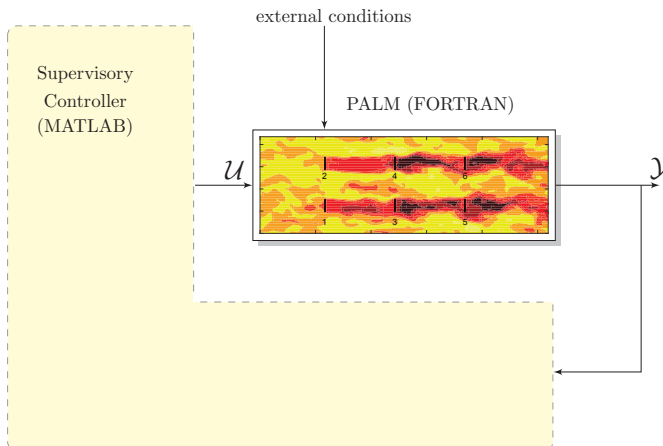


Figure 4.1: Schematic representation of the PALM Supervisory Controller. The signals  $\mathcal{Y}$  and  $\mathcal{U}$  are the measurements and control signals, respectively. External conditions are, *i.e.*, boundary conditions.

Table 4.1: Available set of measurements  $\mathcal{Y}$  and control signals  $\mathcal{U}$  for the different turbines models.

PALM+ADM	
$\mathcal{Y}$	wind velocities, generated turbine power, axial force
$\mathcal{U}$	thrust coefficient, yaw angle
PALM+ADM-R	
$\mathcal{Y}$	wind velocities, generated turbine power, axial force, generator speed
$\mathcal{U}$	generator torque, pitch angle, yaw angle

Note again that the developed framework is suitable for any controller programmed in MATLAB and that the developed software is available in the public domain (Boersma, 2018a). Examples where it has already been utilized can be found in (Boersma et al., 2018c; Raach et al., 2018). The specific implementation of the Supervisory Controller used in this work is discussed in the following section.

#### 4.2.3. SUPERVISORY CONTROLLER IMPLEMENTATION PROPOSED IN THIS WORK

In this work, PALM includes the ADM to determine the turbine's forcing terms acting on the flow and power generation. This turbine model is efficient due its lower requirements of grid resolution and coarser allowed time-stepping as compared to having to resolve detailed flow surrounding rotating blades (Meyers and Meneveau, 2010). A consequence of choosing the ADM is that the control signals for turbine  $i$  are the disk-based thrust coefficient  $C'_{T_i}(t)$  following (Meyers and Meneveau, 2010; Boersma et al., 2018b) and yaw angle  $\gamma_i(t)$ . Both of these signals can be used to manipulate the turbine thrust force and power generation (see (4.2)). In this work, the measurements at time  $t$  are 1) the axial force that a turbine exerts on the flow  $F_i(t)$ , 2) the power generated by a turbine  $P_i(t)$  and 3) the rotor-averaged wind velocity  $v_i(t)$  for  $i = 1, 2, \dots, \aleph$  with  $\aleph$  the number of turbines. The rotor-averaged wind velocity is assumed to be known, which could be realized by employing online estimation of the rotor-averaged wind velocity with techniques as presented in (Simley and Pao, 2014; Shapiro et al., 2017b; Doekemeijer et al., 2018). This is however outside the scope of this work. The above defines the sets of measurements and control signals as follows:

$$\mathcal{Y} = \{F_i(t), P_i(t), v_i(t)\}, \quad \mathcal{U} = \{C'_{T_i}(t), \gamma_i(t)\}, \quad \text{for } i = 1, \dots, \aleph \quad (4.1)$$

Figure 4.2 illustrates the specific controller architecture programmed in the Supervisory Controller. The architecture contains two closed loops with in one loop a model predictive controller (MPC) containing a dynamical surrogate model of the wind farm and in the other loop a wind farm controller containing a steady-state surrogate model of the wind farm. The former regulates the thrust coefficients on the seconds-scale to provide power reference tracking, while the latter is utilized when it is desired to increase the available power in the farm. The following section will detail both the dynamical and

steady-state surrogate models.

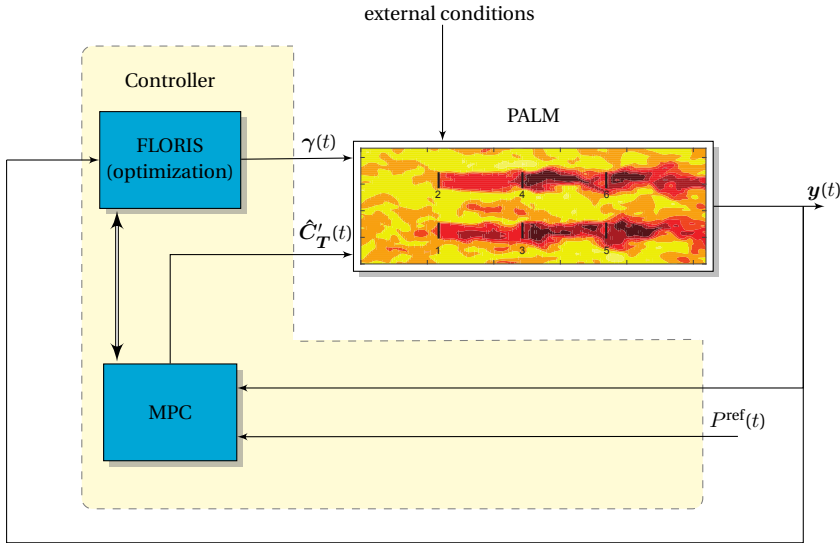


Figure 4.2: Proposed closed-loop control framework with measurements  $\mathbf{y}(t)$  and power reference signal for the farm  $P^{\text{ref}}(t)$ . The control signals are the filtered thrust coefficients  $\hat{C}'_T(t)$  and yaw angles  $\gamma(t)$ . The vertical arrow connecting the MPC and FLORIS represents the information exchange between the different parts of the controller.

## 4.3. CONTROLLER MODELS

The closed-loop controller proposed in this work contains two different surrogate models. Both are in the feedback loop (see Fig. 3.1), but work on different time scales, in different situations and with different control signals. The first loop contains an MPC employing a dynamical wind farm model. This controller works on the seconds-scale and its goal is to track a wind farm reference power signal using the filtered thrust coefficients  $\hat{C}'_T(t)$  as control signals (see Fig. 3.1). The dynamical model used for this control loop is detailed in §4.3.1. The objective of the second control loop is to, when there will not be enough energy in the farm, increase the possible power that can be harvested by finding yaw settings  $\gamma(t)$ . This loop is working on the minutes-scale and employs the FLORIS optimization tool, which utilizes a steady-state model that is detailed in §4.3.2.

### 4.3.1. DYNAMICAL MODEL

An MPC is based on the receding horizon principle in which a constrained optimization problem is solved at each time step using future predictions of the system and it therefore needs a dynamical model. Additionally, we require a computationally efficient model of the wind farm dynamics because we control on the seconds-scale. Yet, due to nonlinear dynamics, uncertain atmospheric conditions and wind farm model dimensions, it is challenging to obtain such a dynamical wind farm model suitable for control. Examples of computationally expensive dynamical control-oriented wind farm models



can be found in (Boersma et al., 2018b; Shapiro et al., 2017a). However, axial induction based wind farm power tracking results that are presented in (van Wingerden et al., 2017; Boersma et al., 2018c) indicate that flow dynamics could be neglected and a wind farm can be modelled as  $\aleph$  uncoupled subsystems, each subsystem consisting of a dynamical turbine model that is based on the actuator disk theory. While wake effects are neglected in the surrogate dynamical model, the turbine dynamics are still affected by the local flow conditions. Hence, the turbine models are updated according to the local rotor-averaged wind velocity, which in reality may or may not be affected by other turbines inside the farm. In this work, the following model for turbine  $i$  is employed

$$\begin{aligned} P_i(t) &= \frac{\pi D^2}{8} \left( v_i(t) \cos[\gamma_i(t)] \right)^3 \hat{C}'_{T_i}(t), \\ F_i(t) &= \frac{\pi D^2}{8} \left( v_i(t) \cos[\gamma_i(t)] \right)^2 \hat{C}'_{T_i}(t), \\ C'_{T_i}(t) &= \tau \frac{d\hat{C}'_{T_i}(t)}{dt} + \hat{C}'_{T_i}(t), \end{aligned} \quad (4.2)$$

for  $i = 1, 2, \dots, \aleph$ , with  $P_i(t)$  the generated power,  $F_i(t)$  the axial force that flow exerts on turbine  $i$ ,  $C'_{T_i}(t)$  the control signal,  $\hat{C}'_{T_i}(t)$  the first-order filtered control signal,  $\gamma_i(t)$  the yaw angle and  $v_i(t)$  the rotor-averaged wind speed perpendicular to the rotor. Notice that  $v_i(t)$  is, *i.a.*, influenced by the upstream turbine settings through wake propagation. We furthermore have  $\tau \in \mathbb{R}^+$ , the time constant of the filter that acts on the control signal such the applied control signal is smooth. Temporally discretizing (4.2) at sample period  $\Delta t$  using the zero-order hold method yields the following state-space representation of turbine  $i$

$$\mathbf{x}_{i,k+1} = A_i \mathbf{x}_{i,k} + B_i(v_{i,k}, \gamma_{i,k}) C'_{T_i,k}, \quad \mathbf{y}_{i,k} = \mathbf{x}_{i,k}, \quad (4.3)$$

with

$$\begin{aligned} A_i &= e^{-\Delta t/\tau} I_3 \in \mathbb{R}^{3 \times 3}, \quad B_i(v_{i,k}, \gamma_{i,k}) = \int_0^{\Delta t} e^{-s/\tau} ds \begin{pmatrix} \frac{\pi D^2}{8} \left( v_i(t) \cos[\gamma_i(t)] \right)^2 \\ \frac{\pi D^2}{8} \left( v_i(t) \cos[\gamma_i(t)] \right)^3 \\ 1/\tau \end{pmatrix} \in \mathbb{R}^3, \\ C'_{T_i,k} &\in \mathbb{R}, \quad \mathbf{x}_{i,k}^T = \left( F_{i,k} \quad P_{i,k} \quad \hat{C}'_{T_i,k} \right) \in \mathbb{R}^3, \quad \mathbf{y}_{i,k} \in \mathbb{R}^3. \end{aligned} \quad (4.4)$$

Lifting the state variables of the turbines and adding the wind farm power error signal to the state variable results in the following wind farm state-space model:

$$\mathbf{x}_{k+1} = A \mathbf{x}_k + B_u(\mathbf{v}_k, \boldsymbol{\gamma}_k) C'_{T,k} + B_r P_k^{\text{ref}}, \quad \mathbf{y}_k = \mathbf{x}_k, \quad (4.5)$$

which is a linear parameter-varying system due to the varying matrix  $B(\mathbf{v}_k, \boldsymbol{\gamma}_k)$ . Furthermore we have:

$$\begin{aligned} \mathbf{x}_k^T &= (\mathbf{x}_{1,k} \quad \mathbf{x}_{2,k} \quad \dots \quad \mathbf{x}_{\mathbb{N},k} \quad e_k) \in \mathbb{R}^{3\mathbb{N}+1}, \\ \mathbf{v}_k^T &= (v_{1,k} \quad v_{2,k} \quad \dots \quad v_{\mathbb{N},k}) \in \mathbb{R}^{3\mathbb{N}}, \\ C'_{T,k} &= \left( C'_{T_1,k} \quad C'_{T_2,k} \quad \dots \quad C'_{T_{\mathbb{N}},k} \right)^T \in \mathbb{R}^{\mathbb{N}}, \\ \hat{C}'_{T,k} &= \left( \hat{C}'_{T_1,k} \quad \hat{C}'_{T_2,k} \quad \dots \quad \hat{C}'_{T_{\mathbb{N}},k} \right)^T \in \mathbb{R}^{\mathbb{N}}, \quad e_k, P_k^{\text{ref}} \in \mathbb{R} \\ \bar{A}_1 &= \text{blkdiag}(A_1, A_2, \dots, A_{\mathbb{N}}) \in \mathbb{R}^{3\mathbb{N} \times 3\mathbb{N}}, \\ \bar{A}_2 &= \begin{pmatrix} 0 & -1 & 0 & \dots & 0 & -1 & 0 \end{pmatrix} \in \mathbb{R}^{1 \times 3\mathbb{N}}, \quad A = \begin{pmatrix} \bar{A}_1 & 0 \\ \bar{A}_2 & 0 \end{pmatrix}, \\ B_u^1(\mathbf{v}_k, \boldsymbol{\gamma}_k) &= \text{blkdiag}(B_1(v_{1,k}, \gamma_{1,k}), B_2(v_{2,k}, \gamma_{2,k}), \dots, B_{\mathbb{N}}(v_{\mathbb{N},k}, \gamma_{\mathbb{N},k})) \in \mathbb{R}^{3\mathbb{N} \times \mathbb{N}}, \\ B_u^2 &= \begin{pmatrix} 0 & 0 & \dots & 0 & 0 \end{pmatrix} \in \mathbb{R}^{1 \times \mathbb{N}}, \quad B_u = \begin{pmatrix} B_u^1(\mathbf{v}_k, \boldsymbol{\gamma}_k) \\ B_u^2 \end{pmatrix}, \\ B_r &= \begin{pmatrix} 0 & 0 & \dots & 0 & 1 \end{pmatrix}^T \in \mathbb{R}^{3\mathbb{N}+1 \times 1}, \end{aligned}$$

where  $\text{blkdiag}(\cdot)$  denotes block diagonal concatenation of matrices or vectors. Furthermore we have the wind farm power reference signal  $P_k^{\text{ref}}$  and tracking error signal  $e_k$ . The model described above will be employed in the controller part presented in §4.4.1.

### 4.3.2. STEADY-STATE MODEL

For the evaluation of the steady-state yaw angles that increase the possible power that can be harvested, the FLOW Redirection and Induction in Steady-state (FLORIS) tool is utilized, which is a low-fidelity steady-state wind farm model and it can be used for the purpose of wind farm control, offline analysis and layout optimization. The most recent version is based on the analytical wake model inspired by Bastankhah and Porté-Agel (Bastankhah and Porté-Agel, 2016) and employed in this work. The interested reader is referred to (Bastankhah and Porté-Agel, 2016) or (Boersma et al., 2018a) for a derivation of the steady-state model that will be employed in the controller as described in §4.4.2.

## 4.4. CONTROL STRATEGY

The proposed closed-loop controller executes two tasks. The first task is executed on the seconds-scale and solves a finite-time constrained predictive optimization problem using the model defined in §4.3.1 assuming full knowledge of the powers, axial forces and rotor-averaged wind velocities. The main objective is to provide power tracking on a farm level. The second task is executed on a 15-minutes scale and consists of an optimization procedure using the steady-state surrogate model defined in §4.3.2 assuming full knowledge of the measured wind direction. The main objective is to increase the possible power extractable from the wind by finding optimal yaw settings. However, the second task will only be executed when the future wind farm reference signal will be above

the maximal possible extractable wind farm power such that unnecessary yaw actuation and consequently potential additional loading (Damiani et al., 2017) will not occur. If more than the maximal possible extractable wind farm power with zero yaw settings is demanded from the farm, optimal yaw settings can be evaluated and applied with the additional second loop. The first and second task will be detailed in §4.4.1 and §4.4.2, respectively.

#### 4.4.1. AXIAL INDUCTION CONTROL FOR POWER TRACKING

The aforementioned MPC is stated to solve the following optimization problem from time  $k_0$  until the prediction horizon  $k_0 + N_h$

$$\min_{C'_{T,k}} \sum_{k=k_0}^{k_0+N_h} e_k^T Q e_k + (F_k - F_{k-1})^T S (F_k - F_{k-1}) \quad (4.6a)$$

$$\text{s.t. } \mathbf{x}_{k+1} = A \mathbf{x}_k + B_u(\mathbf{v}_{k_0}, \gamma_{k_0}) C'_{T,k} + B_r P_k^{\text{ref}}, \quad \mathbf{P}_k \leq \mathbf{P}_{\max}, \quad (4.6b)$$

$$C'_{T,\min} \leq C'_{T_i,k} \leq C'_{T,\max}, \quad |C'_{T_i,k} - C'_{T_i,k-1}| < dC'_{T_i}, \quad (4.6c)$$

with

$$\mathbf{F}_k = (F_{1,k} \quad F_{2,k} \quad \dots \quad F_{N,k})^T \in \mathbb{R}^N, \quad \mathbf{P}_k = (P_{1,k} \quad P_{2,k} \quad \dots \quad P_{N,k})^T \in \mathbb{R}^N,$$

$$\mathbf{P}_{\max} = (P_{1,k_0}^{\text{av}} \quad P_{2,k_0}^{\text{av}} \quad \dots \quad P_{N,k_0}^{\text{av}})^T \in \mathbb{R}^N, \quad e_k = P_k^{\text{ref}} - \sum_{i=1}^N P_{i,k} \in \mathbb{R},$$

and

$$P_{i,k_0}^{\text{av}} = \frac{\pi D^2}{8} (v_{i,k_0} \cos[\gamma_{i,k_0}])^3 C'_{T,\max} \in \mathbb{R}. \quad (4.7)$$

Furthermore,  $C'_{T,\max}$ ,  $C'_{T,\min}$ ,  $dC'_{T_i}$  and  $\mathbf{P}_{\max}$  represent the upper and lower bounds on the thrust coefficients, its variation and upper bound on the turbines power generation, respectively, and  $\gamma_{k_0}$  and  $\mathbf{v}_{k_0}$  the yaw angles and measured rotor-averaged wind velocity at time  $k_0$ , respectively. Note that a constraint on the thrust coefficients is already an indirect constraint on the turbine power signals. However, this generalized framework is beneficial, as it will allow us to investigate different constraints on the power generation of each turbine in future work. We furthermore have the weighting matrices

$$Q = q \in \mathbb{R}, \quad S = I_N \cdot s \in \mathbb{R}^{N \times N} \quad (4.8)$$

with  $q, s \in \mathbb{R}$  controller tuning variables. In fact, by tuning each weight one can increase or decrease the importance of the corresponding term in the cost function. More specifically, by increase the weight  $s$  relative to  $q$ , the controller puts more effort in minimizing the dynamical turbine loading. We would like to stress here that the optimization problem defined in (4.6) tries to find a distribution of control signals among the turbines, such that the tracking error and dynamical loading are minimized. This is different with respect to the work presented in (Boersma et al., 2018c) in which a distribution is imposed before the optimization routine. Clearly, by not imposing a distribution manually as done in this work, the controller is given relatively more freedom to find control signals that minimize tracking error and dynamical loading.

#### 4.4.2. AXIAL INDUCTION CONTROL FOR POWER TRACKING WITH OPTIMIZED YAW SETTINGS

The optimization algorithm described in this paragraph relies on the FLORIS tool described in §4.3.2. In practice, first it is predicted whether the wind farm reference can be tracked for the upcoming 15 minutes.<sup>1</sup> A method to do this could be by taking the maximum value among the upcoming reference signal over a 15 minute horizon and then estimate the available power using an algorithm such as presented in (Göçmen et al., 2014). In this work we are not investigating such a method, but if it is possible to track the wind farm reference signal over the upcoming 15 minutes, then the turbines are yawed in alignment with the mean wind direction (zero yaw settings) so that no unnecessary yaw actuation will occur. However, when it is estimated that tracking will not be ensured, first the steady-state surrogate model should be adjusted to match the present atmospheric conditions inside the farm such as for example demonstrated in (Bottasso and Schreiber, 2018). These atmospheric conditions such as wind direction could be estimated using, e.g., SCADA data and lidar measurements (Raach et al., 2018). Subsequently, the following optimization problem is solved following an interior point method to address the nonlinearity and nonconvexity of the problem:

$$\gamma^* = \operatorname{argmin}_{\gamma^{\text{ss}}} \left( - \sum_{i=1}^{\aleph} P_i^{\text{ss}}(\gamma^{\text{ss}}) \right), \quad (4.9a)$$

$$\text{s.t.} \quad -25^\circ \leq \gamma_i^{\text{ss}} \leq 25^\circ, \quad \text{for } i = 1, \dots, \aleph, \quad (4.9b)$$

where  $\gamma^{\text{ss}} = (\gamma_1^{\text{ss}} \quad \gamma_2^{\text{ss}} \quad \dots \quad \gamma_{\aleph}^{\text{ss}})^T$ . The yaw angle is constrained to suppress the increase in structural loading for strongly yawed turbines (Damiani et al., 2017). The optimal yaw settings,  $\gamma^*$ , are then distributed to the turbines and turbine models (see (4.2)), and maintained for a fifteen minute period, upon which the above described cycle is repeated. The steady-state power expression is defined as

$$P_i^{\text{ss}} = \left( \frac{\pi D^2}{8} \right) \cdot \left( v_i^{\text{ss}} \cos[\gamma_i^{\text{ss}}] \right)^3 \cdot \overline{C}_{T_i}'. \quad (4.10)$$

For more details, the reader is referred to Bastankhah and Porté-Agel (2016); Boersma et al. (2018a).

## 4.5. SIMULATION RESULTS

PALM simulation results are all of a neutral atmospheric boundary layer and will be discussed in this section. In all simulation cases, the controller is applied to a wind farm with specifications as described in Table 4.2. A  $C_P/C_T$ -curve of a single turbine is depicted in Fig 3.16.

The time constant  $\tau$  is chosen following (Munters and Meyers, 2017) and as a consequence, no fast dynamics such as structural vibrations are captured with the turbine model. However, it results in smooth control signals that are fed to the turbines in PALM.

<sup>1</sup>The necessity of using optimized yaw settings or non-yawed turbines to track the future reference is evaluated every 15 minutes, but this time-span can be adapted according to atmospheric conditions. Additionally, it is assumed that the reference is known for the upcoming 15 minutes throughout this work.

Table 4.2: Summary of the simulation set-up.

$L_x \times L_y \times L_z$	$15.3 \times 3.8 \times 1.3 \text{ [km}^3\text{]}$	$D, z_h$	120, 90 [m]
$\Delta x \times \Delta y \times \Delta z$	$15 \times 15 \times 10 \text{ [m}^3\text{]}$	Turbine spacing	$5D \times 3D$ [m]
$\Delta t$	1 [s]	$U_\infty, V_\infty, W_\infty$	8, 0, 0 [m/s]
$N, \tau, N_h$	850, 5, 10 [s]	$\text{TI}_\infty$ ,	6%
$C'_{T,\max}, C'_{T,\min}, dC'_T$	2, 0.1, 0.2		

The prediction horizon  $N_h$  is found after tuning the controller. The influence of  $\tau, N_h$  is not further investigated in this work. The value for  $C'_{T,\max}$  corresponds to the Betz-optimal value and hence no overinductive axial induction control is considered. Furthermore,  $C'_{T,\min} = 0.1$  indicating that we do not allow turbines to shut down completely, which is common practice in wind farms. The bound on the thrust coefficient variation  $dC'_T = 0.2$  is set such that turbines can not de- and uprate instantaneously, but it also provides an upper and lower bound on the maximum allowable dynamical loading (see (4.2)).

The topology under consideration is illustrated in Fig. 4.3 and contains heavily waked wind turbines due to the fact that turbines are aligned with the mean wind direction. Although farms are designed such that the occurrence of this situation is minimized, it remains an interesting case study to investigate farm dynamics in these worst case scenarios (Fleming et al., 2016a). This section is organised as follows. Firstly in §4.5.1, two performance measures are introduced such that controllers with different settings can be evaluated. Secondly, in §4.5.2, a brief summary on how PALM is initialized is given. In §4.5.3, we investigate the influence of the controller parameter  $s$  (see (4.8)) on the tracking performance, the dynamical loading and consequently the differences between the found control signal distributions. Then in §4.5.4, we illustrate by example that a wind farm power reference signal that temporarily exceed the maximal possible extractable wind farm power with zero yaw can be tracked when yawing turbines in an optimized way.

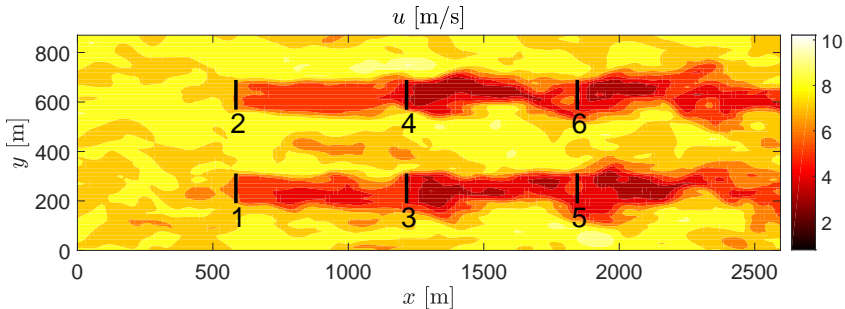


Figure 4.3: Initial longitudinal flow velocity component at hub-height. The flow is going from west to east and the black vertical lines represent the wind turbines.

### 4.5.1. PERFORMANCE MEASURES

In order to evaluate the controller performance under different settings, two criteria is introduced.

$$dF_i = \sum_{k=1}^N (F_{i,k} - F_{i,k-1})^2, \quad \text{for } i = 1, \dots, \aleph \quad \text{and,} \quad dF = \sum_{i=1}^{\aleph} dF_i. \quad (4.11)$$

The turbine performance index,  $dF_i$ , represents the turbine's force variations and the quantity  $dF$  represents the force variations on a farm level, both evaluated over the complete simulation horizon. Clearly, a lower performance index indicates less force variations over the simulation horizon.

### 4.5.2. SIMULATION INITIALIZATION

Simulations are initialized as follows: a fully developed flow field is generated in the precursor such that the free-stream wind speeds are  $U_\infty=8$  [m/s] and  $V_\infty=W_\infty=0$  [m/s] in the longitudinal, lateral and vertical direction, respectively, and a turbulence intensity in front of the farm of approximately 6% at hub-height in front of the wind farm (see 4.A for definition of turbulence intensity used in this work). Then, for the specific topology considered in this work, the flow is propagated  $N$  seconds in advance with  $C'_{T_i,k} = 2$  (corresponding to the Betz-optimal value) and  $\gamma_{i,k} = 0$  for  $i = 1, \dots, \aleph$  for the complete  $N$  seconds so that the wakes are fully developed. Here, non-cyclic boundary conditions and time-dependent turbulent inflow data are imposed by using a turbulence recycling method (Maronga et al., 2015). The flow field obtained after these  $N$  seconds is utilized as initial flow field (see Fig. 4.3) for the simulation results presented in this work.

The greedy power ( $P^{\text{greedy}}$ ) is defined as the time-averaged wind farm power harvested with  $C'_{T_i,k} = 2$  and  $\gamma_{i,k} = 0$  for  $i = 1, \dots, \aleph$  and  $N$  seconds of simulation starting with the previous described initial flow field. With unyawed turbines, a wind farm can potentially harvest above the  $P^{\text{greedy}}$  threshold for only a relatively short period of time. Clearly, this period is defined by the wake propagation time. In this work,  $P^{\text{greedy}}$  is defined as the maximal possible extractable wind farm power.

### 4.5.3. POWER TRACKING WHILE MINIMIZING DYNAMICAL TURBINE LOADING

In this section, the controller parameter  $s$  is varied so that its influence on the previously defined performance measures and control signal distribution can be studied. The value of controller parameter  $q = 10^4$  is found after tuning such that tracking is ensured. The wind farm power reference signal is defined as:

$$P_k^{\text{ref}} = 0.7P^{\text{greedy}} + 0.2P^{\text{greedy}} \delta P_k, \quad (4.12)$$

with  $\delta P_k$  a normalized ‘‘RegD’’ type AGC signal (Pilong, 2013) coming from an operator and  $P^{\text{greedy}} \approx 7.5$  [MW]. As can be seen in (4.12), the reference will never exceed  $P^{\text{greedy}}$  during the simulation period and hence turbines are in derate mode for the complete simulation period. Consequently, the problem described in §4.4.1 is exclusively solved with Yalmip and CPLEX to provide power tracking, and the problem described in §4.4.2

is not due to the fact that it is possible to track the reference signal given in (4.12) with unyawed turbines over the complete simulation horizon.

In Fig. 4.4, it can be observed that tracking is ensured for all presented cases and hence we can conclude that, for the presented cases, the controller parameter  $s$  does not have a significant impact on the tracking performance. However, in Fig. 4.5, it can be seen that the performance index  $dF$  as defined in (4.11) reduces when  $s$  increases indicating that dynamical loading can be reduced on a farm level. This is expected since  $dF$  can be found in the controller's objective function as defined in (4.6). However, Fig. 4.5 also depicts the turbine's performance indices as defined in (4.11), and it can be observed that, although dynamical loading on a farm level is reduced, it can increase for specific turbines in the farm (see for example turbine 5). We note, but do not show, that for  $s > 50$  no significant changes in the dynamical loading can be observed.

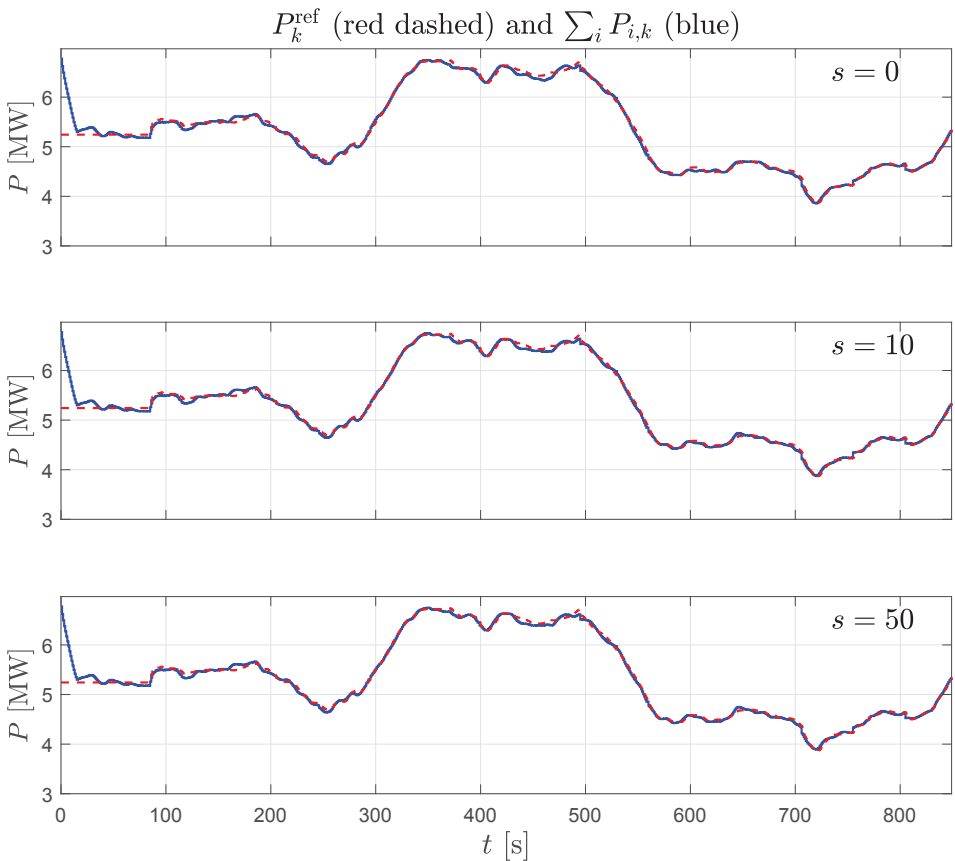


Figure 4.4: Wind farm power and reference for different controller settings  $s$ .

Furthermore, from Fig. 4.6 it can be concluded that the control signal distribution significantly changes for a varying controller parameter  $s$ . In fact, an increasing penalty on the dynamical loading results in a decrease of the downstream thrust coefficients,

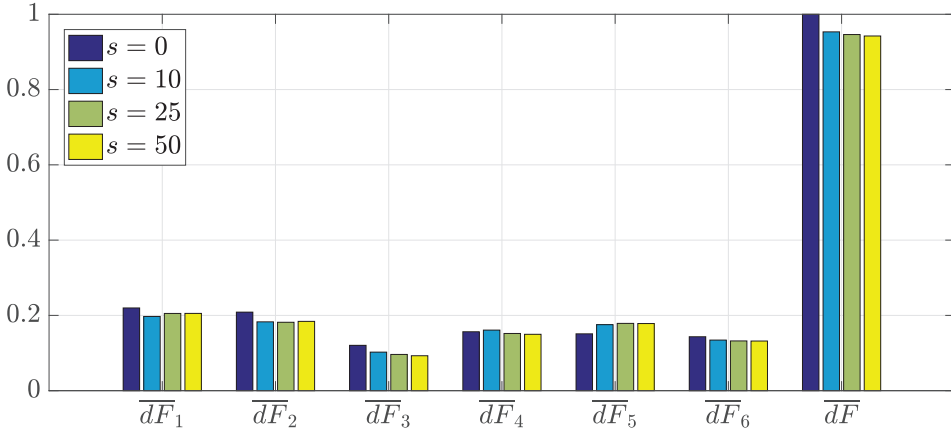


Figure 4.5: Normalized performance indices as defined in (4.11) for different controller settings  $s$ .

while upstream turbines receive increased thrust coefficients. The latter results in a decreased rotor-averaged flow velocity and its variation, which reduces the fatigue loading (see (4.2)). In other words, the dynamical loading of the upstream turbines is reduced when increasing the weight  $s$ , while such a simple relation can not be observed for the downstream turbines. This could possibly be due to the complex wake dynamics that influence the dynamical loading of the downstream turbines. However, Fig. 4.5 indicates that, on a farm level, the dynamical loading is reduced when increasing  $s$ , which is expected since the weight  $s$  increases the penalty on the sum of the individual turbine dynamical loading (see 4.6). Figure 4.7 additionally depicts the turbine power signals for different controller settings. We observe that in all cases, the upstream turbines produce relatively the most power since the wind speed in front of these turbines is the highest and that an increase in  $s$  results in incremental power production of the upstream turbines.

#### 4.5.4. POWER TRACKING WITH OPTIMIZED YAW SETTINGS

In this section, the controller is evaluated with the following reference signal

$$P_k^{\text{ref}} = 0.8P^{\text{greedy}} + 0.5P^{\text{greedy}}\delta P_k. \quad (4.13)$$

Observe that, for a period, more power is demanded from the farm than the averaged power harvested under greedy control. Consequently, the optimization problem described in §4.4.2 is solved firstly for the measured wind direction and topology under consideration to increase the maximum possible power that can be harvested by the farm. Solving the problem given in (4.9) takes approximately 30 seconds on a regular notebook and single i7 core. The optimized yaw settings were found to be

$$\gamma_k^* = (-24.3 \quad -24.3 \quad -16.2 \quad -16.2 \quad 0 \quad 0)^T \text{ [deg]}. \quad (4.14)$$

These yaw settings are kept constant throughout the simulation case presented in this section and applied instantaneously in the initial flow field. See Fig. 4.8 for instantana-



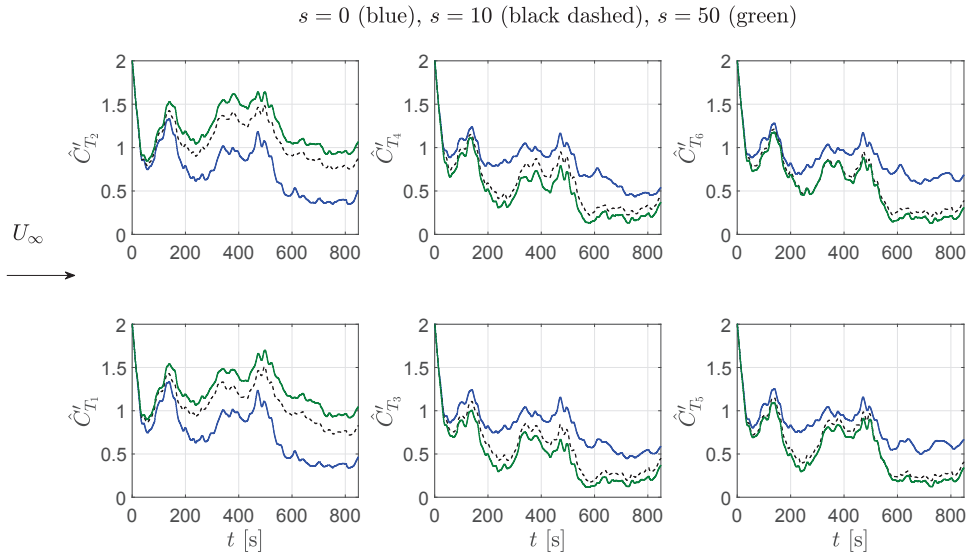


Figure 4.6: Thrust coefficients for different controller settings  $s$ . The arrow on the left indicates the wind direction.

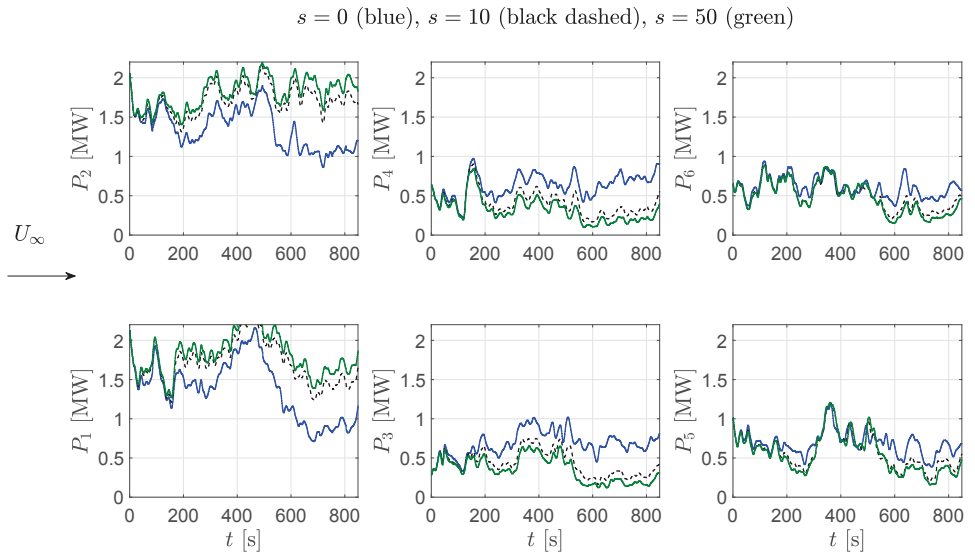


Figure 4.7: Turbine power signals for different controller settings  $s$ . The arrow on the left indicates the wind direction.

neous longitudinal flow velocity components at hub-height. Note that we assume no deviation of the mean wind direction and free-stream wind speed during the simulation period since we update yaw settings every 15 minutes.

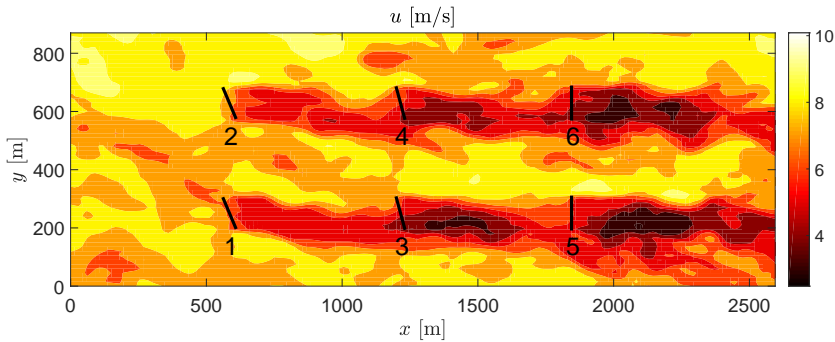


Figure 4.8: Instantaneous longitudinal flow velocity component at hub-height at  $t = 600$  [s]. The flow is going from west to east and the black vertical lines represent the wind turbines.

Secondly, the problem described in §4.4.1 is solved during the complete simulation horizon and power tracking is provided with yawed turbines. On a regular note book and single core, it takes approximately 0.07 seconds to solve the problem described in §4.4.1. Hence, due to the fact that the sample time is chosen to be one second, online power tracking can be achieved. The controller parameters  $q, s$  were found after tuning such that tracking is ensured and set to  $q = 10^4, s = 25$ . Note that during the simulation time, the wake mainly alters due to the changed yaw settings, which makes it extra challenging for the MPC to track the reference signal. Figure 4.9 depicts simulation results of two simulations.

In the top plot, tracking results are depicted that are obtained with unyawed turbines. Here it can be seen that indeed, the reference can not be tracked sufficiently over the complete simulation horizon, which is due to the absence of sufficient wind power. Interestingly, from  $t = 300$  [s] to  $t = 450$  [s], the wind farm power produces more than  $P^{\text{greedy}}$ , which is due to the fact that wakes of upstream turbines are not fully developed yet. However, when the wake changes arrive at downstream turbines, the available wind power decreases and the power production converges to  $P^{\text{greedy}}$  from  $t = 450$  [s] to  $t = 520$  [s]. In the below plot, it can be observed that power tracking can be ensured over the complete simulation horizon, which is due to the fact that the yawed turbines increase the possible power that can be harvested by the farm.

Figure 4.10 depicts the thrust coefficients that are found by the MPC and it can be seen that in the non-yawed turbine case (*i.e.*,  $\gamma_{i,k} = 0$ ), the thrust coefficients reach their boundaries from  $t = 300$  [s] to  $t = 450$  [s] and sufficient power tracking can not be ensured during this timespan. However, when the found optimized yaw settings  $\gamma_k^*$  are applied, the wind speed is higher in front of the upstream turbines hence more power can be harvested with these turbines. In order to track the reference, it is therefore possible to reduce the thrust coefficients.

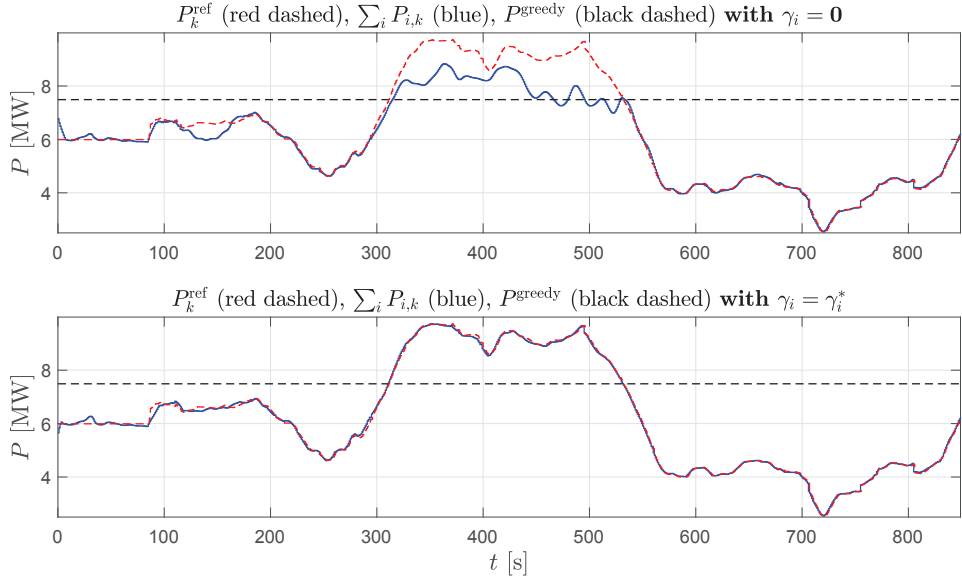


Figure 4.9: Wind farm tracking results of the controller with  $\gamma_{i,k} = 0$  (above) and optimized settings  $\gamma_k^*$  (below).

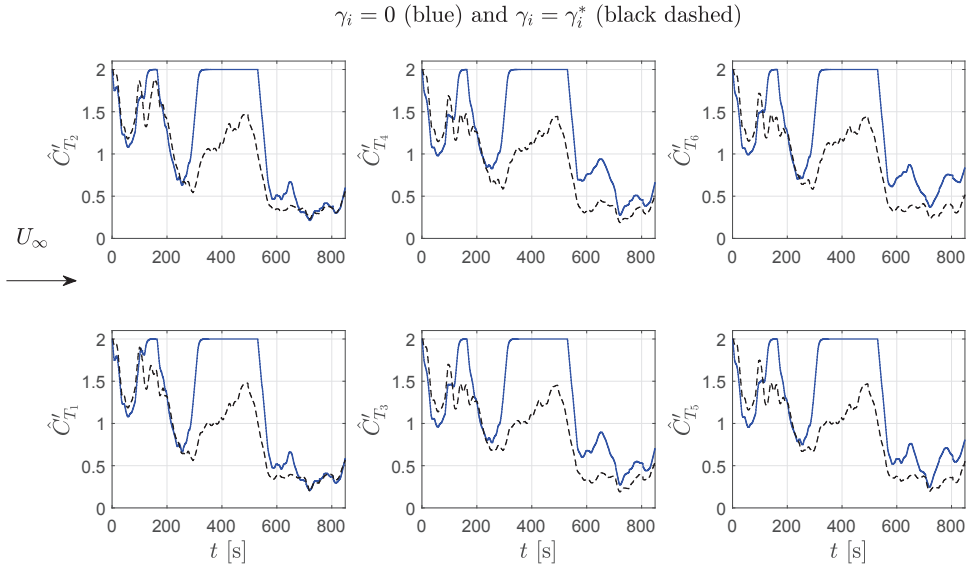


Figure 4.10: Thrust coefficients with  $\gamma_{i,k} = 0$  and optimized settings  $\gamma_k^*$ . The arrow on the left indicates the wind direction.

#### 4.5.5. POWER TRACKING UNDER ATMOSPHERIC PERTURBATIONS

The proposed controller is in this section evaluated under time varying lateral flow velocity components  $\tilde{v}_k$ . The controller settings are found to be  $q = 10^4, s = 0$ , and the simulation results are obtained with non-yawed turbines. The following perturbation is applied in PALM:

$$\bar{v}_k = \tilde{v}_k + 0.01, \quad \text{if } 150 < k < 250, \quad \text{or } 550 < k < 600. \quad (4.15)$$

This perturbation is applied before time integration of the Navier-Stokes equations in PALM. Hence PALM resolves, after perturbing the lateral flow velocity component, the flow velocity components at time  $k + 1$ . Figure 4.11 depicts the longitudinal flow velocity components at two different time steps. Clearly, after perturbing the lateral flow velocity component, a cross-wind can be observed and consequently, less wake interaction occurs. Nevertheless, Fig. 4.12 indicates that the controller is able to provide power tracking. Figure 4.13 depicts the thrust coefficients for the complete simulation horizon. Due to the imposed cross-wind, wakes are steered right from downstream turbines and consequently, the averaged rotor flow velocity of downstream turbines increases. This results in higher power production and thus, to maintain power tracking, thrust coefficients can be reduced. The latter can be observed in Fig. 4.13. It can thus be concluded that the proposed controller is able to provide power tracking when a cross-wind, possibly initiated by a butterfly far away, finds its way through the farm.

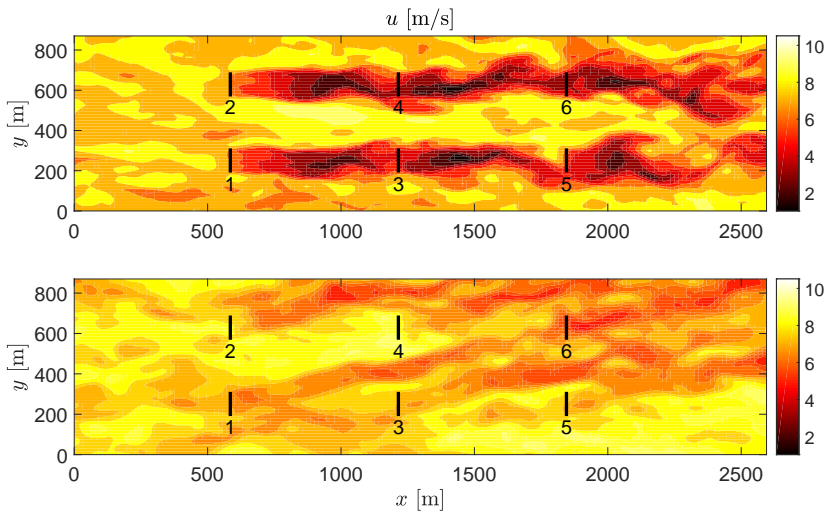


Figure 4.11: Instantaneous longitudinal flow velocity component at hub-height at  $t = 50$  [s] (above) and  $t = 600$  [s] (below). The flow is going from west to east and the black vertical lines represent the wind turbines.

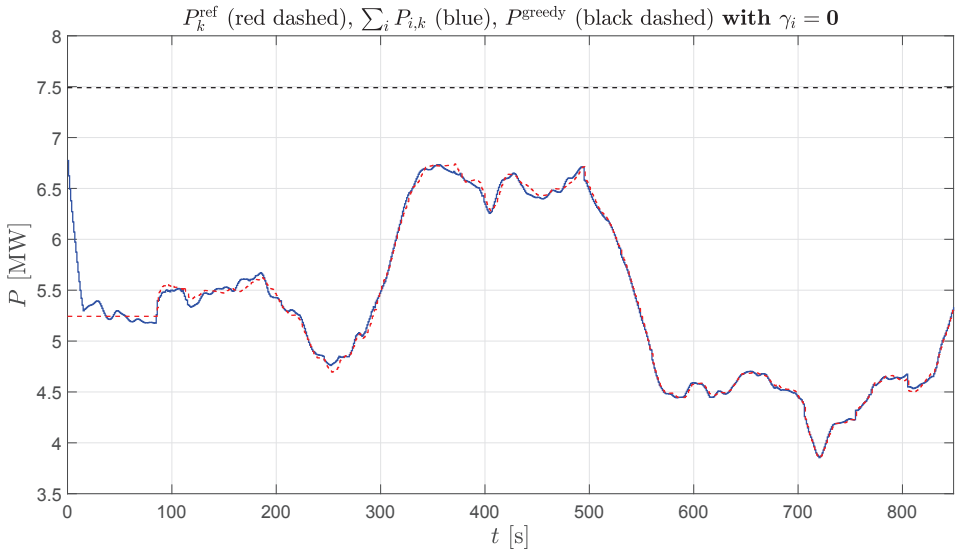


Figure 4.12: Wind farm power signal and its reference under perturbation in the lateral flow velocity component.

4

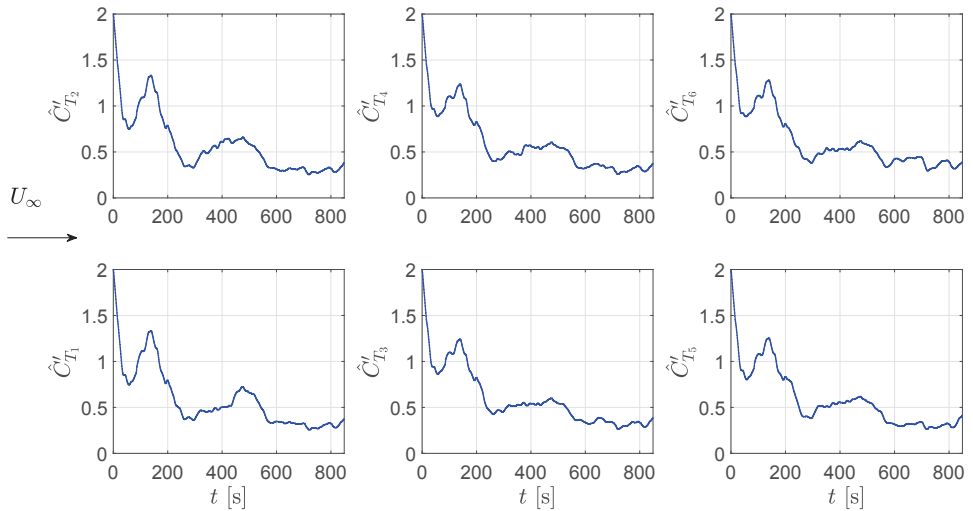


Figure 4.13: Thrust coefficients with  $\gamma_{i,k} = 0$  and under under perturbation in the lateral flow velocity component. The arrow on the left indicates the wind direction.

#### 4.5.6. POWER TRACKING UNDER TURBINE FAILURE

In this section, the controller is tested under the situation in which one turbine fails to produce power after a certain time instant. The same controller settings were used in §4.5.5. During the first period of the simulation, all 6 turbines contribute to the power tracking task, but at  $t = 99$  [s], the third turbine is completely shut down and consequently, the other turbines have to compensate for this loss. Figure 4.14 depicts the wind farm power signal and its reference, and it can be seen that power tracking is again ensured. At  $t = 99$  [s], there is a dip in the power production, but this is recovered after a few time instances. This is due to the fact that thrust coefficients of the other turbines are increased, as can be seen in Fig. 4.15. It can therefore be concluded that the proposed controller is also able to cope with turbine shut downs, given that the remaining turbines are able to provide enough power for the imposed reference signal. However, if this appears not to be the case, optimized yaw settings can be found and applied that increase the maximum possible power that can be harvested by the farm as discussed in §4.5.4.

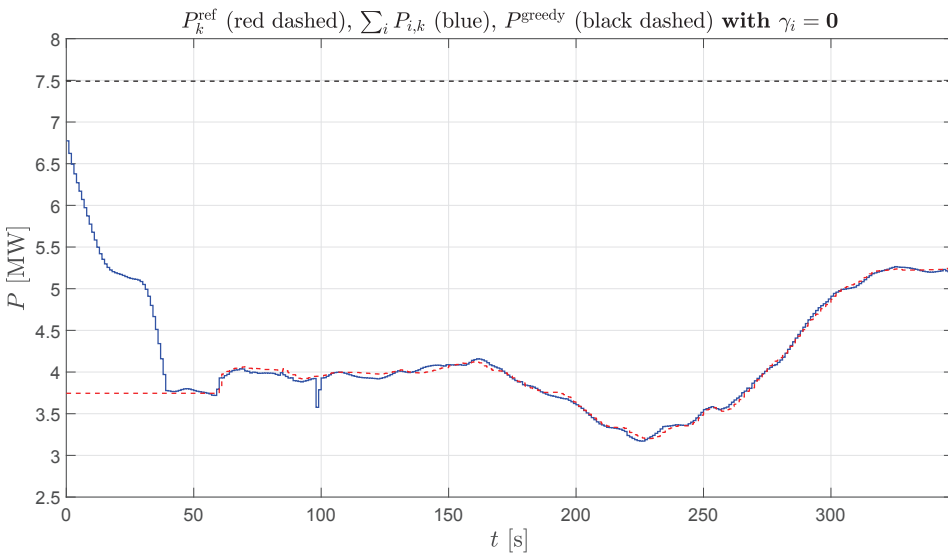


Figure 4.14: Wind farm power signal and its reference under turbine failure condition at  $t = 99$  [s].

#### 4.5.7. POWER TRACKING CLOSE TO AND ABOVE GREEDY POWER

Greedy power ( $P^{\text{greedy}}$ ) has been defined as the time-averaged wind farm power harvested with  $C'_{T_{i,k}} = 2$  and  $\gamma_{i,k} = 0$   $i = 1, \dots, \aleph$  over the entire simulation horizon. This section presents reference tracking results where the reference is constant over the simulation horizon, but increases in amplitude for each simulation case. In order to study the controller's performance when it is pushed to its limit, the reference was increased towards and over the  $P^{\text{greedy}}$  level. The same controller settings were used in §4.5.5 and Fig. 4.16 depicts the results. The upper plot shows the wind farm's power production with

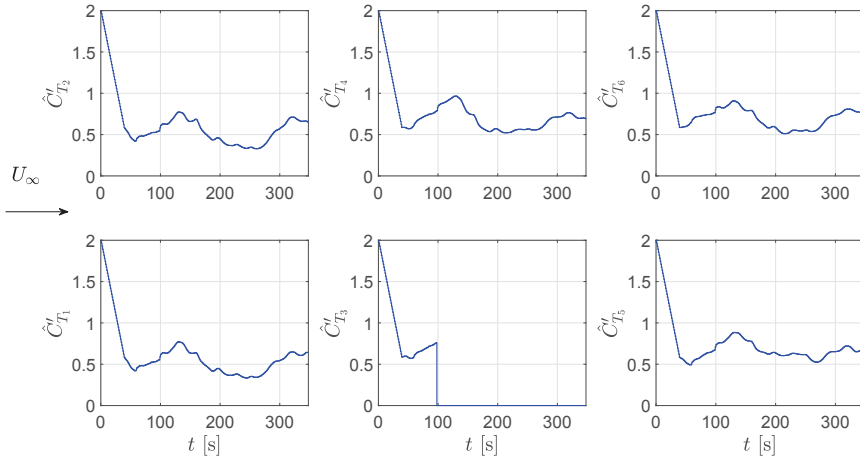


Figure 4.15: Thrust coefficients with  $\gamma_{i,k} = 0$  and under turbine failure condition at  $t = 99$  [s]. The arrow on the left indicates the wind direction.

$C'_{T_{i,k}} = 2$  and  $\gamma_{i,k} = 0$ , so no control is activated. The other plots illustrate the controller's performance when reference signals are defined as percentages of  $P^{\text{greedy}}$ . In the bottom plot for example, the wind farm's power reference signal is one percent above  $P^{\text{greedy}}$ .

The  $0.8P^{\text{greedy}}$  case shows good tracking results. However, the tracking deteriorates around 100-150 seconds for the cases  $0.9P^{\text{greedy}}$  and above. This is mainly due to the definition of  $P^{\text{greedy}}$  since it is an average over the complete horizon. In the upper plot, the wind farm power is between 1-1.5 [MW] lower than  $P^{\text{greedy}}$  around 100-150 seconds. Hence it is impossible to track power reference signals that are close to  $P^{\text{greedy}}$  around this period, simply because this power is not available in the farm. This is due to the fact that the rotor-averaged wind velocities are not high enough and the control signals are pushed to their maximum. However, when the amplitude of the oscillations around  $P^{\text{greedy}}$  decrease (from 400 seconds until the end), it can be observed that good tracking can be ensured for cases below or equal to  $P^{\text{greedy}}$ . Table 4.3 illustrates the root mean squared level of the error between reference and wind farm power for the different cases. From the table it can be concluded that the level increases if the reference gets closer to the  $P^{\text{greedy}}$  level or goes above this level.

Table 4.3: Root mean squared level of the error (Reference-WF power) signal for the different tracking cases.

Case	RMSE [MW]	Case	RMSE [MW]
$0.7P^{\text{greedy}}$	0.10	$1.0P^{\text{greedy}}$	0.50
$0.8P^{\text{greedy}}$	0.07	$1.01P^{\text{greedy}}$	0.55
$0.9P^{\text{greedy}}$	0.20	$1.02P^{\text{greedy}}$	0.60
$0.95P^{\text{greedy}}$	0.32	$1.03P^{\text{greedy}}$	0.65

Figure 4.17 depicts three simulation cases. In the upper plot, the wind farm power

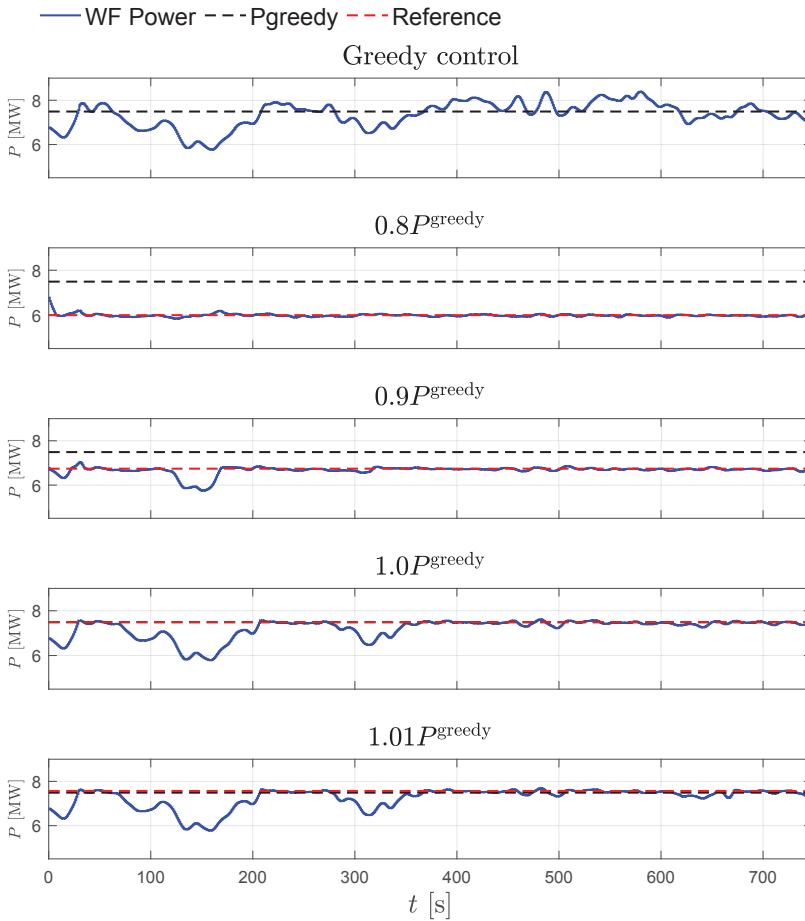


Figure 4.16: Wind farm power (WF Power) reference tracking results.

reference is equal to  $P^{\text{greedy}}$ . Then a case where the reference is one percent higher than  $P^{\text{greedy}}$  and the last plot depicts a case where the reference is 2 percent higher than  $P^{\text{greedy}}$ . Note that the depicted results are a zoom in of the complete simulation horizon. From these specific cases it can be concluded that the reference signal can be tracked only when there is in fact enough power available in the farm. The more the reference increases relative to  $P^{\text{greedy}}$ , the more the tracking performance deteriorates since there are more time intervals in which more power is demanded than there is actually available. However, since the controller does not contain a full wake model, information regarding future available wind farm power is not accessible for the controller. Hence it aims to (when more power is demanded than available) capture the current maximum available power for each time step.



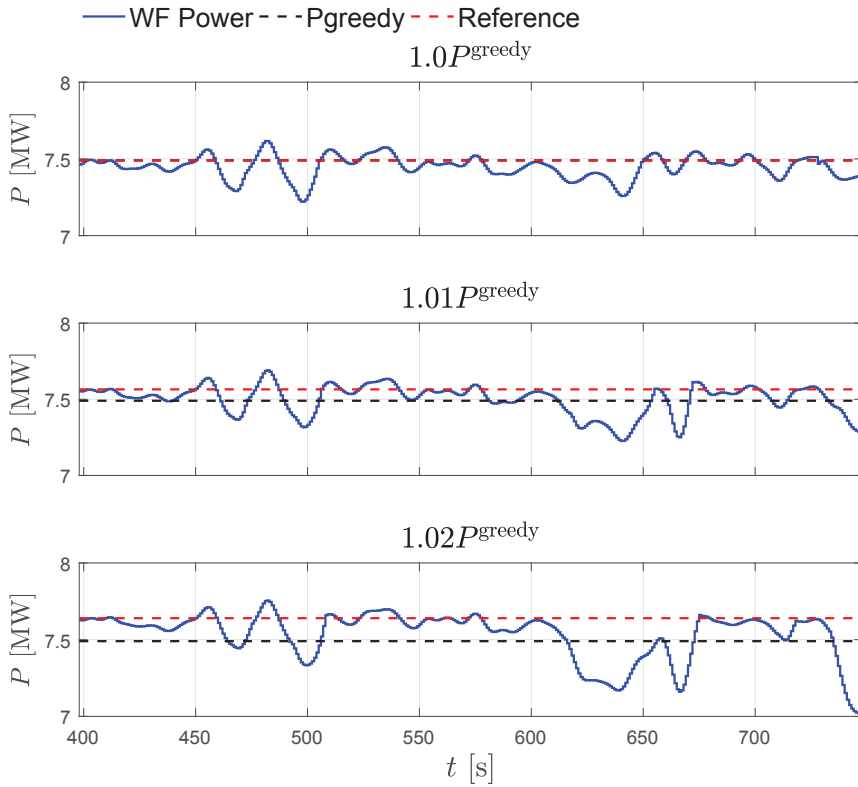


Figure 4.17: Wind farm power (WF Power) reference tracking results for the  $P^{\text{greedy}}$  and above  $P^{\text{greedy}}$  case.

#### 4.5.8. COMPUTATION TIME

In this section we briefly investigate the computation time that the controllers take for evaluating new thrust coefficients, *i.e.*, for solving the problem given in (4.6). In the closed-loop control framework presented in this chapter, the controller evaluates every second new thrust coefficients. Hence, the problem given in (4.6) should be solved within a second because online control is desired. Table 4.4 gives the mean computation time as a function of the number of turbines  $\aleph$ . Obviously, the mean computation time increases as the number of turbines increases, which is due to the fact that the optimization problem given in (4.6) becomes larger. The controller can evaluate new thrust coefficients within one second for wind farms that have less than 36 turbines. However, when a farm has 49 turbines, the mean computation time is already approximately 1.5 seconds, which is higher than the desired one second. In such a case it should be investigated if the proposed closed-loop controller also can provide power tracking when every two seconds new thrust coefficients are evaluated instead of every one second. Another possible option is to partition the problem given in (4.6) in sub problems that can be solved within a second (hierarchical approach as proposed in, *e.g.*, Spudic et al. (2010)) or use a more powerful computer. This is however not investigated in this work. Further-

more, this work does not investigate the mean computation time necessary to evaluate new yaw settings, *i.e.*, for solving the problem given in (4.9) as a function of the number of turbines in the farm.

Table 4.4: Mean computation time per controller time step  $\Delta t^{\text{CPU}}$  versus number of turbines  $\aleph$ . Computations are performed on a regular notebook with one core.

$\aleph$	$\Delta t^{\text{CPU}}$ [s]	$\aleph$	$\Delta t^{\text{CPU}}$ [s]	$\aleph$	$\Delta t^{\text{CPU}}$ [s]	$\aleph$	$\Delta t^{\text{CPU}}$ [s]	$\aleph$	$\Delta t^{\text{CPU}}$ [s]
3	0.049	6	0.068	9	0.091	12	0.10	15	0.16
20	0.22	25	0.38	36	0.77	49	1.5	64	2.9

## 4.6. CONCLUSIONS

Ancillary services in wind farms are important to increase the wind power penetration in the energy market. One example is secondary frequency regulation in which the objective is to have the wind farm's power generation track a power reference signal generated by transmission system operators during a time span of several minutes. Due to the uncertain wake dynamics, a closed-loop control solution with a dynamical surrogate model is needed to provide this so called power tracking. Since dynamical wake models are generally complex, approximations are required such that the surrogate model can be employed in a controller that should work in a real time application. In this chapter, we present such a dynamical surrogate wind farm model and utilize it in a model predictive controller that provides power tracking, and additionally is able to reduce the dynamical loading on a farm level by finding for each simulation second new optimized thrust coefficients in approximately 0.07 seconds for the presented case study. We note here that the dynamical loading is parametrized via the rate of change in the axial forces of the turbines. This is obviously a simplification (*e.g.*, no partial wake overlap is considered), but the control framework can still easily be used when more complex linear models are included that parametrize the fatigue in a more complex way.

To push the possible range of traceable power signals, wake steering is used when future reference signals exceed the maximum power that can be harvested with non-yawed turbines. Optimized yaw settings that maximize the possible power that can be harvested are then found by employing a steady-state surrogate model and set for a simulation period of fifteen minutes. The necessity of applying optimized or zero yaw settings to track the future reference can then be re-evaluated. Note that the optimized yaw settings maximize the possible power that can be harvested, which can result in unnecessary turbine yawing. In future work, a more sophisticated method could be incorporated in the controller for determining yaw settings that exactly increase the possible power that can be harvested to the maximal value of the future reference. Nonetheless, it takes approximately 30 seconds to find new optimized yaw settings and hence, this part of the controller is also suitable for online control. In this chapter, we give an example where the reference can not be tracked sufficiently when turbines are non-yawed, while power tracking is ensured when optimized yaw settings are applied. Additional simulation case studies were also presented that indicate that the proposed controller can deal with alternating atmospheric conditions and a turbine shut down. The controller is

evaluated in a high-fidelity simulation environment for which software is developed that allows for programming controllers in MATLAB and evaluating these in a high-fidelity simulation environment.

#### 4.A. TURBULENCE INTENSITY

The turbulence intensity in front of the wind farm  $\text{TI}_\infty$  is computed as follows: take the longitudinal flow velocity at hub-height for the area defined by the vertices  $x \in (30, 150)$  [m] and  $y \in (375, 525)$  [m] for  $L$  seconds. Define this local time-varying flow field as  $u_k^l$ . Define:

$$u_k' = u_k^l - \mu_u \quad \text{with} \quad \mu_u = \frac{1}{L} \sum_{k=1}^L u_k^l. \quad (4.16)$$

Using the above to compute the turbulence intensity yields:

$$\text{TI}_\infty = \mu_s \left( \text{rms}(u_k') \cdot \mu_u^{-1} \right), \quad (4.17)$$

with  $\text{rms}(u_k')$  the root-mean-square level of  $u_k'$  along the time axis and  $\mu_s(\cdot)$  the spatial average in the  $x$ - and  $y$ -direction.

# 5

## CONCLUSION AND RECOMMENDATIONS

One way to reduce the overall cost of wind energy is by placing turbines in each other's proximity in what is called a wind farm. Doing so has the advantage of reducing maintenance and cabling costs. However, an upwind turbine develops a wake, which impacts the performance of downstream turbines. In wind farm control, the aim is to take these interactions into account and provide improved performance on a farm level, by deviating from the standard turbine control strategy. A wind farm control objective can be the combination of energy production maximization, fatigue loading minimization or providing an ancillary service such as wind farm power tracking. Wind farm control is expected to be crucial in further decreasing the cost of wind energy over the next several decades. However, serious steps towards a practical wind farm control solution have to be made in order to demonstrate its full potential. This thesis dealt with important questions that need to be addressed in order to make these steps.

### 5.1. CONCLUSIONS

The first research question that we introduced in this thesis is:

- |  |
|--|
| I. What is the state-of-the art in wind farm modelling and control, what is missing and contributes to the current state of wind farm control? |
|--|

Based on a thorough literature review, it has been concluded that there is still uncertainty on the necessary fidelity of the controller model and that closed-loop wind farm controllers evaluated in a high-fidelity simulation environment are scarce. More specifically, no results are published with a closed-loop wind farm control solution that employs a medium-fidelity dynamical wind farm model, based on the unsteady Navier-Stokes equations, online. Such a model allows for convenient adaptation of its

fidelity by the capacity to vary the temporal and spatial resolution. Proposing such a closed-loop control framework is an answer to the first research question presented in Chapter 1. A closed-loop control framework is essential in wind farm control since it can partially compensate for model mismatches and it can reject time-varying disturbances. Additionally, since the framework presented in this thesis employs a dynamical control-oriented model<sup>1</sup>, wake delays and transients are captured and hence taken into account by the controller. A last reason for utilizing a dynamical model in the controller is that it allows for utilizing a sophisticated control methodology like Model Predictive Control (MPC), which allows for constrained control. One key ingredient of MPC is a control-oriented (surrogate) model. One contribution of this thesis is the development of such a control-oriented model, which has been detailed in Chapter 3.

This brings us to the second research question that we introduced in this thesis is:

II. Which wind farm dynamics need to be captured in a control-oriented wind farm model such that the model can be employed in the online closed-loop control framework, while the control objective is ensured?

The derivation of the control-oriented model starts with the three-dimensional unsteady Navier-Stokes equations. Modeling assumptions, reducing the fidelity, were made to make the controller model suitable for online control. The model is employed in an Ensemble Kalman filter (Doekemeijer et al., 2018) and an adjoint-based model predictive wind farm controller (Vali et al., 2018a). Hence, leaps are taken towards a practical implementation of the closed-loop control scheme proposed in this thesis. A first serious step towards practical implementation would be to evaluate the proposed closed-loop control solution in a high-fidelity simulation environment. This test can provide insight on the necessary information/dynamics that the control-oriented model should contain. If the test results are not successful or it is desired to improve the controller's performance, the scope of dynamics captured inside the control-oriented model may need to be reconsidered. Since the developed model is derived from the three-dimensional unsteady Navier-Stokes equations, it is relatively easy to include dynamics that are neglected in the first place. Nevertheless, it can be concluded from the presented cases in Chapter 3 that the developed dynamical control-oriented model is able to estimate high-fidelity flow (at hub-height) and power data in a fraction of the time with the high-fidelity model. Two novel contributions that resulted in this successful estimation are:

1. A correction factor has been included in the continuity equation, which reduces the unrealistic speed up effect (wind velocity increase) on both sides behind each turbine. This effect is a consequence of neglecting the vertical dimension, but the correction factor partially compensates for that.
2. A spatially dependent mixing length parametrization has been proposed that al-

<sup>1</sup>Note that the framework is not limited to dynamical control-oriented models, but can also employ a steady-state wind farm model.

lows for local adaptation of wake characteristics. The mixing length value depends on the spatial distance downstream each turbine.

To provide leverage for answering the second research question, the control-oriented model developed in Chapter 3 can be utilized. However, conclusive statements can not be made since the controller model has not been employed in a controller that has been evaluated in a high-fidelity simulation environment. However, it can be stated that, when wake interactions should be taken into account, employing a steady-state model can be seen as the minimum, whereas a model with the full Navier-Stokes equations as the maximum. The model presented in Chapter 3 can be tailored as a compromise (in terms of speed and accuracy) according to the specified controller objective.

Another, more specific, research question posed in this thesis is:

III. Which wind farm dynamics need to be captured in a control-oriented wind farm model such that the model can be employed in the online closed-loop control framework, while wind farm power tracking is ensured?

In Chapter 4 it has been shown that for power reference tracking, no full wake model (such as the WFSim model presented in this thesis) has to be included in the controller to ensure tracking in a high-fidelity simulation environment. The proposed model predictive controller provides power reference tracking by employing a dynamical parameter-varying model. The latter does not contain a full wake model, which results in a model predictive controller that is time efficient and suitable for online control. The closed-loop control solution presented in this part of the thesis also demonstrates that by applying optimized yaw angles, the set of trackable wind farm power reference signals can be increased. The optimized yaw angles are found by employing a steady-state wind farm model. Hence, this online closed-loop control solution contains both a dynamical and steady-state wind farm model. It can be concluded that, for this application, no full wake model has to be present in the controller to provide power tracking, but to find optimized yaw settings that increase the set of trackable wind farm power reference signals, a full wake model (minimal steady-state) needs to be employed.

The last research question that is posed in this thesis is:

IV. Can we impose additional objectives on the controller while providing wind farm power tracking and what is the consequence on the control signal distribution among the turbines?

This thesis showed that, by including additional performance measures in the model predictive controller, different solutions (distributions of the control signals among the turbines) can be found, while still ensuring power tracking. Additionally it has been shown that different control signal distributions affect the turbine's dynamical loading, which in this thesis is parametrized as the variation in axial force on the rotor. In a

real wind farm, this variable is normally not measured, but it can easily be replaced by, *e.g.*, the out of plane blade bending moments when these are captured in the control-oriented model. As such, the presented closed-loop control solution provides an illustration of how it can be utilized in a real wind farm.

## 5.2. RECOMMENDATIONS

Although this thesis presented steps towards closed-loop dynamical wind farm control, still many roads need to be discovered. In the following, research recommendations are given.

- The controller presented in Chapter 4 should be tested in a wind tunnel or better, a real wind farm so that its performance can be evaluated in a more realistic environment.
- A control-oriented model that contains more wake dynamics should be included in the controller presented in Chapter 4. Then, controller performance and computational time can be compared, and it can be determined whether a model of increased fidelity results in increased controller performance.
- The controller presented in (Vali et al., 2018a) is not tested in a high-fidelity wind farm model, *i.e.*, the wind farm model and controller model are equivalent. It is recommended to test the controller in a high-fidelity wind farm model since this provides information on the online feasibility. In addition, the necessary dynamics that should be included in the control-oriented model can be studied. Secondly, (Doekemeijer et al., 2018) and (Vali et al., 2018a) need to be coupled and tested in a high-fidelity wind farm model. Then, a full solution to the problem stated in Chapter 1 can be given (see Fig. 1.5).
- The online wind farm control framework presented in this thesis requires a controller model. It has been explained that this is a challenge in this framework. Exploring the possibilities of distributing the controller model such that each partition can be solved separately could be interesting. Generally it holds that subdividing large mathematical problems into small problems, solve these and then gather the results reduces the total computational time with respect to directly solving for the large problem itself. Additionally, distributed control methodologies exist that provide techniques that could possibly be applied in wind farms.
- Modelling directions such as those presented in (Annoni and Seiler, 2016) can be explored in more detail for a wind farm application. The linear parameter-varying models can be employed for offline controller synthesis.
- A direction hardly explored in wind farm control is the application of an offline synthesized dynamic feedback controller. One example is presented in (Soleimanzadeh et al., 2013). An advantage is that online controller evaluation and propagation in time (like in MPC) is not necessary, since synthesis can be done offline and consequently, the computational time is less critical. The idea is to design a

dynamical controller that ensures closed-loop stability and performance employing a wind farm model as presented in Chapter 3. Advanced controller synthesis techniques exist or need to be adapted or developed for this research direction. Closed-loop dynamic feedback control in wind farms is mainly suitable for power tracking and reducing fatigue loading. Due to the lack of results in the literature, this research direction can provide the wind community with new insights, but can also provide the control community with new controller synthesis methods with a wind farm as practical application.

- Another open research direction is the exploration of system identification techniques (Birpoutsoukis et al., 2017) in wind farm modelling and control. The general idea here is to excite the wind farm and measure its response. The input/output data can be utilized to identify a control-oriented wind farm model, online or offline.
- A practical implementable control solution as presented in (Munters and Meyers, 2018b) should be tested in a wind tunnel or real wind farm. It is interesting to explore this direction of wind farm control further in which standard periodic functions are applied as control signals and consequently, additional wake recovery is introduced and power yield is increased.





# BIBLIOGRAPHY

- Abkar, M. and Porté-Agel, F.: The effect of atmospheric stability on wind-turbine wakes: A large-eddy simulation study, *Journal of Physics: Conference Series*, DOI: 10.1088/1742-6596/524/1/012138, 2016.
- Aho, J., Buckspan, A., Laks, J., Fleming, P. A., Jeong, Y., Dunne, E., Churchfield, M., Pao, L. Y., and Johnson, K.: A tutorial of wind turbine control for supporting grid frequency through active power control, *American Control Conference*, DOI: 10.1109/ACC.2012.6315180, 2012.
- Ainslie, J. E.: Calculating the flowfield in the wake of wind turbines, *Journal of Wind Engineering and Industrial Aerodynamics*, vol. 27(1-2), pp. 213-224, 1988.
- Anderson, P. S., Ladkin, R. S., and Renfrew, I. A.: An Autonomous Doppler Sodar Wind Profiling System, *Journal of Atmospheric and Oceanic Technology*, vol. 22(9), pp. 1309-1325, 2005.
- Annoni, J. and Seiler, P.: A low-order model for wind farm control, *American Control Conference*, DOI: 10.1109/ACC.2015.7170981, 2015.
- Annoni, J. and Seiler, P.: A method to construct reduced-order parameter-varying models, *International Journal of Robust and Nonlinear Control*, vol. 27(4), pp. 582-597, 2016.
- Annoni, J., Seiler, P., Johnson, K., Fleming, P. A., and Gebraad, P. M. O.: Evaluating wake models for wind farm control, *American Control Conference*, DOI: 10.1109/ACC.2014.6858970, 2014.
- Annoni, J., Gebraad, P. M. O., Scholbrock, A., Fleming, P. A., and van Wingerden, J. W.: Analysis of axial-induction-based wind plant control using an engineering and a high-order wind plant model, *Wind Energy*, vol. 19(6), pp. 1135-1150, 2016a.
- Annoni, J., Gebraad, P. M. O., and Seiler, P.: Wind Farm Flow Modeling Using an Input-Output Reduced-Order Model, *American Control Conference*, DOI: 10.1109/ACC.2016.7524964, 2016b.
- Annoni, J., Scholbrock, A., Churchfield, M., and Fleming, P. A.: Evaluating Tilt Control for Wind Farms, *American Control Conference*, DOI: 10.23919/ACC.2017.7963037, 2017.
- Aström, K. J. and Murray, R. M.: *Feedback Systems*, Princeton University Press, 2008.
- Avila, M., Folch, A., Houzeaux, G., Eguzkitza, B., Prieto, L., and Cabezon, D.: A Parallel CFD Model for Wind Farms, *Procedia Computer Science*, vol. 18, pp. 2157-2166, 2013.

- Barthelmie, R., Frandsen, S., Nielsen, M. N., Pryor, S. C., Rethore, P. E., and Jørgensen, H. E.: Modelling and Measurements of Power Losses and Turbulence Intensity in Wind Turbine Wakes at Middelgrunden Offshore Wind Farm, *Wind Energy*, vol. 10(6), pp. 517-528, 2007.
- Barthelmie, R., Frandsen, S., Hansen, K., Schepers, J., Rados, K., Schlez, W., Neubert, A., Jensen, L., and Neckelmann, S.: Modelling the impact of wakes on power output at Nysted and Horns rev, *European Wind Energy Conference*, DOI: 10.1175/2010JTECHA1398.1, 2009.
- Barthelmie, R., Pryor, S. C., Frandsen, S., Hansen, K., Schepers, J., Rados, K., Schlez, W., Neubert, A., Jensen, L., and Neckelmann, S.: Quantifying the Impact of Wind Turbine Wakes on Power Output at Offshore Wind Farms, *Journal of Atmospheric and Oceanic Technology*, vol. 27(8), pp. 1302-1317, 2010.
- Barthelmie, R. J., Folkerts, L., Ormel, F. T., Sanderhoff, P., Eecen, P. J., Stobbe, O., and Nielsen, N. M.: Offshore Wind Turbine Wakes Measured by Sodar, *Journal of Atmospheric and Oceanic Technology*, vol 20(4), pp. 466-477, 2003.
- Bartl, J. and Sætran, L.: Blind test comparison of the performance and wake flow between two in-line wind turbines exposed to different atmospheric inflow conditions, *Wind Energy Science*, vol. 2, pp. 55-76, 2016.
- Bastankhah, M. and Porté-Agel, F.: Experimental and theoretical study of wind turbine wakes in yawed conditions, *Journal of Fluid Mechanics*, vol. 806(10), pp. 506-541, 2016.
- Bastine, D., Witha, B., Wächter, M., and Peinke, J.: Towards a Simplified Dynamic Wake Model Using POD Analysis, *Energies*, vol. 8(2), pp. 895-920, 2015.
- Bay, C. J., Annoni, J., Taylor, T., Pao, L. Y., and Johnson, K.: Active power control for wind farms used distributed model predictive control and nearest neighbor communication, *American Control Conference*, DOI: 10.23919/ACC.2018.8431764, 2018.
- Berglind, B. and Wisniewski, R.: Fatigue Estimation Methods Comparison for Wind Turbine Control, eprint arXiv:1411.3925, 2014.
- Betz, A.: Das Maximum der theoretisch möglichen Ausnutzung des Windes durch Windmotoren, *Zeitschrift für das gesamte Turbinenwesen*, 1920.
- Betz, A.: *Wind-Energie und ihre Ausnutzung durch Windmühlen*, 1926.
- Bianchi, F. D., Battista, H. D., and Mantz, R. J.: *Wind Turbine Control Systems; Principles, modelling and gain scheduling design*, Springer-Verlag London, 2007.
- Biegel, B., D. Madjidian, D., Spudić, V., Rantzer, A., and Stoustrup, J.: Distributed low-complexity controller for wind power plant in derated operation, *International Conference on Control Applications*, DOI: 10.1109/CCA.2013.6662758, 2013.

- Birpoutsoukis, G. Marconato, A., Lataire, J., and Schoukens, J.: Regularized nonparametric Volterra kernel estimation, *Automatica*, vol. 82, pp. 324-327, 2017.
- Blazek, J.: *Computational Fluid Dynamics: Principles and Applications*, Elsevier, 2001.
- Boersma, S.: <https://github.com/TUDELFT-DataDrivenControl/PALMSuperController>, 2018a.
- Boersma, S.: <https://github.com/TUDELFT-DataDrivenControl/WFSim>, 2018b.
- Boersma, S., Korniienko, A., Laib, K., and van Wingerden, J. W.: Robust Performance Analysis for a Range of Frequencies, *American Control Conference*, DOI: 10.1109/ACC.2016.7526558, 2016a.
- Boersma, S., Vali, M., van Wingerden, J. W., and Kühn, M.: Quasi Linear Parameter Varying modeling for wind farm control using the 2D Navier Stokes equations, *American Control Conference*, DOI: 10.1109/ACC.2016.7525616, 2016b.
- Boersma, S., Doekemeijer, B. M., Gebraad, P. M. O., Fleming, P. A., Annoni, J., Scholbrock, A. K., Frederik, J. A., and van Wingerden, J. W.: A tutorial on control-oriented modelling and control of wind farms, *American Control Conference*, DOI: 10.23919/ACC.2017.7962923, 2017.
- Boersma, S., Doekemeijer, B. M., Siniscalchi-Minna, S., and van Wingerden, J. W.: A constrained wind farm controller providing secondary frequency regulation: an LES study, *Renewable Energy*, 2018a.
- Boersma, S., Doekemeijer, B. M., Vali, M., Meyers, J., and van Wingerden, J. W.: A control-oriented dynamic wind farm model: WFSim, *Wind Energy Science*, vol. 3, pp. 75-95, 2018b.
- Boersma, S., Rostampour, V., Doekemeijer, B. M., and van Wingerden, J. W.: A centralized model predictive wind farm controller in PALM providing power reference tracking, *Journal of Physics: Conference Series*, DOI: 10.1088/1742-6596/1037/3/032023, 2018c.
- Boersma, T. and Losz, A.: The New International Political Economy of Natural Gas in the *Handbook of the International Political Economy of Energy and Natural Resources*, ch. 10, pp. 138-153, Edward Elgar Publishing, 2018.
- Bossanyi, E. A.: Individual Blade Pitch Control for Load Reduction, *Wind Energy*, vol. 6(2), pp. 119-128, 2003.
- Bossanyi, E. A.: Further load reductions with individual pitch control, *Wind Energy*, vol. 8(4), pp. 481-485, 2005.
- Bossuyt, J., Howland, M. F., Meneveau, C., and Meyers, J.: Measurement of unsteady loading and power output variability in a micro wind farm model in a wind tunnel, *Experiments in Fluids*, vol. 58(1), 2017.

- Bottasso, C. L. and Schreiber, J.: Online model updating by a wake detector for wind farm control, American Control Conference, DOI: 10.23919/ACC.2018.8431626, 2018.
- Burton, T., Sharpe, D., Jenkins, N., and Bossanyi, E.: Wind energy handbook, John Wiley and Sons, 2001.
- Campagnolo, E., Croce, A., Nanos, E. M., Petrovic, V., Schreiber, J., and Bottasso, C. L.: Wind tunnel testing of a closed-loop wake deflection controller for wind farm power maximization, Journal of Physics: Conference Series, DOI: 10.1088/1742-6596/753/3/032006, 2016a.
- Campagnolo, E., Petrović, V., Bottasso, C. L., and Croce, A.: Wind tunnel testing of wake control strategies, in: American Control Conference, DOI: 10.1109/ACC.2016.7524965, 2016b.
- Churchfield, M., Lee, S., Michalakes, J., and Moriarty, P. J.: A numerical study of the effects of atmospheric and wake turbulence on wind turbine dynamics, Journal of Turbulence, vol. 13(14), 2012.
- Ciri, U., Rotea, M., Santoni, C., and Leonardi, S.: Large Eddy Simulation for an array of turbines with Extremum Seeking Control, American Control Conference, DOI: 10.1109/ACC.2016.7524968, 2016.
- Ciri, U., Rotea, M., and Leonardi, S.: Model-free Control of Wind Farms. A comparative study between individual and coordinated extremum seeking, Renewable Energy, vol. 113, pp. 1033-45, 2017.
- Ciri, U., Rotea, M., and Leonardi, S.: Effect of the turbine scale on yaw control, Wind Energy, vol. 21, pp. 1395-1405, 2018.
- Clayton, B. and Filby, P.: Measured effects of oblique flows and change in blade pitch angle on performance and wake development of model wind turbines, BWEA Wind Energy Conference, 1982.
- Crespo, A., Hernandez, J., Fraga, E., and Andreu, C.: Experimental validation of the UPM computer code to calculate wind turbine wakes and comparison with other models, Journal of Wind Engineering and Industrial Aerodynamics, vol. 27(1-2), pp. 77-88, 1988.
- Crespo, A., Hernandez, J., and Frandsen, S.: Survey of modelling methods for wind turbine wakes and wind farms, Wind Energy, vol. 2(1), pp. 1-24, 1999.
- Cuthill, E. and McKee, J.: Reducing the bandwidth of sparse symmetric matrices, National Conference, ACM, 1969.
- Damiani, R., Dana, S., Annoni, J., Fleming, P. A., Roadman, J., van Dam, J., and Dykes, K.: Assessment of wind turbine component loads under yaw-offset conditions, Wind Energy Science, vol. 3, pp. 173-189, 2017.

- Dar, Z., Kar, K., Sahni, O., and Chow, J. H.: Windfarm Power Optimization Using Yaw Angle Control, *Sustainable Energy*, vol. 8(1), pp. 104-116, 2017.
- Deardorff, J. W.: Stratocumulus-capped mixed layers derived from a three-dimensional model, *Boundary-Layer Meteorology*, vol. 18(4), pp. 495-527, 1980.
- Doekemeijer, B. M., van Wingerden, J. W., Boersma, S., and Pao, L. Y.: Enhanced Kalman filtering for a 2D CFD NS wind farm flow model, *Journal of Physics: Conference Series*, DOI: 10.1088/1742-6596/753/5/052015, 2016.
- Doekemeijer, B. M., Boersma, S., van Wingerden, J. W., and Pao, L. Y.: Ensemble Kalman filtering for wind field estimation in wind farms, *American Control Conference*, DOI: 10.23919/ACC.2017.7962924, 2017.
- Doekemeijer, B. M., Boersma, S., Pao, L. Y., Knudsen, T., and van Wingerden, J. W.: Online model calibration for a simplified LES model in pursuit of real-time closed-loop wind farm control, *Wind Energy Science Discussions*, 2018.
- Dörenkämper, M., Witha, B., Steinfeld, G., Heinemann, D., and Kühn, M.: The impact of stable atmospheric boundary layers on wind-turbine wakes within offshore wind farms, *Journal of Wind Engineering and Industrial Aerodynamics*, vol. 144, pp. 146-153, 2015.
- Ela, E. Gevorgian, V., Fleming, P. A., Zhang, Y. C., Singh, M., Muljadi, E., Scholbrock, A., Aho, J., Buckspan, A., Pao, L. Y., Singhvi, V., Tuohy, A., Pourbeik, P., Brooks, D., and Bhatt, N.: Active power controls from wind power: Bridging the gaps, Tech. rep., National Renewable Energy Laboratory, 2014.
- Enerdata: Global Energy Statistical Yearbook, Tech. rep., 2017.
- España, G., Aubrun, S., Loyer, S., and Devinant, P.: Spatial study of the wake meandering using modelled wind turbines in a wind tunnel, *Wind Energy*, vol 14(7), pp. 923-937, 2011.
- Fleming, P. A., Gebraad, P. M. O., van Wingerden, J. W., Lee, S., Churchfield, M., Scholbrock, A., Michalakes, J., Johnson, K., and Moriarty, P.: The SOWFA super-controller: A high-fidelity tool for evaluating wind plant control approaches, *The European Wind Energy Association*, 2013.
- Fleming, P. A., Gebraad, P. M. O., Lee, S., van Wingerden, J. W., Johnson, K., Churchfield, M., Michalakes, J., Spalart, P., and Moriarty, P.: Evaluating techniques for redirecting turbine wakes using SOWFA, *Renewable Energy*, vol. 70, pp 211-218, 2014a.
- Fleming, P. A., Gebraad, P. M. O., Lee, S., van Wingerden, J. W., Johnson, K., Churchfield, M., Michalakes, J., Spalart, P., and Moriarty, P.: Simulation comparison of wake mitigation control strategies for a two-turbine case, *Wind Energy*, vol. 18(12), pp. 2135-2143, 2014b.

- Fleming, P. A., Ning, A., Gebraad, P. M. O., and Dykes, K.: Wind plant system engineering through optimization of layout and yaw control, *Wind Energy*, vol. 19(2), pp. 329-344, 2015.
- Fleming, P. A., Aho, J., Gebraad, P. M. O., Pao, L. Y., and Zhang, Y.: Computational fluid dynamics simulation study of active power control in wind plants, *American Control Conference*, DOI: 10.1109/ACC.2016.7525115, 2016a.
- Fleming, P. A., Churchfield, M., Scholbrock, A., Clifton, S. S., Johnson, K., Wright, A., Gebraad, P. M. O., Naughton, B., Berg, J., Herges, T., White, J., Mikkelsen, T., Sjöholm, M., and Angelou, N.: Detailed field test of yaw-based wake steering, *Journal of Physics: Conference Series*, DOI: 0.1088/1742-6596/753/5/052003, 2016b.
- Fleming, P. A., Annoni, J., Scholbrock, A., Quon, E., Dana, S., Schreck, S., Raach, S., Haizmann, E., and Schlipf, D.: Full-Scale Field Test of Wake Steering, *Wake Conference*, DOI: 10.1088/1742-6596/854/1/012013, 2017a.
- Fleming, P. A., Annoni, J., Shah, J. J., Wang, L., Ananthan, S., Zhang, Z., Hutchings, K., Wang, P., Chen, W., and Chen, L.: Field Test of Wake Steering at an Offshore Wind Farm, *Wind Energy Science*, vol. 2, pp. 229-239, 2017b.
- Fletcher, T. M. and Brown, R. E.: Simulation of wind turbine wake interaction using the vorticity transport model, *Wind Energy*, vol. 13(7), pp. 587-602, 2010.
- Fortes-Plaza, A., Campagnolo, F., Wang, J., Wang, C., and Bottasso, C. L.: A POD reduced-order model for wake steering control, *Journal of Physics: Conference Series*, DOI: 10.1088/1742-6596/1037/3/032014, 2018.
- Frandsen, S., Barthelmie, R., Pryor, S., Rathmann, O., Larsen, S., Højstrup, J., and Thøgersen, M.: Analytical Modelling of Wind Speed Deficit in Large Offshore Wind Farms, *Wind Energy*, vol. 1(1-2), pp. 39-53, 2006.
- Gaumond, M., Réthoré, P. E., Ott, S., Peña, A., Bechmann, A., and Hansen, K. S.: Evaluation of the wind direction uncertainty and its impact on wake modeling at the Horns Rev offshore wind farm, *Wind Energy*, vol. 17(8), pp. 1169-1178, 2014.
- Gebraad, P. M. O.: Data-Driven Wind Plant Control, Ph.D. thesis, Delft University of Technology, 2014.
- Gebraad, P. M. O. and van Wingerden, J. W.: A Control-Oriented Dynamic Model for Wakes in Wind Plants, *Journal of Physics: Conference Series*, DOI: 10.1088/1742-6596/524/1/012186, 2014.
- Gebraad, P. M. O. and Wingerden, J. W.: Maximum power-point tracking control for wind farms, *Wind Energy*, vol. 18(3), pp. 429-447, 2015.
- Gebraad, P. M. O., Teeuwisse, F. W., van Wingerden, J. W., Fleming, P. A., Ruben, S. D., Marden, J. R., and Pao, L. Y.: Wind plant power optimization through yaw control using a parametric model for wake effects - a CFD simulation study, *Wind Energy*, vol. 19(1), pp. 95-114, 2014.

- Gebraad, P. M. O., Fleming, P. A., and van Wingerden, J. W.: Comparison of Actuation Methods for Wake Control in Wind Plants, American Control Conference, DOI: 10.1109/ACC.2015.7170977, 2015.
- Gebraad, P. M. O., Churchfield, M., and Fleming, P. A.: Incorporating Atmospheric Stability Effects into the FLORIS Engineering Model of Wakes in Wind Farms, Journal of Physics: Conference Series, DOI:10.1088/1742-6596/753/5/052004, 2016a.
- Gebraad, P. M. O., Thomas, J. J., Ning, A., Fleming, P. A., and Dykes, K.: Maximization of the annual energy production of wind power plants by optimization of layout and yaw-based wake control, Wind Energy, vol. 20(1), pp. 97-107, 2016b.
- Göçmen, T., Giebel, G., Poulsen, N. K., and Mahmood, M.: Wind Speed Estimation and Parametrization of Wake Models for Downregulated Offshore Wind Farms within the scope of PossPOW Project, Journal of Physics: Conference Series, DOI: 10.1088/1742-6596/524/1/012156, 2014.
- Göçmen, T., Giebel, G., Sørensen, J. E., and Poulsen, N. K.: Possible Power Estimation of Down-Regulated Offshore Wind Power Plants., Ph.D. thesis, Technical University of Denmark, 2016a.
- Göçmen, T., van der Laan, P., Réthoré, P. E., Diaz, A. P., and Larsen, G. C.: Wind turbine wake models developed at the technical university of Denmark: A review, Renewable and Sustainable Energy Reviews, vol. 60, pp. 752-769, 2016b.
- Goit, J. P. and Meyers, J.: Optimal control of energy extraction in wind-farm boundary layers, Journal of Fluid Mechanics, vol. 768, pp. 5-50, 2015.
- Goossens, S.: Field-test of nacelle-based lidar to explore its applications for Vattenfall as wind park operator, Master's thesis, Delft University of Technology, 2015.
- Grunnet, J. D., Soltani, M., Knudsen, T., Kragelund, M. N., and Bak, T.: Aeolus toolbox for dynamics wind farm model, simulation and control, The European Wind Energy Conference & Exhibition, 2010.
- Guntur, S., Trolldborg, N., and Gaunaa, M.: Application of engineering models to predict wake deflection due to a tilted wind turbine, in: European Wind Energy Conference & Exhibition, 2012.
- Hahm, T. and Wußow, S.: Turbulent Wakes in Wind Farm Configuration, European Wind Energy conference & exhibition, 2006.
- Hamilton, N., Tutkun, M., and Cal, R. B.: Wind turbine boundary layer arrays for Cartesian and staggered configurations: Part II, low-dimensional representations via the proper orthogonal decomposition, Wind Energy, vol. 18(2), pp. 297-315, 2015.
- Hand, M. M. and Balas, M. J.: Systematic controller design methodology for variable-speed wind turbines, Wind Engineering, vol. 24(3), 2002.
- Hansen, M. O. L.: Aerodynamics of wind turbines, third edition, Routledge, 2015.



- Hasager, B., Rasmussen, L., Peña, A., Jensen, L. E., and Réthoré, P. E.: Wind farm wake: The Horns Rev photo case, *Energies*, vol. 6(2), pp. 696-716, 2013.
- Hirth, B. D., Schroeder, J. L., Gunter, W. S., and Guynes, J. G.: Investigating the Impact of Turbine Control on Turbine Wakes using Advanced Doppler Radar, *Windpower*, 2014.
- Horvat, T., Spudić, V., and Baotić, M.: Quasi-stationary optimal control for wind farm with closely spaced turbines, *Information & Communication Technology Electronics & Microelectronics*, 2012.
- Howland, M. F., Bossuyt, J., Martinez-Tossas, L. A., Meyers, J., and Meneveau, C.: Wake structure in actuator disk models of wind turbines in yaw under uniform inflow conditions, *Journal of Renewable Sustainable Energy*, vol. 8, 2016.
- International Energy Agency: *World Energy Outlook*, Tech. rep., 2017.
- International Renewable Energy Agency: *Innovation Outlook: Offshore Wind*, Tech. rep., 2016.
- Iungo, G. V., Santoni-Ortiz, C., Abkar, M., Porté-Agel, F., Rotea, M. A., and Leonardi, S.: Data-driven Reduced Order Model for prediction of wind turbine wakes, *Journal of Physics: Conference Series*, DOI: 10.1088/1742-6596/625/1/012009, 2015a.
- Iungo, G. V., Viola, F., Ciri, U., Rotea, M. A., and Leo: Data-driven RANS for simulations of large wind farms, *Journal of Physics: Conference Series*, DOI: 10.1088/1742-6596/625/1/012025, 2015b.
- Jensen, N. O.: A note on wind generator interaction, Tech. rep., Risø National Laboratory, 1983.
- Jensen, T. N., Knudsen, T., and Bak, T.: Fatigue minimising power reference control of a de-rated wind farm, *Journal of Physics: Conference Series*, DOI: 10.1088/1742-6596/753/5/052022, 2016.
- Jiménez, Á., Crespo, A., and Migoya, E.: Application of a LES technique to characterize the wake deflection of a wind turbine in yaw, *Wind Energy*, vol. 13(6), pp. 559-572, 2010.
- Jinkyoo Park, J., Kwon, S., and Law, K. H.: Wind farm power maximization based on a cooperative static game approach, *The International Society for Optical Engineering*, DOI: 10.1117/12.2009618, 2013.
- Johnson, K. and Fritsch, G.: Assessment of Extremum Seeking Control for Wind Farm Energy Production, *Wind Engineering*, vol. 36(6), pp. 701-15, 2012.
- Johnson, K. and Thomas, N.: Wind farm control: Addressing the aerodynamic interaction among wind turbines, *American Control Conference*, DOI: 10.1109/ACC.2009.5160152, 2009.
- Jonkman, J. M. and Buhl, M. L.: FAST v6.0 user guide, technical report, Tech. rep., National Renewable Energy Laboratory, 2005.

- Jonkman, J. M., Butterfield, S., Musial, W., and Scott, G.: Definition of a 5-MW reference wind turbine for offshore system development, Tech. rep., National Renewable Energy Laboratory, 2009.
- Jonkman, J. M., Annoni, J., Hayman, G., Jonkman, B., and Purkayastha, A.: Development of FAST.Farm: A New Multiphysics Engineering Tool for Wind Farm Design and Analysis, American Institute of Aeronautics and Astronautics, DOI: 10.2514/6.2017-0454, 2017.
- Katic, I., Hojstrup, J., and Jensen, N. O.: A simple model for cluster efficiency, European Wind Energy Conference and Exhibition, 1986.
- King, R. N., Hamlington, P. E., Graf, P., and Dykes, K.: Adjoint Optimization of Wind Farm Layouts for Systems Engineering Analysis, Wind Energy Symposium, DOI: abs/10.2514/6.2016-2199, 2016.
- Knudsen, T. and Bak, T.: Simple Model for Describing and Estimating Wind Turbine Dynamic Inflow, American Control Conference, DOI: 10.1109/ACC.2013.6579909, 2013.
- Knudsen, T., Bak, T., and Svenstrup, M.: Survey of wind farm control: power and fatigue optimization, *Wind Energy*, vol 18(8), pp. 1333-1351, 2015.
- Larsen, G. C., Madsen, H. A., Bingöl, F. Mann, J., Ott, S., Sørensen, J. N., Okulov, V., Troldborg, N., Nielsen, M., Thomsen, K., Larsen, T. J., and Mikkelsen, R.: Dynamic wake meandering modelling, Tech. rep., Risø National Laboratory, 2007.
- Larsen, T. J., Madsen, H. A., Larsen, G. C., and Hansen, K. S.: Validation of the dynamic wake meander model for loads and power production in the Egmond aan Zee wind farm, *Wind Energy*, vol. 16(4), pp. 605-624, 2012.
- Leibniz Universität Hannover: <https://palm.muk.uni-hannover.de/trac>, 2018.
- Madjidian, D.: Scalable minimum fatigue control of dipatchable wind farms, *Wind Energy*, vol. 19(10), pp. 1933-1944, 2016.
- Mann, J., Fisher, D., Kraus, M., Lowndes, E., and York, A.: An Analysis of Engagement Algorithms for Real-Time Weapons Effects, *Journal of Defense Modeling & Simulation*, vol. 3(3), pp. 189-201, 2006.
- Marden, J., Ruben, S. D., and Pao, L. Y.: Surveying game theoretic approaches for wind farm optimization, AIAA aerospace sciences meeting, 2012.
- Marden, J. R., Ruben, S. D., and Pao, L. Y.: A model-free approach to wind farm control using game theoretic methods, *Control Systems Technology*, vol. 21(4), pp. 1207-1214, 2013.
- Maronga, B., Gryscha, M., Heinze, R., Hoffmann, F., Kanani-Sühring, F., Keck, M., Ketelsen, K., Letzel, M. O., Sühring, M., and Raach, S.: The Parallelized Large-Eddy Simulation Model (PALM) version 4.0 for atmospheric and oceanic flows: model formulation, recent developments, and future perspectives, *Geoscientific Model Development*, vol. 8(8), pp. 2515-2551, 2015.

- Marshall, L. and Buhl, J.: A New Empirical Relationship between Thrust Coefficient and Induction Factor for the Turbulent Windmill State, Tech. rep., National Renewable Energy Laboratory, 2005.
- Martinez-Tossas, L. A., Churchfield, M. J., and Leonardi, S.: Large Eddy Simulations of the flow past wind turbines: actuator line and disk modeling, *Wind Energy*, vol. 18(6), pp. 1047-1060, 2014.
- McDonough, J. M.: Introductory lectures on turbulence Physics, Mathematics and Modeling, Tech. rep., University of Kentucky, 2004.
- Medici, D. and Alfredsson, P. H.: Measurements on a wind turbine wake: 3D effects and bluff body vortex shedding, *Wind Energy*, vol. 9(3), pp. 219-236, 2006.
- Menon, A. and Baras, J. S.: Collaborative extremum seeking for welfare optimization, Conference on Decision and Control, DOI: 10.1109/CDC.2014.7039405, 2014.
- Meyers, J. and Meneveau, C.: Large Eddy Simulations of large wind-turbine arrays in the atmospheric boundary layer, Aerospace Sciences Meeting, DOI: abs/10.2514/6.2010-827, 2010.
- Mirzaei, M. and Mann, J.: Lidar configurations for wind turbine control, *Journal of Physics: Conference Series*, DOI: 10.1088/1742-6596/753/3/032019, 2016.
- Mirzaei, M., Soltani, M., Poulsen, N. K., and Niemann, H. H.: Model predictive control of wind turbines using uncertain lidar measurements, American Control Conference, DOI: 10.1109/ACC.2013.6580167, 2013.
- Mirzaei, M., Göçmen, T., Giebel, G., Sørensen, P. E., and Poulsen, N. K.: Turbine control strategies for wind farm power optimization, American Control Conference, DOI: 10.1109/ACC.2015.7170979, 2015.
- Mittal, P., Mitra, K., and Kulkarni, K.: Optimizing the number and locations of turbines in a wind farm addressing energy-noise trade-off: A hybrid approach, *Energy Conversion Management*, vol. 132, pp. 147-160, 2017.
- Moriarty, P. J. and Butterfield, S. B.: Wind turbine modeling overview for control engineers, American Control Conference, DOI: 10.1109/ACC.2009.5160521, 2009.
- Munters, W. and Meyers, J.: Effect of wind turbine response time on optimal dynamic induction control of wind farms, *Journal of Physics: Conference Series*, DOI: 10.1088/1742-6596/753/5/052007, 2016.
- Munters, W. and Meyers, J.: An optimal control framework for dynamic induction control of wind farms and their interaction with the atmospheric boundary layer, *Philosophical Transactions of the Royal Society of London A: Mathematical, Physical and Engineering Sciences*, vol. 375(2091), 2017.
- Munters, W. and Meyers, J.: Dynamic Strategies for Yaw and Induction Control of Wind Farms Based on Large-Eddy Simulation and Optimization, *Energies*, vol 11(1), 2018a.

- Munters, W. and Meyers, J.: Towards practical dynamic induction control of wind farms: analysis of optimally controlled wind-farm boundary layers and sinusoidal induction control of first-row turbines, *Wind Energy Science Discussions*, 2018b.
- Obama, B.: The irreversible momentum of clean energy, *Science Policy Forum*, DOI: 10.1126/science.aam6284, 2017.
- Özdemir, H., Versteeg, M. C., and Brand, A. J.: Improvements in ECN wake model, ICOWES conference, 2013.
- Pao, L. Y. and Johnson, K. E.: A Tutorial on the dynamics and control of wind turbines and wind farms, *American Control Conference*, DOI: 10.1109/ACC.2009.5160195, 2009.
- Parent, O. and Ilinca, A.: Anti-icing and de-icing techniques for wind turbines: Critical review, *Cold Regions Science and Technology*, vol. 65(1), pp. 88-96, 2011.
- Park, J. and Law, K. H.: Cooperative wind turbine control for maximizing wind farm power using sequential convex programming, *Energy Conversion and Management*, vol. 101, pp. 295-316, 2015.
- Park, J. and Law, K. H.: Bayesian Ascent: A Data-Driven Optimization Scheme for Real-Time Control With Application to Wind Farm Power Maximization, *IEEE Transactions on Control Systems Technology*, vol 24(5), pp. 1655-1668, 2016.
- Peña, A., Hasager, C. B., Lange, J., Anger, J., Badger, M., Bingöl, F., Bischoff, O., Cariou, J. P., Dunne, F., Emeis, S., Harris, M., Hofsäs, M., Karagali, I., Laks, J., Larsen, S. E., Mann, J., Mikkelsen, T., Pao, L. Y., Pitter, M., Rettenmeier, A., Sathe, A., Scanzani, F., Schlipf, D., Simley, E., Slinger, C., Wagner, R., and Würth, I.: DTU-Wind-Energy-Report-E-0029, Tech. rep., 2013.
- Peña, A., Réthoré, P. E., and van der Laan, P. M.: On the application of the Jensen wake model using a turbulence-dependent wake decay coefficient: the Sexbierum case, *Wind Energy*, vol. 19(4), pp. 763-776, 2015.
- Pilong, C.: PJM Manual 12: Balancing Operations, Technical report, PJM, 2013.
- Porté-Agel, F. and Niayifar, A.: Analytical Modeling of Wind Farms: A New Approach for Power Prediction, *Energies*, vol. 9(9), 2016.
- Prandtl, L.: Bericht über Untersuchungen zur ausgebildeten Turbulenz, *Z. Angew. Math. Mech*, 1925.
- Raach, S., Schlipf, D., Haizmann, F., and Cheng, P. W.: Three dimensional dynamic model based wind field reconstruction from lidar data, *Journal of Physics: Conference Series*, DOI: 10.1088/1742-6596/524/1/012005, 2014.
- Raach, S., Schlipf, D., Borisade, F., and Cheng, P. W.: Wake redirecting using feedback control to improve the power output of wind farms, *American Control Conference*, DOI: 10.1109/ACC.2016.7525111, 2016.

- Raach, S., Boersma, S., Wingerden, J. W., Schlipf, D., and Cheng, P. W.: Robust lidar-based closed-loop wake redirection for wind farm control, vol. 50(1), pp. 4498-4503, International Federation of Automatic Control, 2017a.
- Raach, S., van Wingerden, J. W., Boersma, S., Schlipf, D., and Cheng, P. W.: Hinf Controller Design for Closed-Loop Wake Redirection, American Control Conference, DOI: 10.23919/ACC.2017.7963035, 2017b.
- Raach, S., Boersma, S., Doekemeijer, B. M., Wingerden, J. W., and Cheng, P. W.: Lidar-based closed-loop wake redirection in high-fidelity simulation, Journal of Physics: Conference Series, DOI: 10.1088/1742-6596/1037/3/032016, 2018.
- Rettenmeier, A., Schlipf, D., Wurth, I., and Cheng, P. W.: Power performance measurements of the NREL CART-2 wind turbine using a nacelle-based lidar scanner, Journal of Atmospheric and Oceanic Technology, vol. 31(10), pp. 2029-2034, 2014.
- Rosen, A. and Sheinman, Y.: The power fluctuations of a wind turbine, Journal of Wind Engineering and Industrial Aerodynamics, vol. 59(1), pp. 51-68, 1995.
- Rostampour, V., Margellos, K., Vrakopoulou, M., Prandini, M., Andersson, G., and Lygeros, J.: Reserve Requirements in AC Power Systems With Uncertain Generation, Innovative Smart Grid Technologies Europe, DOI: 10.1109/ISGTEurope.2013.6695354, 2013.
- Rotea, M. A.: Dynamic Programming Framework for Wind Power Maximization, The International Federation of Automatic Control, vol. 47(3), pp. 3639-3644, 2014.
- Rott, A., Boersma, S., van Wingerden, J. W., and Kühn, M.: Dynamic flow model for real-time application in wind farm control, Wake Conference, DOI: 10.1088/1742-6596/854/1/012039, 2017.
- Rowley, C. W., Colonius, T., and Murray, R. M.: Model reduction for compressible flows using POD and Galerkin projection, Physica D: Nonlinear Phenomena, vol. 189(1-2), pp. 115-129, 2004.
- Sagaut, P.: Large Eddy Simulation for Incompressible Flows, 2006.
- Sakagami, Y., Santos, P. A., Haas, R., Passos, J., and Taves, F. T.: Effects of turbulence, wind shear, wind veer, and atmospheric stability on power performance: a case study in Brazil, European Wind Energy Association, 2015.
- Sanderse, B.: Aerodynamics of wind turbine wakes, Literature Review, Report 16, Energy research Centre of the Netherlands, 2009.
- Sanderse, B., van der Pijl, S. P., and Koren, B.: Review of computational fluid dynamics for wind turbine wake aerodynamics, Wind Energy, vol. 14(7), pp. 799-819, 2011.
- Santoni, C., Ciri, U., Rotea, M., and Leonardi, S.: Development of a high fidelity CFD code for wind farm control, American Control Conference, DOI: 10.1109/ACC.2015.7170980, 2015.

- Schepers, J. G. and van der Pijl, S. P.: Improved modelling of wake aerodynamics and assessment of new farm control strategies, *Journal of Physics: Conference Series*, DOI: 10.1088/1742-6596/75/1/012039, 2007.
- Schlipf, D.: Prospects of multivariable feedforward control of wind turbines using lidar, *American Control Conference*, DOI: 10.1109/ACC.2016.7525112, 2016.
- Schlipf, D., Kapp, S., Anger, J., Bischoff, O., Hofsäß, M., Rettenmeier, A., Smolka, U., and Kühn, M.: Field testing of feedforward collective pitch control on the CART2 using a nacelle-based lidar scanner, *European Wind Energy Association*, 2011a.
- Schlipf, D., Kapp, S., Anger, J., Bischoff, O., Hofsäß, M., Rettenmeier, A., Smolka, U., and Kühn, M.: Prospects of optimization of energy production by lidar assisted control of wind turbines, *European Wind Energy Association*, 2011b.
- Schlipf, D., Schlipf, D. J., and Kühn, M.: Nonlinear model predictive control of wind turbines using lidar, *Wind Energy*, vol. 16(7), pp. 1107-1129, 2013.
- Schlipf, D., Grau, P., Raach, S., Duraiski, R., Trierweiler, J., and Cheng, P. W.: Comparison of linear and nonlinear model predictive control of wind turbines using lidar, *American Control Conference*, DOI: 10.1109/ACC.2014.6859205, 2014.
- Schmid, P. J.: Dynamic mode decomposition of numerical and experimental data, *Journal of Fluid Mechanics*, vol. 656, pp. 5-28, 2010.
- Scholbrock, A., Fleming, P. A., Schlipf, D., Wright, A. D., Johnson, K., and Wang, N.: Lidar-Enhanced Wind Turbine Control: Past, Present, and Future, *American Control Conference*, DOI: 10.1109/ACC.2016.7525113, 2016.
- Selvam, K., Kanev, S., van Wingerden, J. W., van Engelen, T., and Verhaegen, M.: Feedback-Feedforward Individual Pitch Control for wind turbine load reduction, *International Journal of Robust and Nonlinear Control*, special issue on Wind turbines: New challenges and advanced control solutions, vol. 19(1), pp. 72-91, 2009.
- Shapiro, C. R., Meyers, J., Meneveau, C., and Gayme, D. F.: Wind farms providing secondary frequency regulation: Evaluating the performance of model-based receding horizon control, *Journal of Physics: Conference Series*, DOI: 10.1088/1742-6596/753/5/052012, 2016.
- Shapiro, C. R., Bauweraerts, P., Meyers, J., Meneveau, C., and Gayme, D. F.: Model-based receding horizon control of wind farms for secondary frequency regulation, *Wind Energy*, vol. 20(7), pp. 1261-1275, 2017a.
- Shapiro, C. R., Meyers, J., Meneveau, C., and Gayme, D. F.: Dynamic wake modeling and state estimation for improved model-based receding horizon control of wind farms, *American Control Conference*, DOI: 10.23919/ACC.2017.7963036, 2017b.
- Simley, E. and Pao, L. Y.: Evaluation of a wind speed estimator for effective hub-height and shear components, *Wind energy*, vol. 19(1), pp. 167-184, 2014.

- Siniscalchi-Minna, S., Bianchi, F. D., De Prada Gil, M., and Ocampo-Martinez, C.: A wind farm control strategy for power reserve maximization, *Renewable Energy*, vol. 131, pp. 37-44, 2018a.
- Siniscalchi-Minna, S., Bianchi, F. D., and Ocampo-Martinez, C.: Predictive control of wind farms based on lexicographic minimizers for power reserve maximization, *American Control Conference*, DOI: 10.23919/ACC.2018.8431865, 2018b.
- Soleimanzadeh, M., Wisniewski, R., and Kanev, S.: An optimization framework for load and power distribution in wind farms, *Journal of Wind Engineering and Industrial Aerodynamics*, vol. 107, pp. 256-262, 2012.
- Soleimanzadeh, M., Wisniewski, R., and Johnson, K.: A distributed optimization framework for wind farms, *Journal of Wind Engineering and Industrial Aerodynamics*, vol. 123, pp. 88-98, 2013.
- Soleimanzadeh, M., Wisniewski, R., and Brand, A.: State-space representation of the wind flow model in wind farms, *Wind Energy*, vol. 17(4), pp. 627-639, 2014.
- Spudic, V., Jelavic, M., Baotic, M., and Peric, N.: Hierarchical wind farm control for power/load optimization, *Journal of Physics: Conference Series*, 2010.
- Spudić, V., Conte, C., Baotić, M., and Morari, M.: Cooperative distributed model predictive control for wind farms, *Optimal Control Applications and Methods*, vol. 36(3), pp. 333-352, 2014.
- Steinbuch, M., de Boer, W. W., Bosgra, O. H., Peters, S. A. W. M., and Ploeg, J.: Optimal control of wind power plants, *Journal of Wind Engineering and Industrial Aerodynamics*, vol. 27(1-3), pp. 237-246, 1988.
- Stevens, R. J. A. M.: Dependence of optimal wind turbine spacing on wind farm length, *Wind Energy*, vol. 19(4), pp. 651-663, 2015.
- Sutherland, H. and Herbert, J.: On the Fatigue Analysis of Wind Turbines, Tech. rep., Sandia National Laboratories, 1999.
- Tang, Y., He, H., Ni, Z., Wen, J., and Sui, X.: Reactive power control of grid-connected wind farm based on adaptive dynamic programming, *Neurocomputing*, vol. 125, pp. 125-133, 2014.
- Tong, W.: *Wind power generation and wind turbine design*, Wit Press, 2010.
- Trabucchi, D., Vollmer, L., and Kühn, M.: Shear layer approximation of Navier-Stokes steady equations for non-axisymmetric wind turbine wakes: Description, verification and first application, *Journal of Physics: Conference Series*, DOI: 10.1088/1742-6596/753/3/032030, 2016.
- Ungurán, R. and Kühn, M.: Combined individual pitch and trailing edge flap control for structural load alleviation of wind turbines, *American Control Conference*, DOI: 10.1109/ACC.2016.7525262, 2016.

- Vali, M., van Wingerden, J. W., Boersma, S., Petrović, V., and Kühn, M.: A predictive control framework for optimal energy extraction of wind farms, *Journal of Physics: Conference Series*, DOI: 10.1088/1742-6596/753/5/052013, 2016.
- Vali, M., Petrović, V., Boersma, S., van Wingerden, J. W., and Kühn, M.: Adjoint-based model predictive control of wind farms: Beyond the quasi steady-state power maximization, *International Federation of Automatic Control*, vol. 50(1) pp. 4510-4515, 2017.
- Vali, M., Petrović, V., Boersma, S., van Wingerden, J. W., Pao, L. Y., and Kühn, M.: Adjoint-based model predictive control of wind farms: Beyond the quasi steady-state power maximization, *Control Engineering Practice* (under review), 2018a.
- Vali, M., Petrović, V., Boersma, S., van Wingerden, J. W., Pao, L. Y., and Kühn, M.: Model Predictive Active Power Control of Waked Wind Farms., *American Control Conference*, 2018b.
- van der Laan, M. P., Sørensen, N. N., Réthoré, P.-E., Mann, J., Kelly, M. C., and Troldborg, N.: The  $k$ - $\epsilon$ -fP model applied to double wind turbine wakes using different actuator disk force methods, *Wind Energy*, vol 18(12), pp. 2223-2240, 2015.
- van Dijk, M. T., van Wingerden, J. W., and Ashuri, T. Li, T.: Wind farm multi-objective wake redirection for optimizing power production and loads, *Energy*, vol. 121, pp. 561-569, 2017.
- van Kuik, G. and Peinke, J.: Long-term Research Challenges in Wind Energy - A Research Agenda by the European Academy of Wind Energy, *Wind Energy Science*, vol. 1, pp. 1-39, 2016.
- van Wingerden, J. W., Pao, L. Y., Aho, J., and Fleming, P.A.: Active power control of waked wind farms, *International Federation of Automatic Control*, vol. 50(1), pp. 4484-4491, 2017.
- Vermeer, L. J., Sorensen, J. N., and Crespo, A.: Wind turbine wake aerodynamics, *Progress in Aerospace Sciences*, vol. 39(6-7), pp. 467-510, 2003.
- Versteeg, H. K. and Malalasekera, W.: *An introduction to computational fluid dynamics: The finite volume method*, 2007.
- Vollmer, L., Steinfeld, G., Heinemann, D., and Kühn, M.: Estimating the wake deflection downstream of a wind turbine in different atmospheric stabilities: An LES study, *Wind Energy Science*, vol. 1, pp. 129-141, 2016.
- Wagenaar, J. W. and Schepers, J. G.: Wake Measurements in ECN's Scaled Wind Farm, *Journal of Physics: Conference Series*, DOI: 10.1088/1742-6596/555/1/012105, 2012.
- WindEurope: Annual combined onshore and offshore wind energy statistics, Tech. rep., 2018.



- Yang, Z., Li, Y., and Seem, J. E.: Optimizing energy capture of cascaded wind turbine array with nested-loop extremum seeking control, *Journal of Dynamic Systems, Measurement, and Control*, vol. 137(12), 2015.
- Zalkind, D. S. and Pao, L. Y.: The fatigue load effects of yaw control for wind plants, *American Control Conference*, DOI: 10.1109/ACC.2016.7524969, 2016.
- Zhao, H., Wu, Q., Guo, Q., Sun, H., and Xue, Y.: Distributed Model Predictive Control of a Wind Farm for Optimal Active Power ControlPart I: Clustering-Based Wind Turbine Model Linearization, *IEEE Transactions on Sustainable Energy*, vol. 6(3), pp. 831-839, 2015.

# ACKNOWLEDGEMENTS

At the age of 25, I had worked for approximately 3 years in a kitchen and subsequently 4 years in a highly automated factory. After finishing an internal education in the latter, I got a contract of indefinite duration and started asking myself the question if this is what I would like to do for the rest of my life. Although I learned a lot, enjoyed working with my colleagues and enjoyed my spare time to the fullest until that point, I concluded that staying would not be an option. During my factory work, I fixed robotics and injection moulding errors that occurred. However, if the error involved, *e.g.*, programming or installing the robot, I had to step aside since other people were there to do this job. I decided that I wanted to learn this and started the Bachelor of Engineering track “Automation” in Utrecht. Part of this education involved PLC programming etcetera, but also parts approached engineering from a more theoretical perspective. To my own surprise, these courses were the ones I enjoyed the most. Of course, it helps when they were given by teachers such as Albert Moes, Ruud Luttmmer and Jacques Stuifbergen who made me enjoy systems&control, mechanics and mathematics, respectively. Their knowledge and enthusiasm contributed greatly to my increasing enthusiasm and I only wanted to learn and especially understand more. I want to thank all three for transferring a part of their knowledge and enthusiasm to me.

Since I wanted to learn more about systems&control and its theory, the place to be is Delft. A great university where it is possible to indulge yourself in theoretical matter, something that I did. Underlying theory regarding systems&control is taught by renowned experts. A few names that enlightened me the most and made me more enthusiastic are prof T. Young (systems&signals), K. Wakker (astrodynamics), A. van den Berg (complex function theory), R. Babuška, T. Keviczky (both control theory), M. Verhaegen (filtering), R. Tóth (process dynamics), G. Lopes (robotics) and X. Bombois (system identification). How much I enjoyed their lectures and studied their material to try to understand. The latter is something I can do by reading, discussing and iterating this process. I was lucky to find somebody who studies in an equivalent way, Georgios. By discussing we did not only learn a lot, I also learned a different level of understanding. It was not a few iterations, but many times, the iterations went on in the middle of the night until the pages were turned over many many times and every letter was discussed. There was always one objective, and that was to understand things from a theoretical point of view. Try to predict the model or controller we programmed before running it and not running it 100 times and try to explain all these results. Xavier Bombois gave me the opportunity to do my masters thesis in Lyon where I ended up working with Anton and Khaled. I enjoyed my stay in Lyon mostly since the main goals were 1) understand underlying theory and 2) scientifically contribute. I had many discussions and laughs with Anton and Khaled and this all gave me more motivation to pursue a PhD.

In my master thesis defence committee was, *i.a.*, Jan-Willem. He asked me to pursue my PhD in Delft and work on wind farm control. I want to thank Jan-Willem for giving me this opportunity and support. During my PhD I met and worked with the “klasbakken” Bart, Sebastiaan and Joeri. We had great discussions and laughs and these guys are one of the reasons that I got through my PhD. During my PhD I also got the opportunity to work for a short period with Johan Meyers. I am grateful that you took the time to discuss and share a small part of your knowledge with me during the few discussions we had. Other collaborators I would like to thank are the NREL researchers, Steffen, Vahab, Sara, Mehdi, Andreas and Will. From all of them I learned something. Thanks to my committee members, for taking the time and providing feedback.

Also many thanks to all my friends and obviously, during my life, there is always my family. Jan, Ieke, Tim, Susana and Nynke who always supported and endured me being me. I cannot thank you enough, but will just say that you guys are the best. At last I want to thank Catherine, mon amour. I met her during my period in Lyon and ever since, she always kept supporting and challenging me.

*SJOERD BOERSMA  
Delft, August 2018*

# CURRICULUM VITÆ

## SJOERD BOERSMA

15-01-1982      Born in Hardenberg, Holland.

### EDUCATION

- 2007–2010      B.Eng. Automation (with honours)  
University of Applied Sciences Utrecht  
*Thesis:*          Modelling, identification and control of the Robotic  
                         Soccer Goalkeeper  
*Supervisor:*    ir. A. Moes  
*Supervisor:*    prof. dr. ir. R. Babuška
- 2010–2011      Pre-Master Systems and Control  
Delft University of Technology
- 2012–2015      M.Sc. Systems and Control (cum laude)  
Delft University of Technology  
*Thesis:*          Analysis of the Robust Performance of Large-Scale  
                         Linear Systems using a Hierarchical Approach: PLL  
                         Network Application  
*Supervisor:*    dr. ir. A. Korniienko  
*Supervisor:*    prof. dr. ir. X. Bombois
- 2015–2019      PhD. Engineering  
Delft University of Technology  
*Thesis:*          Towards closed-loop dynamical wind farm control:  
                         model development and control applications  
*Promotor:*      prof. dr. ir. J.W. van Wingerden  
*Promotor:*      prof. dr. ir. M. Verhaegen

### GRANTS

- 2014              Erasmus scholarship to do research in the Ecole Centrale de Lyon, France
- 2017              IPID4all travel grant to do research in ForWind, Oldenburg, Germany

## VISITING SCHOLAR

- |      |   |
|------|---|
| 2014 | Research in the Ecole Centrale de Lyon, France (1 year) |
| 2017 | Research in ForWind, Oldenburg, Germany (1 month)       |

# LIST OF PUBLICATIONS

## JOURNAL ARTICLES

**S. Boersma, B.M. Doekemeijer, S. Siniscalchi-Minna and J.W. van Wingerden**, *A constrained wind farm controller providing secondary frequency regulation: an LES study*, [Renewable Energy](#) 2018.

**B.M. Doekemeijer, S. Boersma, L.Y. Pao, T. Knudsen and J.W. van Wingerden**, *Online model calibration for a simplified LES model in pursuit of real-time closed-loop wind farm control*, [Wind Energy Science](#) 2018.

**M. Vali, V. Petrović, S. Boersma, J.W. van Wingerden, L.Y. Pao and M. Kühn**, *Adjoint-based model predictive control of wind farms: Beyond the quasi steady-state power maximization*, [Control Engineering Practice](#) 2018 (under review).

**S. Boersma, B.M. Doekemeijer, M. Vali, J. Meyers and J.W. van Wingerden**, *A control-oriented dynamic wind farm model: WFSim*, [Wind Energy Science](#) 2018.

## TUTORIAL ARTICLES

**S. Boersma, B.M. Doekemeijer, P.M.O. Gebraad, P.A. Fleming, J. Annoni, A.K. Scholbrock, J.A. Frederik and J.W. van Wingerden**, *A tutorial on control-oriented modelling and control of wind farms*, [American Control Conference](#) 2017.

## BOOK CHAPTERS

**B.M. Doekemeijer, S. Boersma, J. Annoni, P.A. Fleming and J.W. van Wingerden**, *Wind Plant Controller design*, ModSim book 2018.

## PEER-REVIEWED CONFERENCE ARTICLES

(Abbreviated list.)

**S. Boersma, T. Keviczky and J.W. van Wingerden**, *Stochastic Model Predictive Control: uncertainty impact on wind farm power tracking*, [American Control Conference 2019](#) (under review).

**R. Ungurán, S. Boersma, V. Petrović, J.W. van Wingerden, L.Y. Pao and M. Kühn**, *Feedback-feedforward individual pitch control design with uncertain measurements*, [American Control Conference 2019](#) (under review).

**S. Boersma, V. Rostampour, B.M. Doekemeijer, J.W. van Wingerden and T. Keviczky**, *A Model Predictive Wind Farm Controller with Linear Parameter-Varying Models*, [IFAC Conference on Nonlinear Model Predictive Control](#) 2018.

- B.M. Doekemeijer, S. Boersma, L.Y. Pao and J.W. van Wingerden**, *Joint state-parameter estimation for a control-oriented LES wind farm model*, [Journal of Physics: Conference Series 2018](#).
- S. Raach, S. Boersma, B.M. Doekemeijer, J.W. van Wingerden and P.W. Cheng**, *Lidar-based closed-loop wake redirection in high-fidelity simulation*, [Journal of Physics: Conference Series 2018](#).
- S. Boersma, V. Rostampour, B.M. Doekemeijer, W. van Geest and J.W. van Wingerden**, *A constrained model predictive wind farm controller providing active power control: an LES study*, [Journal of Physics: Conference Series 2018](#).
- B.M. Doekemeijer, S. Boersma, J.W. van Wingerden and L.Y. Pao**, *Ensemble Kalman filtering for wind field estimation in wind farms*, [American Control Conference 2017](#).
- S. Raach, S. Boersma, J.W. van Wingerden, D. Schlipf and P.W. Cheng**, *Robust lidar-based closed-loop wake redirection for wind farm control*, [International Federation of Automatic Control 2017](#).
- A. Rott, S. Boersma, J.W. van Wingerden and M. Kühn**, *Dynamic flow model for real-time application in wind farm control*, [Wake Conference 2017](#).
- M. Vali, J.W. van Wingerden, S. Boersma, V. Petrović and M. Kühn**, *A predictive control framework for optimal energy extraction of wind farms*, [Journal of Physics: Conference Series 2016](#).
- S. Boersma, P.M.O. Gebraad, M. Vali, B.M. Doekemeijer and J.W. van Wingerden**, *A control-oriented dynamic wind farm flow model: WFSim*, [Journal of Physics: Conference Series 2016](#).
- S. Boersma, A. Korniienko, K. Laib and J.W. van Wingerden**, *Robust Performance Analysis for a Range of Frequencies*, [American Control Conference 2016](#).
- S. Boersma, M. Vali, J.W. van Wingerden and M. Kühn**, *Quasi Linear Parameter Varying modeling for wind farm control using the 2D Navier Stokes equations*, [American Control Conference 2016](#).